AD-A118 554 STANFORD UNIV CA INFORMATION SYSTEMS LAB F/G 17/4
RESEARCH ON ADAPTIVE ANTENNA TECHNIQUES. IV.(U)
AUG 80 B WIDROW, T SAXE, K DUVALL, W NEWMAN N00019-79-C-0331
UNCLASSIFIED NL

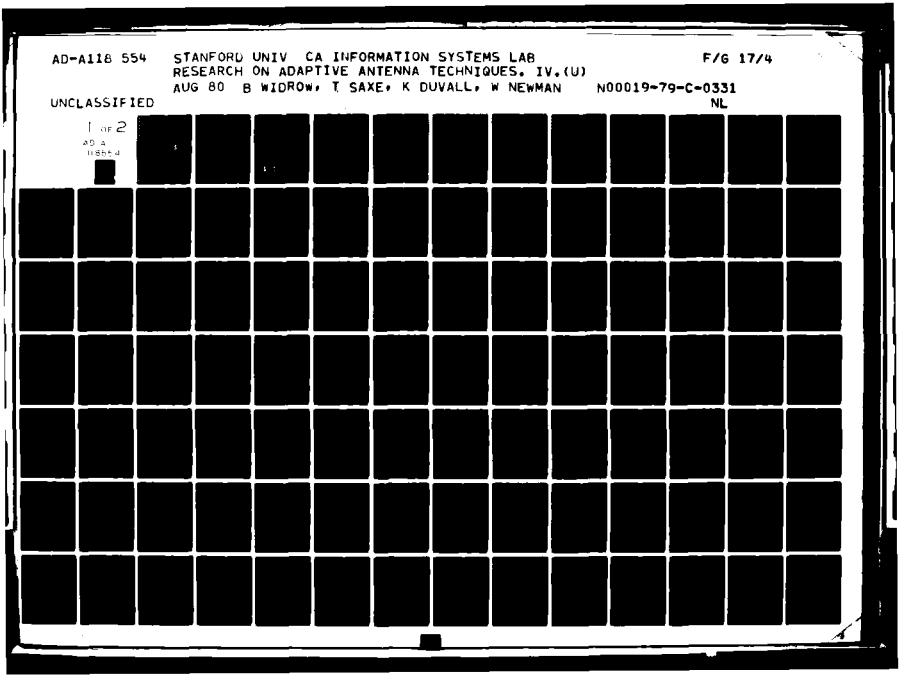

RESEARCH ON ADAPTIVE ANTENNA TECHNIQUES IV

(1)

FINAL REPORT

by

B. Widrow
T. Saxe
K. Duvall
W. Newman
R. Gooch

August 6, 1980

Information Systems Laboratory
Department of Electrical Engineering
Stanford University
Stanford, CA 94305

This research was supported by the
Naval Air Systems Command of the Department of Defense
under Contract N00019-79-C-0331

The views and conclusions contained in this document
are those of the authors and should not be interpreted as
necessarily representing the official policies, either expressed or implied
of the Naval Air Systems Command or the U.S. Government.

APPROVED FOR PUBLIC RELEASE:
DISTRIBUTION UNLIMITED

FOREWORD

This final report describes the research performed during the past year on adaptive antenna techniques. The research included new work on the topic of signal cancellation in adaptive arrays as well as a further investigation of power-separation techniques that was begun under a prior contract (N00019--78-C-0276) with the Naval Air Systems Command. The report has been divided into two parts to reflect the different thrusts of the new and the continuing investigations.

Part I of the report is concerned with the phenomenon of signal cancellation that occurs in standard adaptive beamformers when the environment demands rapid adaptation. The signal-cancellation effect that results from jammer/signal interaction with the adaptive beamformer is described and is likened to the notch-filtering effect that occurs in much simple adaptive noise cancelling systems. Two different techniques that are currently being pursued to alleviate signal cancellation are described, and simulation results are presented that indicate significant peformance improvement over conventional beamformers.

Part II is based on a doctoral dissertation by T. Saxe and represents a refinement of earlier work on adaptive power separators. This part discusses the design of adaptive power separators for discriminating between powerful jammer signals and a weaker desired signal. Three different single-channel, low-power-pass adaptive separators are analyzed. Each structure consists of a power-spectrum estimator, a filter designer that analyzes the power spectrum and designs filters that reject frequencies where the spectral estimate exceeds a selected threshold, and a filter that actually processes the input to reject powerful spectral components.

PART I

JAMMING OF ADAPTIVE ARRAYS BY SIGNAL CANCELLATION: THE PHENOMENON AND TWO REMEDIES

B. Widrow, K. Duvall, R. Gooch, and W. Newman

I. INTRODUCTION

Adaptive antennas have been under development in various forms during the past two decades or so. Although adaptive antennas have only been used in small numbers thus far, they have proven themselves capable of rejecting jamming signals to an extent that is unprecedented. Most high performance radar and communications systems being designed to work in jamming environments currently incorporate adaptive antennas. The development of spread spectrum techniques simultaneously with adaptive antennas provides a formidable set of technologies for jam resistant systems. These technologies are compatible and are frequently used in the same system. An adaptive antenna is relied upon to attenuate strong jamming signals as they appear at the receiver "front end." Spread spectrum techniques are used to neutralize large numbers of weak jammers that may not be eliminated totally by the adaptive antenna.

The question arises, are adaptive antennas susceptible to certain jammers? Or, stated differently, can jammers be devised specifically for use against adaptive antennas? Under certain circumstances, the answer to this question is yes. This paper is concerned with jamming signals that could defeat or partially defeat known adaptive antenna algorithms. The existence of jammers that could trouble known adaptive arrays motivates the development of new adaptive signal processing and array processing algorithms, two of which are proposed herein.

The goals of this paper are threefold:

(a) Examine the signal cancellation phenomenon in adaptive beamformers.

(b) Formulate approaches toward the elimination of the adaptive signal cancellation phenomenon, based on the work of K. Duvall.

(c) Introduce spatial dither algorithms for the purposes of combating signal cancellation and modulating "smart" jammer signals at the receiving array.

II. SIGNAL CANCELLATION JAMMING

Any adaptive beamformer, either the Howells-Applebaum sidelobe canceller [1,2], Widrow's pilot signal beamformer [3], Griffith's beamformer [4], Frost's beamformer [5], Zahm's beamformer [6] or combinations and variations of these, is susceptible to attack by a simple jammer which may be band-pass noise, or a sinusoid, or a sum of sinusoids suitably spaced in frequency. The interaction of such jammers with the desired signal in these adaptive algorithms can cause cancellation of signal components, even when these adaptive beamformers are working perfectly.

To understand how this comes about, consider the Frost beamformer which functions in the following manner. A beam is formed toward a user selected "look direction." The receiving sensitivity in this direction is then constrained. A typical constraint is one that forces the array to have a unit gain magnitude and zero phase over a selected passband of frequencies in the look direction. The beamformer is adapted (its weights are varied) to minimize its output power, subject to the constraint which sustains the beam in the look direction. Adaptation subject to the constraint causes the array to accept a signal with gain one if this signal arrives from the look direction, and causes any other signals, jammer signals for example, to be rejected as well as possible (in the minimum total power sense) so long as they do not arrive from the look direction. Other adaptive beamformers behave more or less like the Frost beamformer except that the Frost algorithm imposes a "hard" constraint on the signal gain in the look direction. The Widrow and Griffiths beamformers create "soft" constraints in this direction. The Howells-Applebaum and Zahm

beamformers apply soft constraints omnidirectionally rather than along a look direction.

Suppose that the Frost beamformer has a sinusoidal input signal arriving from the look direction. This signal should appear at the beamformer output, going through a unit gain. Now suppose a jammer is turned on, a very strong sinusoidal jammer at the same frequency as the signal and arriving off the look direction. The jamming sinusoid would normally be rejected by the adaptive beamformer, if the signal were not present. But with signal present, minimizing the total output power will cause the jammer to be admitted with just the right magnitude and phase to cancel the sinusoidal signal. Thus, the signal sinusoid is admitted with a gain of one. On the other hand, just a trickle of the powerful jammer sinusoid is admitted to perfectly cancel the signal sinusoid and produce a net output of zero. The output power is minimized and the constraint is preserved, as it should be with a perfectly working Frost beamformer. But the result is loss of the signal. This amounts to *jamming by signal cancellation*, rather than *jamming by overwhelming* the signal with interference.

If the input signal in the look direction is broadband rather than sinusoidal and the jammer is sinusoidal, the adaptive algorithm will modulate the sinusoidal jammer in such a manner that it will cancel some signal components at the jammer frequency and at neighboring frequencies. If the jammer signal contains a sum of sinusoids at spaced frequencies within the passbands, the output signal spectrum will be notched at each of the jammer frequencies. This phenomenon could be troublesome for bandpass and spread spectrum communications.

This signal cancellation phenomenon has been observed and analyzed in the context of simple adaptive noise cancelling systems, much simpler systems than adaptive beamformers. A brief discussion and analysis of adaptive noise

cancelling follows.

III. ADAPTIVE NOISE CANCELLING

An adaptive noise canceller is shown in Fig. 1. In the terminology of that field, the "primary input" contains a useful signal s, plus interference n_0. The "reference input" is separately obtained in practical systems. It contains interference n_1, related to that of the primary input. The relationship between the two interferences is generally unknown a priori. The adaptive filter has the job of shaping the reference interference to replicate (in the least squared error sense) the primary interference so that subtraction will remove the interference from the primary input and thereby deliver a much more useful output. It has been shown in [7] that an adaptive filter minimizing mean squared error, minimizes output power of the system of Fig. 1. This causes the system output to be a best least squares estimate of the useful signal s. The Howells-Applebaum sidelobe canceller is more complicated than this in several ways (useful signals and jammer signals appear at both primary and reference inputs; spatial, i.e. array, processing is also involved), but works basically on the cancelling principle described above.

If the reference input is a sinusoid, as shown in Fig. 2, then the signal flow path from primary input to the output behaves like a sharp, linear, time-invariant notch filter. When first discovered, this was a surprise because the adaptive filter itself is intrinsically nonlinear and time variable. An analysis, by John Glover of the notch filter effect was presented in a 1975 Proceedings of the IEEE paper by Widrow, et al, on the subject of adaptive noise cancelling [7]. A more detailed analysis is contained in Glover's Ph.D. thesis entitled "Adaptive Noise Cancelling of Sinusoidal Interferences", Department of Electrical Engineering, Stanford University, 1975 [8]. A published work based on Glover's thesis has since appeared [9]. This work treats both single and multiple notch

cases. Analysis of the simplest case, a single notch created by a two weight adaptive filter, is presented next.

IV. AN ADAPTIVE NOTCH FILTER

In this section, an analysis of the notch filter effect of the adaptive noise canceller, is presented. This analysis deals with the formation of a notch at a single frequency. Analytical and experimental results show, however, that if more than one frequency is present in the reference input, a notch for each frequency will be formed.

Figure 2 shows an adaptive noise canceller with two adaptive weights. The primary input is assumed to be an arbitrary signal--stochastic, deterministic, periodic, transient, etc. The reference input is assumed to be a pure cosine wave $C\cos(\omega_o t+\varphi)$. The primary and reference inputs are sampled at the frequency $\Omega = 2\pi/T$ rad/s. The reference input is sampled directly, giving x_{1j}, and after undergoing a 90° phase shift, it is sampled, giving x_{2j}. The samplers are synchronous and strobe at $t = 0,\ T,\ 2T$, etc.

A transfer function for the noise canceller of Fig. 2 may be obtained by analyzing signal propagation from the primary input to the system output.* Weight updating in the system is carried out according to the LMS algorithm [10,11]:

$$w_{1j+1} = w_{1j} + 2\mu\varepsilon_j x_{1j}$$

$$w_{2j+1} = w_{2j} + 2\mu\varepsilon_j x_{2j}\,, \tag{1}$$

where the subscripts indicate the time index and μ is a constant controlling the rate of adaptation. Refering to Fig. 3, the sampled reference inputs are

*It is not obvious, from inspection of Fig. 2, that a transfer function for this propagation path in fact exists. Its existence is shown, however, by the subsequent analysis.

$$x_{1j} = C\cos(\omega_o jT+\varphi)\,. \tag{2}$$

and

$$x_{2j} = C\sin(\omega_o jT+\varphi)\,. \tag{3}$$

The first step in the analysis is to obtain the isolated impulse response from the error ε_j, point C, to the filter output, point G, with the feedback loop from point G to point B broken. Let an impulse of amplitude α be applied at point C at discrete time $j = k$; that is,

$$\varepsilon_j = \alpha\delta(j-k) \tag{4}$$

The $\delta(j-k)$ is a Kronecker delta function, defined as

$$\delta(j-k) = \begin{cases} 1, & \text{for } j = k \\ 0, & \text{otherwise}\,. \end{cases} \tag{5}$$

The impulse causes a response at point D of

$$\varepsilon_j x_{1j} = \begin{cases} \alpha C\cos(\omega_o kT+\varphi), & \text{for } j = k \\ 0, & \text{otherwise}\,, \end{cases} \tag{6}$$

which is the input impulse scaled in amplitude by the instantaneous value of x_{1j} at $j = k$. The signal flow path from point D to point E is that of a digital integrator with transfer function $2\mu/(z-1)$ and impulse response $2\mu u(j-1)$, where $u(j)$ is the discrete unit step function

$$u(j) = \begin{cases} 0, & \text{for } j < 0 \\ 1, & \text{for } j \geq 0. \end{cases} \tag{7}$$

Convolving $2\mu u(j-1)$ with $\varepsilon_j x_{1j}$ yields a response at point E of

$$w_{1j} = 2\mu\alpha C\cos(\omega_o kT+\varphi)\,, \tag{8}$$

where $j \geq k + 1$. When the scaled and delayed step function is multiplied by x_{1j}, the response at point F is obtained as

$$y_{1j} = 2\mu\alpha C^2\cos(\omega_o jT+\varphi)\cos(\omega_o kT+\varphi)\,. \tag{9}$$

where $j \geq k + 1$. The corresponding response at point J, obtained in a similar manner, is

$$y_{2j} = 2\mu\alpha C^2 \sin(\omega_o jT+\varphi) \sin(\omega_o kT+\varphi), \tag{10}$$

where $j \geq k + 1$. Combining (9) and (10) yields the response at the filter output, point G:

$$\begin{aligned} y_{2j} &= 2\mu\alpha C^2 \cos(\omega_o T(j-k)) \\ &= 2\mu\alpha C^2 u(j-k-1) \cos(\omega_o T(j-k)). \end{aligned} \tag{11}$$

Note that (11) is a function only of $(j-k)$ and is thus a time invariant impulse response, proportional to the input impulse.

A linear transfer function for the noise canceller may now be derived in the following manner. If the time k is set equal to zero, the unit impulse response of the linear time-invariant signal-flow path from point C to point G is

$$y_j = 2\mu C^2 u(j-1) \cos(\omega_o jT), \tag{12}$$

and the transfer function of this path is

$$\begin{aligned} C(z) &= 2\mu C^2 \left[\frac{z(z - \cos\omega_o T)}{z^2 - 2z\cos\omega_o T + 1} - 1 \right] \\ &= \frac{2\mu C^2(z \cos \omega_o T - 1)}{z^2 - 2z \cos \omega_o T + 1}. \end{aligned} \tag{13}$$

This function can be expressed in terms of a radian sampling frequency $\Omega = 2\pi/T$ as

$$C(z) = \frac{2\mu C^2[z \cos(2\pi\omega_o\Omega^{-1}) - 1]}{z^2 - 2z \cos(2\pi\omega_o\Omega^{-1}) + 1}. \tag{14}$$

If the feedback loop from point G to point B is now closed, the transfer function $H(z)$ from the primary input, point A, to the noise canceller output, point C, can be obtained from the feedback formula:

$$H(z) = \frac{z^2 - 2z \cos(2\pi\omega_o\Omega^{-1}) + 1}{z^2 - 2(1-\mu C^2)z \cos(2\pi\omega_o\Omega^{-1}) + 1 - 2\mu C^2}. \tag{15}$$

Equation (15) shows that the noise canceller with a cosine reference input has the properties of a notch filter at the reference frequency ω_o along the signal flow path from primary input to output. The zeros of the transfer function are located in the Z plane at

$$z \approx \exp(\pm i 2\pi\omega_o \Omega^{-1}) \tag{16}$$

and are precisely on the unit circle at angles of $\pm 2\pi\omega_o\Omega^{-1}$ rad. The poles are located at

$$z = (1-\mu C^2)\cos(2\pi\omega_o{}^{-1}) \pm i[(1-2\mu C^2) - (1-\mu C^2)\cos^2(2\pi\omega_o\Omega^{-1})]^{1/2} . \tag{17}$$

The poles are inside the unit circle at a radial distance $(1 - 2\mu C^2)^{1/2}$, approximately equal to $1 - \mu C^2$, from the origin at angles of

$$\pm \text{arc cos}[(1-\mu C^2)(1-2\mu C^2)^{-1/2}\cos(2\pi\mu\Omega^{-1})] .$$

For slow adaptation (that is, small values of μC^2) these angles depend on the factor

$$\begin{aligned} \frac{1-\mu C^2}{(1-2\mu C^2)^{1/2}} &= \left[\frac{1 - 2\mu C^2 + \mu^2 C^4}{1 - 2\mu C^2}\right]^{1/2} \\ &= (1 - \mu^2 C^4 + \cdots)^{1/2} \\ &\doteq 1 - \frac{1}{2}\mu^2 C^4 \end{aligned} \tag{18}$$

which differs only slightly from a value of one. The result is that, in practical instances, the angles of the poles are almost identical to those of the zeros.

The location of the poles and zeros and the magnitude of the transfer function in terms of frequency are shown in Fig. 4. Since the zeros lie on the unit circle, the depth of the notch in the transfer function is infinite at the frequency $\omega = \omega_o$. The sharpness of the notch is detemined by the closeness of the poles to the zeros. Corresponding poles and zeros are separated by a dis-

tance approximately equal to μC^2. The arc length along the unit circle (centered at the position of a zero) spanning the distance between half-power points is approximately $2\mu C^2$. This length corresponds to a notch bandwidth of

$$\begin{aligned}(BW) &= \mu C^2 \Omega/\pi \\ &= 2\mu C^2 F \text{ Hz}, \end{aligned} \tag{19}$$

where F is the sampling frequency in Hz. The Q of the notch is determined by the ratio of the center frequency to the bandwidth.

$$Q \doteq \frac{\omega_o \pi}{\mu C^2 \Omega}. \tag{20}$$

The time constant of the mean square error "learning curve" for the LMS algorithm has been shown to be [6,9]

$$\tau_{mse} = \frac{n}{4\mu \; trace \; R} \text{ iterations}, \tag{21}$$

where R is the covariance matrix of the inputs to the weights, and n is the number of weights. Formula (21) applies when the eigenvalues are all equal. This is the case for the system of Fig. 2. Multiplying by the sampling period T, the time constant is expressed in seconds of real time as

$$\tau_{mse} = \frac{nT}{4\mu \; trace \; R} \text{ sec.} \tag{22}$$

For the two-weight adaptive filter of Fig. 2,

$$\begin{aligned} trace \; R &= \frac{1}{2}C^2 + \frac{1}{2}C^2 \\ &= C^2. \end{aligned} \tag{23}$$

This is the sum of the power into the weights. Combining equations (23), (22), and (19) yields

$$(BW) = \frac{1}{\tau_{mse}} \text{ Hz.} \tag{24}$$

Thus, the bandwidth of the notch is the reciprocal of the time constant of the

tance approximately equal to μC^2. The arc length along the unit circle (centered at the position of a zero) spanning the distance between half-power points is approximately $2\mu C^2$. This length corresponds to a notch bandwidth of

$$\begin{aligned}(BW) &= \mu C^2 \Omega / \pi \\ &= 2\mu C^2 F \text{ Hz}, \end{aligned} \tag{19}$$

where F is the sampling frequency in Hz. The Q of the notch is determined by the ratio of the center frequency to the bandwidth.

$$Q \doteq \frac{\omega_o \pi}{\mu C^2 \Omega}. \tag{20}$$

The time constant of the mean square error "learning curve" for the LMS algorithm has been shown to be [6,9]

$$\tau_{mse} = \frac{n}{4\mu \, trace \, R} \text{ iterations}, \tag{21}$$

where R is the covariance matrix of the inputs to the weights, and n is the number of weights. Formula (21) applies when the eigenvalues are all equal. This is the case for the system of Fig. 2. Multiplying by the sampling period T, the time constant is expressed in seconds of real time as

$$\tau_{mse} = \frac{nT}{4\mu \, trace \, R} \text{ sec.} \tag{22}$$

For the two-weight adaptive filter of Fig. 2,

$$\begin{aligned} trace \, R &= \frac{1}{2}C^2 + \frac{1}{2}C^2 \\ &= C^2. \end{aligned} \tag{23}$$

This is the sum of the power into the weights. Combining equations (23), (22), and (19) yields

$$(BW) = \frac{1}{\tau_{mse}} \text{ Hz.} \tag{24}$$

Thus, the bandwidth of the notch is the reciprocal of the time constant of the

learning process, for the simple system of Fig. 2.

Figure 5 shows the results of two experiments performed to demonstrate that the adaptive system acts like a notch filter. In the first, the primary input was a cosine wave of unit power stepped at 512 discrete frequencies. The reference input was a cosine wave with frequency ω_0 of $\pi/2T$ rad/s. The value of C was 1, and the value of μ was 1.25×10^{-2}. The frequency resolution of the fast Fourier transform was 512 bins. The output power at each frequency is shown in Fig. 5(a). As the primary frequency approaches the reference frequency, significant cancellation occurs. The weights do not converge to stable values but "tumble" at the difference frequency,* and the adaptive filter behaves like a modulator, converting the reference frequency into the primary frequency. The theoretical notch width between half-power points, $1.59 \times 10^{-2}\ \omega_0$, compares closely with the measured notch width of $1.62 \times 10^{-2}\ \omega_0$.

In the second experiment, the primary input was composed of uncorrelated samples of white noise of unit power. The reference input and the processing parameters were the same as in the first experiment. An ensemble average of 4096 power spectra at the noise canceller output is shown in Fig. 5(b). An infinite null was not observed in this experiment because of the finite frequency resolution of the spectral analysis algorithm.

In these experiments, the filtering of a reference cosine wave of a given frequency caused cancellation of primary input components at adjacent frequencies. This result indicates that, under some circumstances, primary input components may be partially cancelled and distorted even though they are not correlated with the reference input. In practice this kind of cancellation is of concern only when the adaptive process is rapid; that is, when it is effected with

*When the primary and reference frequencies are held at a constant difference, the weights develop a sinusoidal steady state at the difference frequency. In other words, they converge on a dynamic rather than a static solution.

large values of μ. When the adaptive process is slow, the weights converge to values that are nearly fixed, close to the Wiener solution, and though signal cancellation as described in this section occurs, it is generally not significant due to the fact that the notch is extremely narrow. In any event, the primary input appears at the output having gone through a notch filter.

V. SIGNAL CANCELLATION PHENOMENA WITH A FROST ADAPTIVE BEAMFORMER

Figure 6 shows the antenna array and Frost beamformer that were used in the series of computer simulation experiments to be presented below. The signal was assumed to be incident from broadside and the look direction constraint was set to unit gain and zero phase from zero frequency to half the sampling rate, i.e. to a flat response over all frequencies. The jammer was sinusoidal at one quarter the sampling frequency. In these experiments, ambient noise and receiver noise were negligible. A typical converged beam pattern is shown in Fig. 6, plotted at the jammer frequency. Only half the symmetrical pattern is plotted. One can see that the look direction gain is unity, and that the gain in the jammer direction is .019, 34 dB below the main beam gain. Observation of the beam pattern gives the appearance that the beamformer is working perfectly.

A bandpass signal was received by this adaptive beamformer whose spectrum is shown in Fig. 7(a). The spectrum of the sinusoidal jammer is shown in Fig. 7(b). The output signal spectrum is shown in Fig. 7(c). The input signal appears at the output having gone through a notch filter. The notching effect is evident in the output signal spectrum and is indicative of gross signal distortion at the beamformer output. The notch width is not exactly equal to the reciprocal of the learning curve time constant, but exceeds it by a factor of 2.

The conditions for the derivation of the notch width formula (24), i.e., sinusoidal signals appearing with exact 90° separation at the inputs to the two weights, are not precisely met with the 16-weight Frost processor under the above stated experimental conditions. Nevertheless, the simple formula (24) does give at least an approximate prediction of notch width that is applicable at most jammer angles.

The notching phenomenon in adaptive beamformers is somewhat more complicated than in adaptive noise cancelling systems. The useful signal arriving from the look direction encounters a unit gain due to the main beam constraint. This is analogous to the direct primary signal path of Fig. 1. The jammer signal arriving at other than the look direction encounters an adaptive filter, analogous to the reference signal path of Fig. 1. The weights in the adaptive beamformer are not completely free as they are in the adaptive filter of Fig. 1. The Frost constraint reduces the number of degrees of freedom to be equal to the number of weights multiplied by the factor $(k-1)/k$, where k is equal to the number of antenna elements. Also, the spatial processing effects of the array and the multichannel structure of the adaptive processor introduce differences in the dynamics of convergence between the adaptive beamformer and the adaptive noise canceller.

Additional experiments were conducted with the system of Fig. 6. The jammer was again sinusoidal, while the look-direction signal was composed of white noise of unit power. The jammer power was varied. Spectra of the beamformer outputs are shown in Fig. 8. With the jammer power set at its lowest level, the signal cancellation notch is at its smallest bandwidth as is seen in Fig. 8a. As the jammer power is increased and other parameters held constant, the notch width increases. Figure 8(c) shows the widest notch for the strongest jammer signal that was applied. In all of the illustrated cases, the relationship between

notch width and reciprocal adaptive time constant has been preserved.

The results of another experiment are shown in Fig. 9. Here, the signal was white, and the jammer was a strong bandpass noise. Signal components were partially cancelled over the entire jammer spectral band, corresponding to extensive signal distortion. It should be realized that results of this type would only occur in cases of very rapid adaptation. For the experiment of Fig. 9, the time constant of the adaptive process was approximately equal to 20 sampling periods. The bandwidth of the jammer was approximately equal to 15% of the sampling rate.

Two remedies to the signal notching or cancellation problem will be discussed. The first is a method devised by K. Duvall based on the use of two signal processing systems, one to perform the adaptation, the other to generate the system output signal.

VI. THE DUVALL BEAMFORMER

In order to prevent signal cancellation, the useful signal arriving from the look direction is excluded from the beamformer in which the adaptive process takes place. In the system shown in Fig. 10, the adaptive process is only used to derive a set of weights. These weights are copied into a separate, identical "slaved" processor used to form the output signal. The adaptive process could be the Frost algorithm, as indicated in Fig. 10, or it could be any one of a number of adaptive beamformer algorithms that have appeared in the literature.

The antenna array elements in Fig 10 are assumed to be uniformly spaced along a line. It is clear from the block diagram shown in this figure that, because of the subtractive preprocessing, the look direction signal will not appear at the Frost adaptive beamformer inputs but that the jammer signals

will be present as indicated. Receiver noise and ambient noise are neglected in this discussion. The Frost algorithm will null jammer J. The strength and character of signal S will have no effect on the weights. Copying the weights will cause the slaved processor to have a main beam which conforms to the Frost constraints established for the look direction, and to have a null in the exact direction of the jammer J. The correct alignment of the null is assured since the relative phases of the jammer components are the same in the slaved beamformer as in the Frost adaptive beamformer, where the nulls originate. The phasor diagram in Fig. 10 verifies this in accord with the following argument.

The jammer components received by the antenna elements are indicated by a set of equal amplitude uniformly-spaced phasors J_0, J_1, J_2, J_3, and J_4. The phasor inputs to the Frost beamformer are J_1-J_0, J_2-J_1, J_3-J_2, and J_4-J_3. They too are uniform-amplitude, equally-spaced, and separated by the same angles as the received jammer components J_0, J_1, J_2, J_3, and J_4. Since the relative phase angles are the same in the slaved processor as in the Frost processor, the beam pattern notch is formed at the proper bearing angle.

The Duvall beamformer uses a standard adaptive beamformer as one of its components. Beam steering in any direction can be accomplished simply by including beam steering delays in the antenna circuits. Phase shifters would be adequate for narrowband processes; delay lines would be required for broadband processes. It should be noted that although the phasor argument applies only to one jammer at one frequency, linearity and superposition show that the principle is applicable to multiple jammers and to broadband as well as to narrowband jammers and signals.

Experiments have been performed with this system, and results are given in Figs. 11 and 12. Figure 11 compares the output spectrum of the Frost beam-

former with that of the Duvall beamformer (using a Frost beamformer), both adapting with a time constant of .05, with the same array and with the same signal and jammer. The array and jammer were as shown in Fig. 6. After performing the comparative experiments, the Frost beamformer showed evidence of strong signal cancellation, while the Duvall beamformer showed no evidence of signal cancellation. In the time domain, Fig. 12 compares the look-direction input signal with the output signals of the Frost and Duvall beamformers. In both cases the weights were initialized to zero, and adaptive transients are visible at the beginnings of the output tracings. Beyond the region where the transient exists, substantial signal distortion in the Frost beamformer output is present. The distortion power was measured to be 6 dB below the input signal power. Such distortion is not apparent at the output of the Duvall beamformer. Here the distortion was measured to be 110 dB below signal level.

The Duvall beamformer appears to be an important development toward mitigating the effects of signal cancellation. It is, however, a recent development, and possible limitations on its performance have yet to be assessed. Effects of component inaccuracies and array imperfections are not yet understood. How to use it with other than straight line, evenly spaced arrays is not yet determined. Other methods for eliminating or reducing signal cancellation effects are also being pursued, such as spatial dither algorithms.

VII. SPATIAL DITHER ALGORITHMS

Spatial dither algorithms have been newly conceived for the purpose of applying locally controlled modulation to signals arriving at angles other than the look direction while leaving inputs from the look direction unmodulated and undistorted. The effect is to cause jammer power to be spread spectrally, thereby reducing jammer power density. When used with a conventional adaptive beamformer, spatial dither reduces signal cancellation effects. The same

process has the additional capability of modulating a "smart" jammer signal in a way that is totally unpredictable to the jammer, thus in many cases rendering it "less smart."

A conceptually simple form of spatial dither algorithm is the "3/4-inch plywood" approach, pictured in Fig. 13. The elements of an antenna array may be imagined to be fixed to a piece of plywood which provides a rigid insulating support, so that the entire array may be moved mechanically. In either one or two dimensions, the array is moved in directions which are orthogonal to the look direction. Far-field emanations arriving from the look direction will be undistorted by the mechanical motion, while emissions from off axis sources will be distorted by an unusual shift-of-time-base form of modulation. (Electronic means of implementation of this spatial dither process are being devised.)

The outputs of the antenna elements of Fig. 13 could be applied to a time delay and sum (nonadaptive) beamformer, to a conventional adaptive beamformer, or to a Duvall adaptive beamformer. Spatial dither could be beneficial in each case. By reducing jammer power density, some antijam protection is provided without adaptive beamforming, and additional antijam protection is provided with adaptive beamforming. Reduction of signal cancellation effect in a Frost beamformer can be obtained by using spatial dither preprocessing. Breakup of jammer signal structure is a possible form of signal preprocessing applicable to all types of adaptive and nonadaptive beamformers.

The 3/4-inch plywood approach has been computer simulated, and results are presented in Fig. 14. The motion was random and was done along a line perpendicular to the look direction. At every fourth sample time, the plywood position was switched; the new position was drawn randomly from a uniform distribution which ranged from zero to eight wavelengths. Figure 14(a) shows the spectrum of the look-direction input signal, in this case a random bandpass sig-

nal. The sinusoidal jammer spectrum is shown in Fig. 14(b). The spectrum of the jammer from the physical reference frame of the array is shown in Fig. 14(c). It is clear that the jammer power is greatly spread, that jammer power density is significantly reduced, and that the jammer signal is severely distorted from its original form. In the simulation, bandpass filters were used with each antenna output to represent the effects of a receiver for each antenna. The filtered signals were then applied to a conventional Frost adaptive beamformer. Some signal distortion is evident, but the amount of distortion is greatly reduced by the spatial dither. The output spectrum shown in Fig. 14(d) is far less distorted than that of Fig. 7(c), a comparable spectrum obtained without spatial dither.

VIII. CONCLUSION

Signal cancellation effects occur in conventional adaptive beamformers when jammer power and adaptation rate are high. These effects can cause signal loss in the case of narrowband signals or cause significant signal distortion in the case of wideband signals. Means of combatting signal cancellation have been proposed, namely the Duvall beamformer and the spatial dither algorithm. The latter approach will probably not be as effective as the former against signal cancellation but has the capability of destroying "smart" jammer signals.

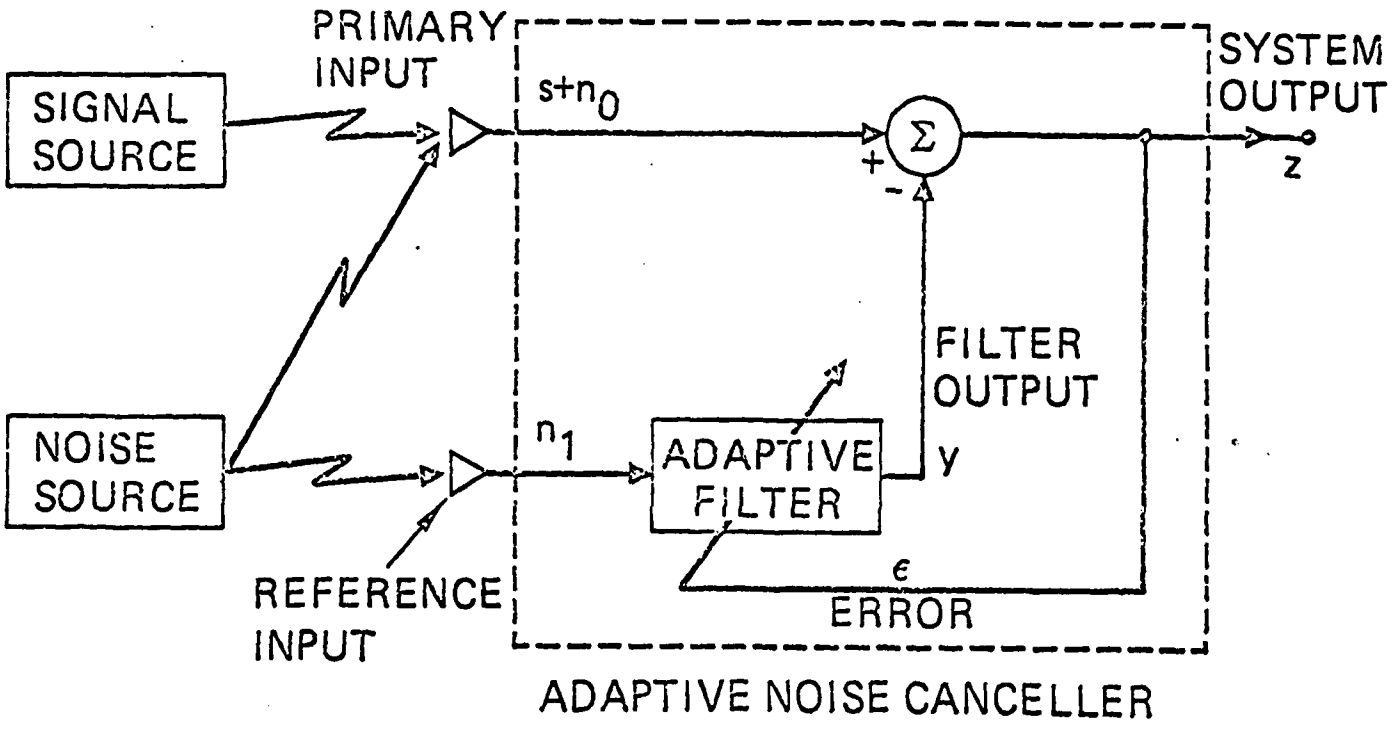

Fig. 1. The adaptive noise cancelling concept.

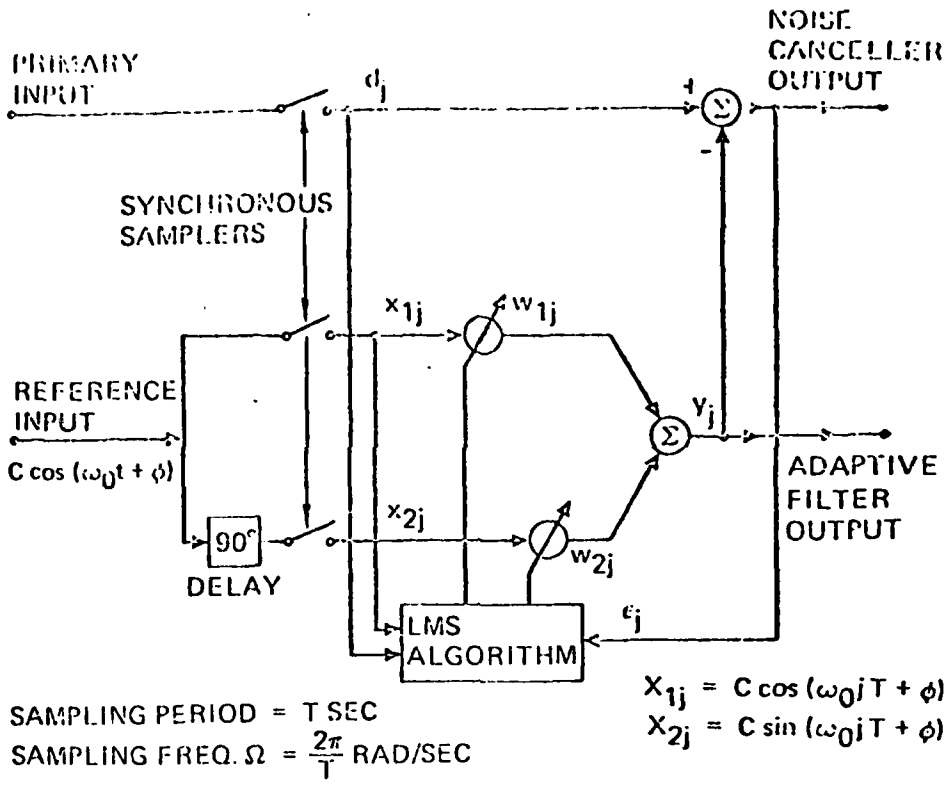

Fig. 2. Two-weight noise canceller.

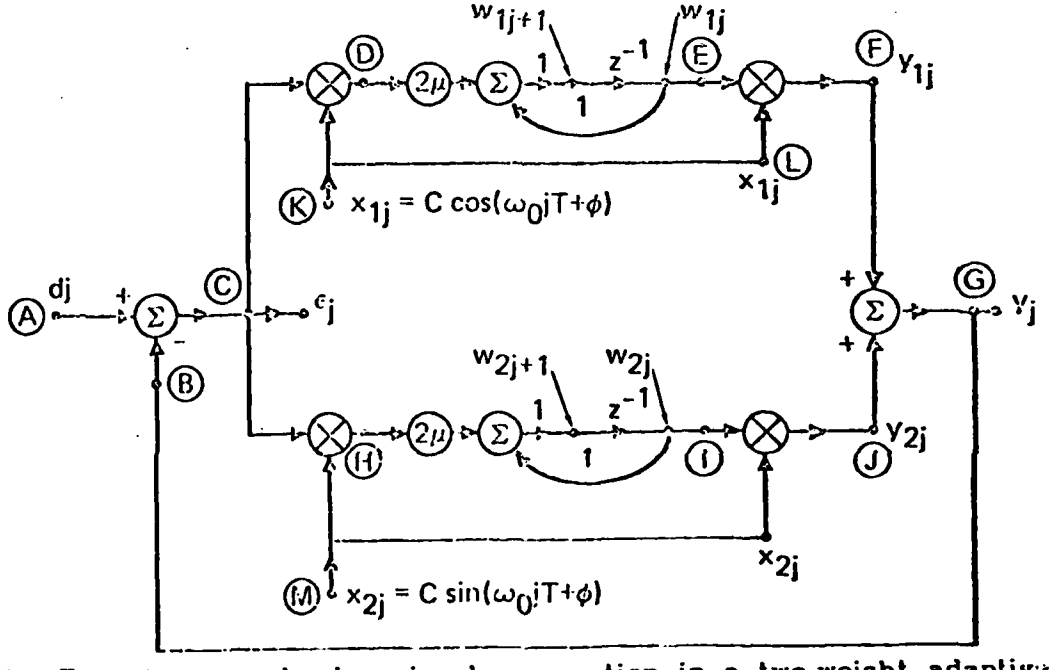

Fig. 3. Flow diagram showing signal propagation in a two-weight adaptive noise canceller.

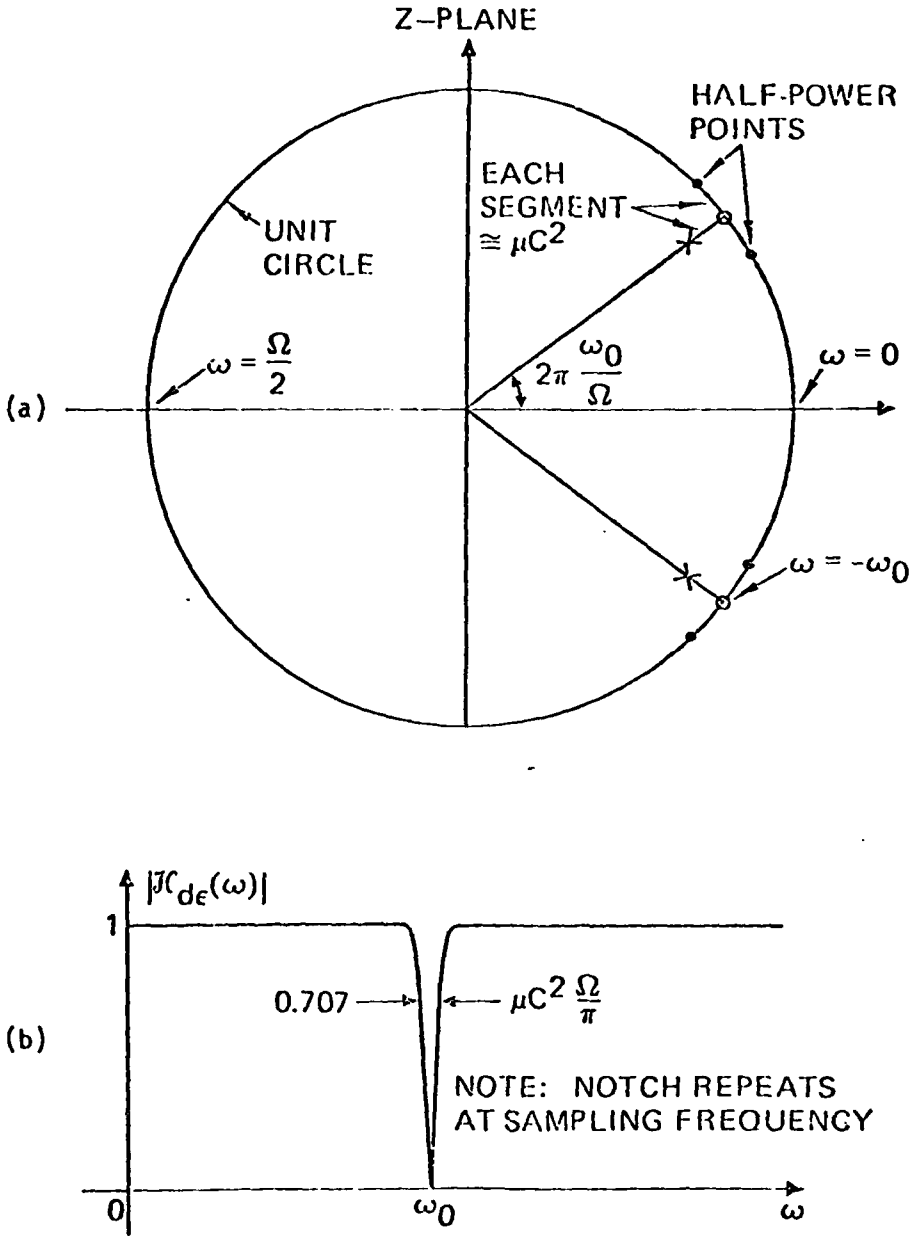

Fig. 4. Properties of transfer function of two-weight adaptive noise canceller. (a) Location of poles and zeros. (b) Magnitude of transfer function.

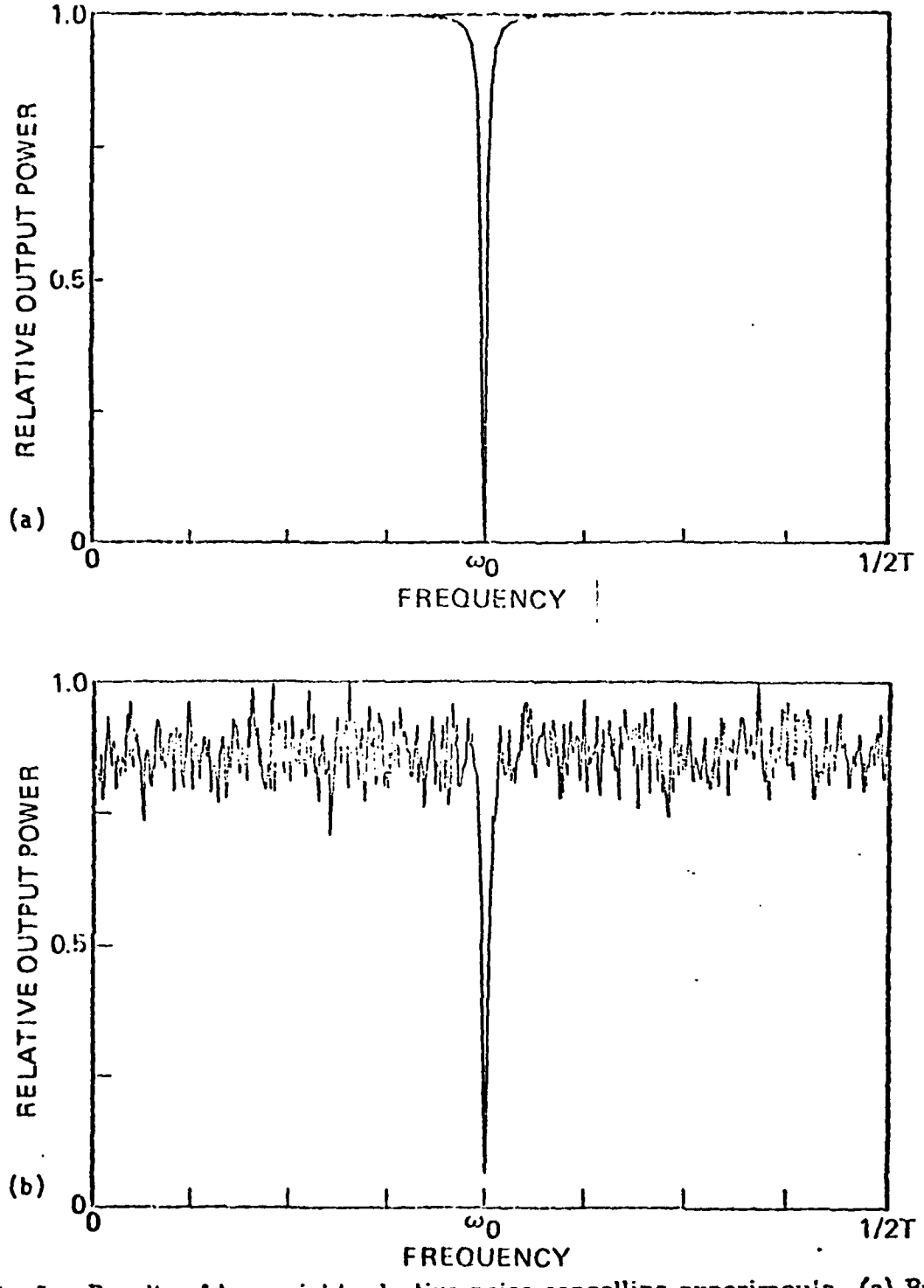

Fig. 5. Results of two-weight adaptive noise cancelling experiments. (a) Primary input composed of cosine wave at 512 discrete frequencies. (b) Primary input composed of uncorrelated samples of white noise.

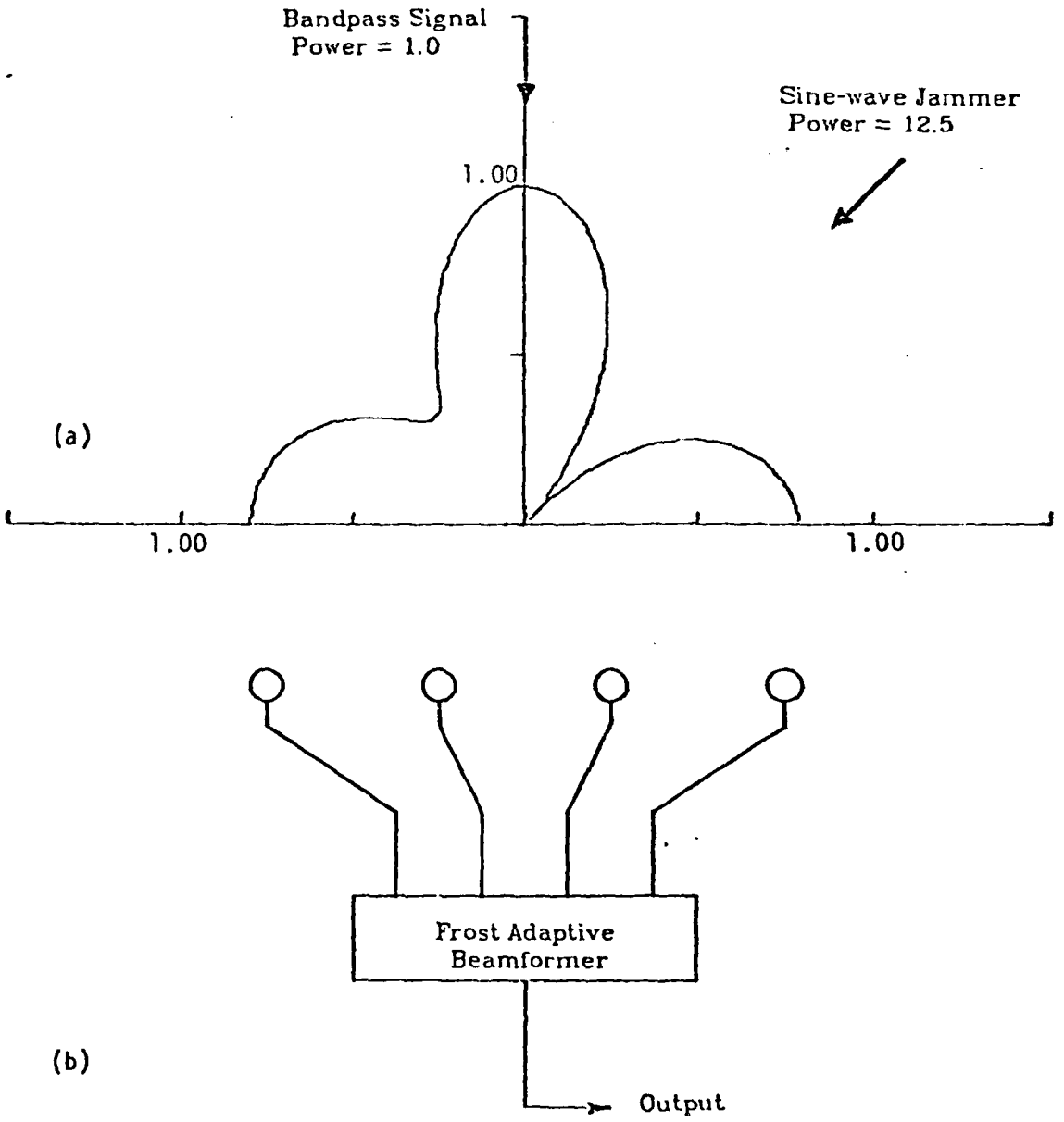

Fig. 6. Frost adaptive beamformer with signal and jammer.

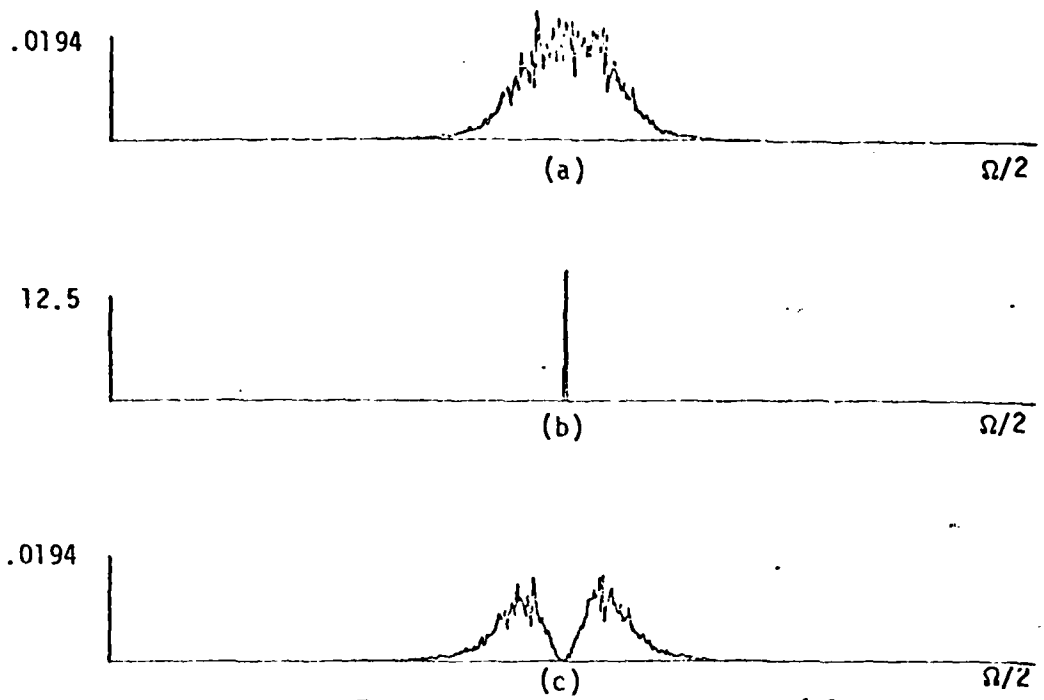

Fig. 7. Power spectra of Frost beamformer simulation. (a) Input signal spectrum. (b) Jammer spectrum. (c) Beamformer output spectrum.

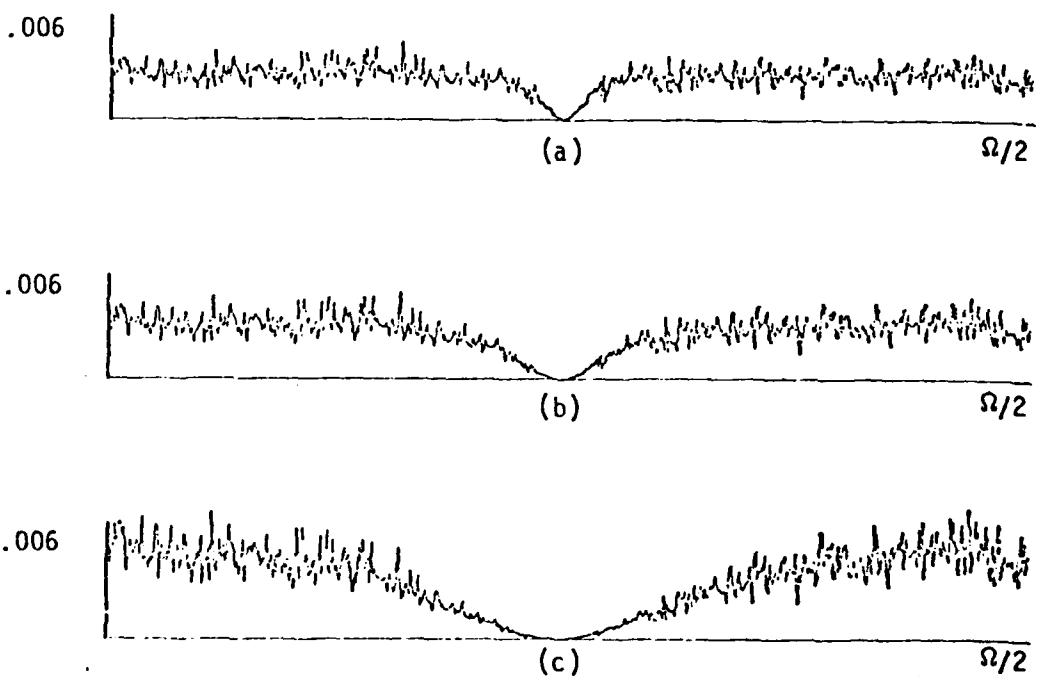

Fig. 8. Frost beamformer output spectra for white-noise signal of power 1.0 and sinusoidal jammer. (a) Jammer power = 12.5 (b) Jammer power = 25.0 (c) Jammer power = 50.0

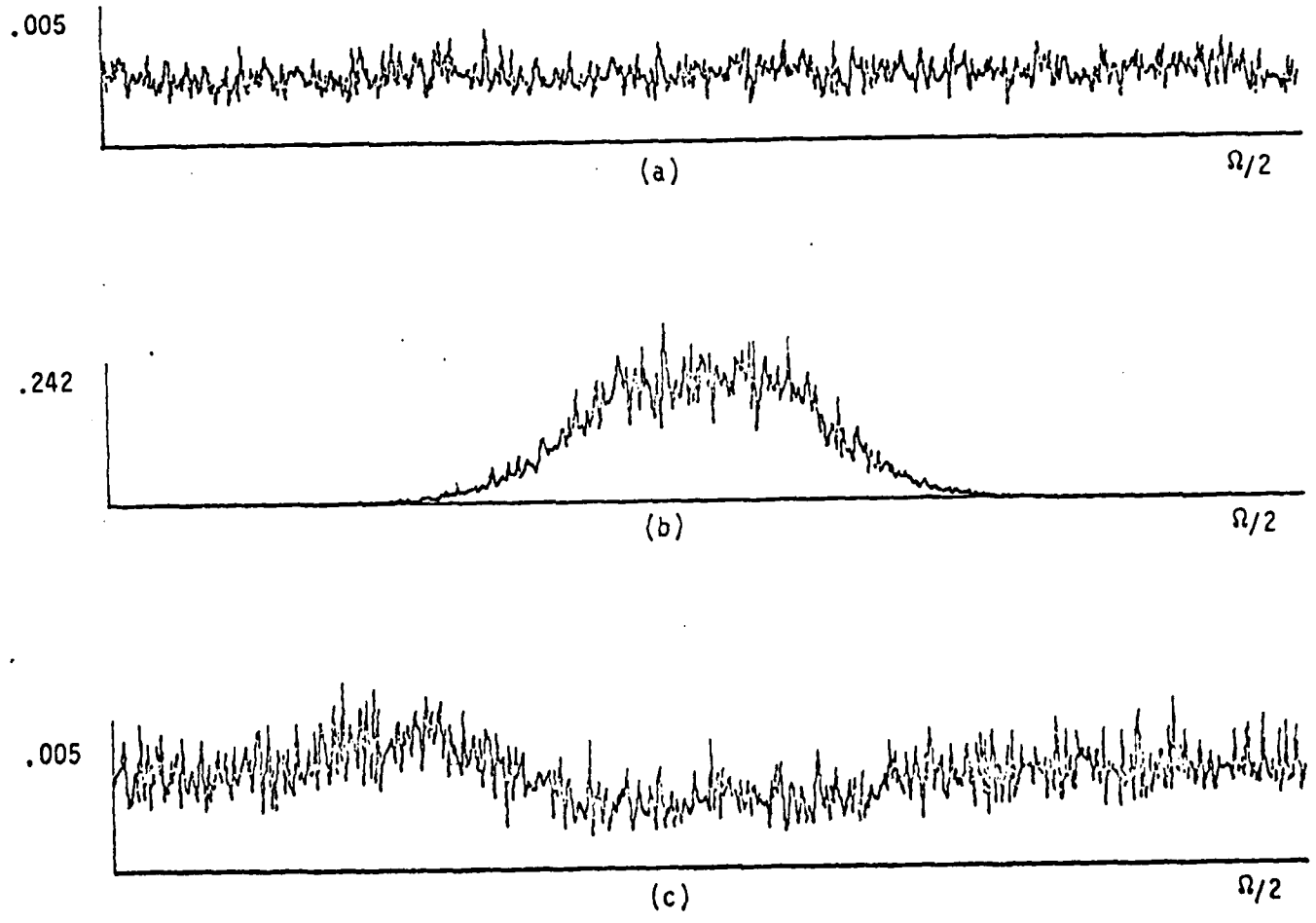

Fig. 9. Power spectra of Frost beamformer simulation with wide-band signal. (a) Input signal spectrum. (b) Jammer spectrum. (c) Beamformer output spectrum.

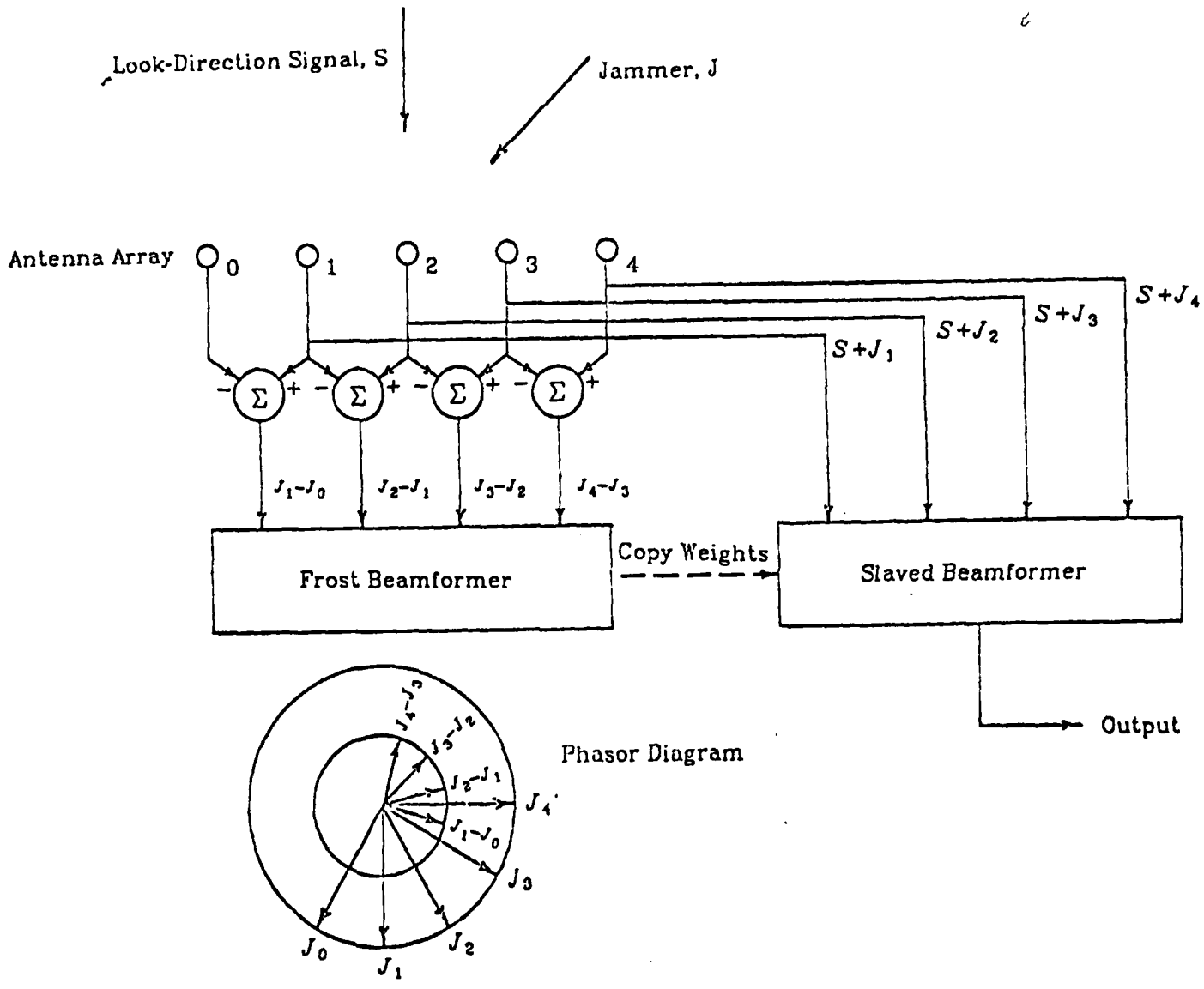

Fig. 10. Duvall beamformer for eliminating cancellation jamming.

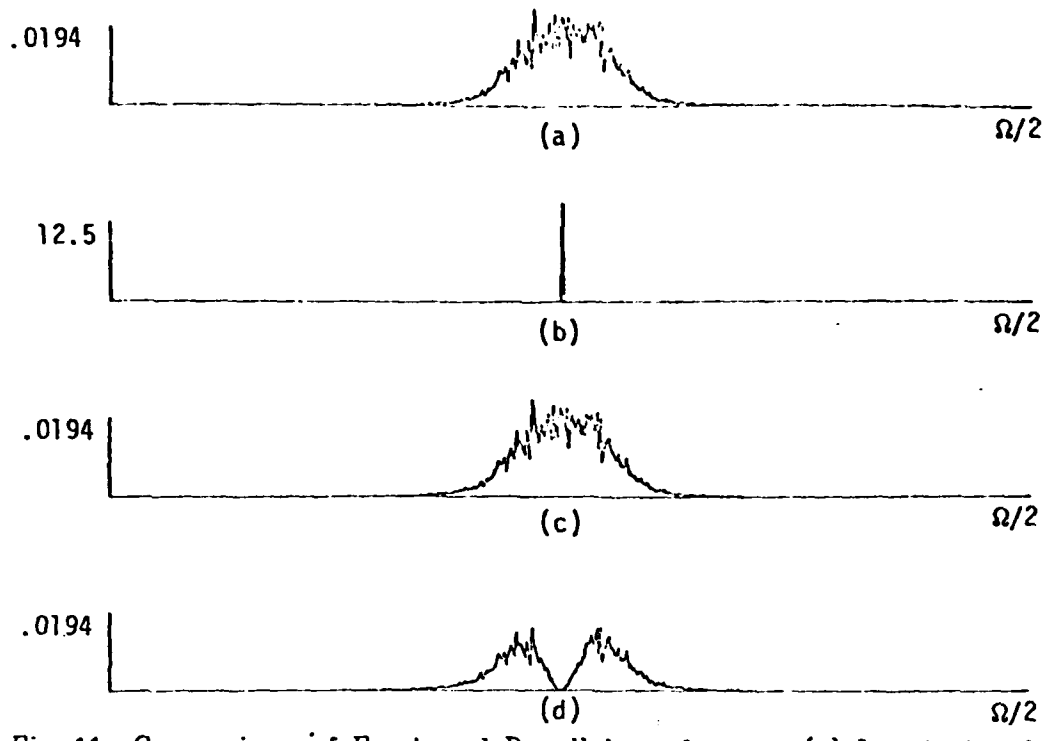

Fig. 11. Comparison of Frost and Duvall beamformer. (a) Input signal spectrum. (b) Jammer spectrum. (c) Duvall beamformer output spectrum. (d) Frost beamformer output spectrum.

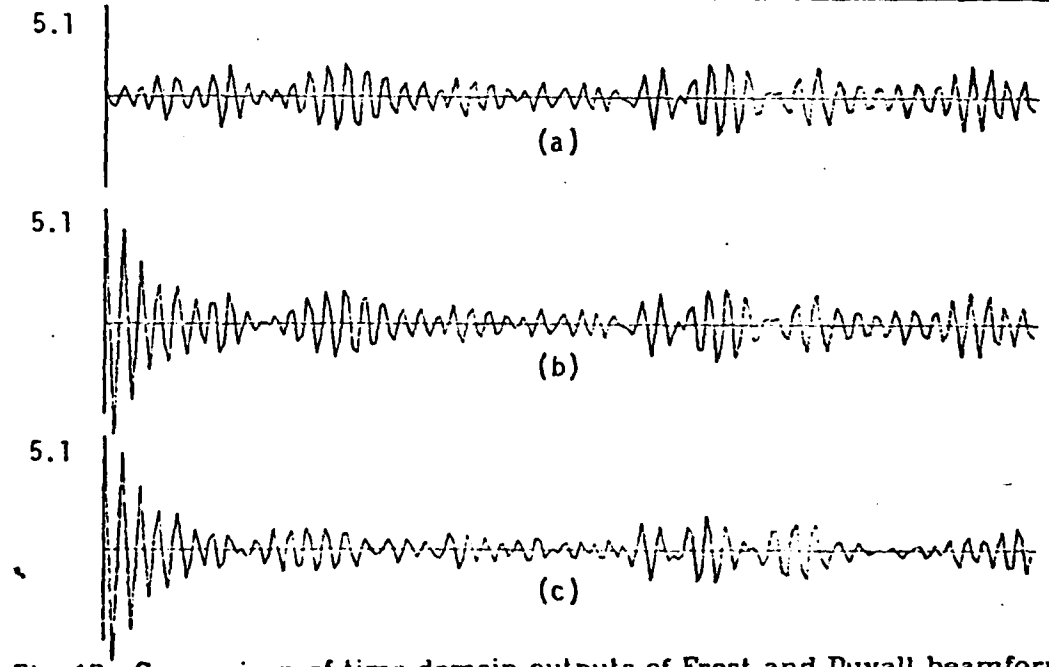

Fig. 12. Comparison of time-domain outputs of Frost and Duvall beamformers. (a) Signal input. (b) Duvall beamformer output. (c) Frost beamformer output.

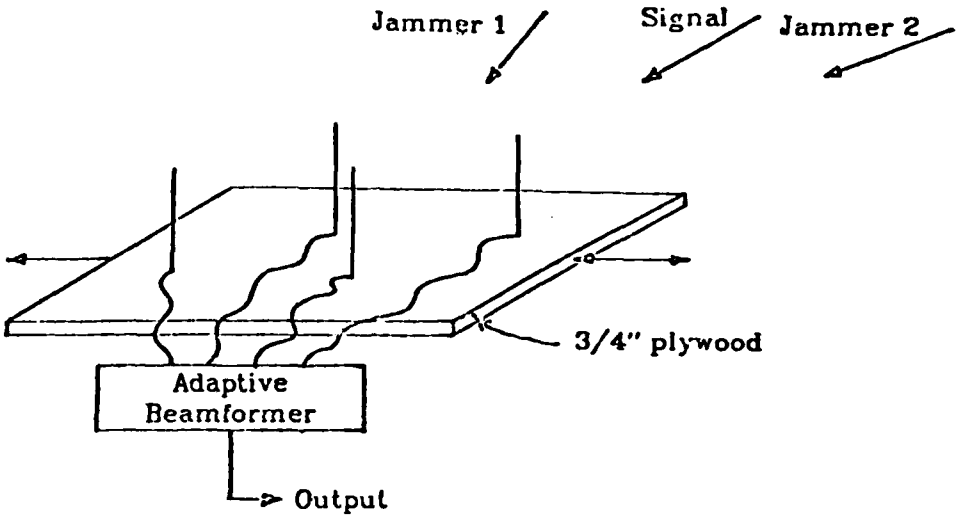

Fig. 13. Spatial dither algorithm (3/4" plywood approach).

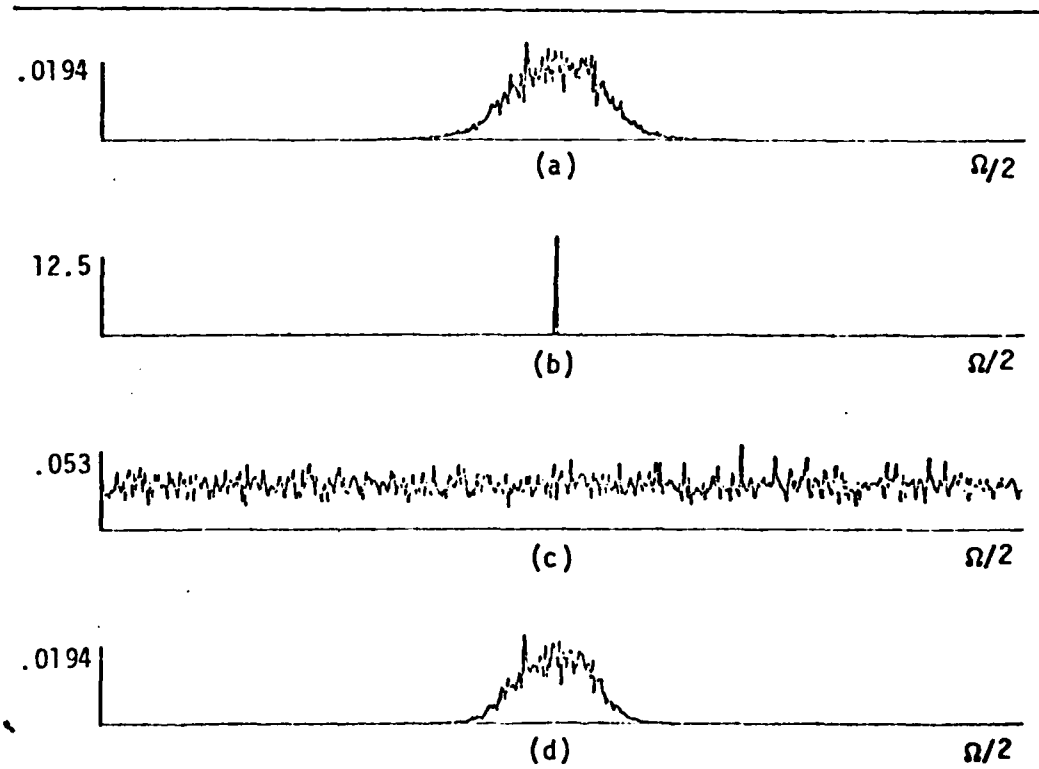

Fig. 14. Input and output power spectra of Frost beamformer with spatial dither preprocessing. (a) Input signal spectrum. (b) Undithered jammer spectrum. (c) Dithered jammer spectrum. (d) Adaptive array output spectrum.

References

1. Howells, P., Aug. 24, 1965, "Intermediate Frequency Side-Lobe Canceller," U. S. Patent 3 202 990.

2. Sept. 1976, Special Issue on Adaptive Antennas, IEEE Transactions on Antennas and Propagation, Vol. Ap-24. No. 5.

3. Widrow, B., Dec. 1967, "Adaptive Antenna Systems," Proceedings of the IEEE, Vol. 55, No. 12, pp. 2143-2159.

4. Griffiths, L. J., Oct. 1969, "A Simple Adaptive Algorithm For Real-Time Processing In Antenna Arrays," Proceedings of the IEEE, Vol. 57, No. 10, pp. 1696-1704.

5. Frost, III, O. L., Aug. 1972, "An Algorithm For Linearly Constrained Adaptive Array Processing," Proceedings of the IEEE, Vol. 60, No. 8, pp. 926-935.

6 Zahm, C. L., 1973, "Applications of Adaptive Arrays to Suppress Strong Jammers in the Prescence of Weak Signals," IEEE Transactions on Aerosp. Electron. Systems, Vol. AES-9, pp. 260-271.

7. Widrow, B., et al., Dec. 1975, "Adaptive Noise Cancelling: Principles and Applications," Proceedings of the IEEE, Vol. 63, No. 12, pp. 1692-1716.

8. Glover, J., Dec. 1975 (Ph.D. dissertation), "Adaptive Noise Cancelling of Sinusoidal Interference," Stanford Electronics Laboratories, Stanford University.

9. Glover, J., Dec. 1977, "Adaptive Noise Cancelling Applied to Sinusoidal Interferences," IEEE Transactions on Acoustics, Speech and Signal Processing, Vol. ASSP-25, No. 6, pp. 484-491.

10. Widrow, B., and M. E. Hoff, Jr., 1960, "Adaptive Switching Circuits," IRE WESCON Conv. Rec., pt. 4, pp. 96-104.

11. Widrow, B., et al., Aug. 1976, "Stationary and Nonstationary Learning Characteristics of the LMS Adaptive Filter, " Proceedings of the IEEE, Vol. 64, No. 8, pp. 1151-1162.

PART II

ADAPTIVE POWER SEPARATORS

Timothy Saxe

1 -- INTRODUCTION

An adaptive power separator (APS) is an adaptive filter that discriminates between signals on the basis of their powers. There are different varieties of APS. Some pass low power signals and reject high power signals (low-power pass APS), some pass only high power signals (high-power pass APS), and others pass only signals with power within a specified range. A low-power pass APS could be used in the "front end" of a radio receiver to eliminate powerful signals from nearby transmitters while still passing weak signals from distant transmitters. Of course, a single channel APS cannot distinguish between two signals that overlap spectrally.

This paper develops and analyses three different single channel low-power pass adaptive power separators. Therefore, in this paper the term adaptive power separator is understood to mean a single channel power separator that passes only low power signals. However, the power separators developed in this paper can be easily altered to pass high power signals or even signals in a specified power range.

Previous workers in the field of adaptive filtering [Wid, Zah, Tre, Che] have noted that some adaptive filters have a property called power inversion. Power inversion is a weak form of power separation in which signals with high power at the input to the adaptive system have less output power than signals with low input power. However, the transition from low gain to high gain is not sharp so these filters cannot discriminate between two signals that have nearly the same power.

The purpose of this work is to develop an APS with a sharp transition that will be able to discriminate between two signals with nearly the same power.

Any APS is a nonlinear system. However, all of the adaptive power separators described in this work become linear filters if the adaptive process is stopped. The adaptive process produces linear filters that use frequency discrimination to reject high power signals. Consequently, a single channel APS cannot discriminate between two signals that overlap in frequency. This limitation may be overcome by using a multichannel APS if the signals are spatially separated. For example, an APS built into an antenna array could discriminate between two signals provided that they either had different angles of arrival or they did not overlap in frequency.

2 -- PREVIOUS WORK: THE LALE APS

The single channel adaptive system which is called the adaptive (spectral) line enhancer (ALE) was first proposed by Widrow [Wid2] for the detection of sinusoidal components buried in noise. He showed that the gain of the ALE was a function of the signal-to-noise ratio. Thus the ALE can be used as an APS. However, the threshold power* of the ALE is difficult to control since it is a function of the input noise power as well as the signal power. Widrow and Treichler [Wid3, Wid4, Tre] proposed a modified ALE, called the "leaky" ALE (LALE), that algorithmically simulates the effect of added input noise without actually adding noise to the input. By this means the effective signal-to-noise ratio, and hence the threshold power of the LALE, can be controlled by altering a parameter of the adaptive process. Thus the LALE is an APS with a selectable threshold power.

In this chapter we will analyze the performance of the LALE and show that it can be used as a either a high-power pass APS or a low-power pass APS. A brief intuitive explanation of the LALE is presented first to aid in understanding the mathematical analysis of the LALE.

As was mentioned earlier, the ALE can be used as an APS. Since the ALE is simpler to understand than the LALE, we will first study the operation of the ALE. Figure 2-1 shows a block diagram of an ALE. The heart of the ALE is the LMS (Least Mean Square) adaptive filter

---

*The threshold power of an APS is defined as the signal power for which the voltage gain of the APS is 1/2.

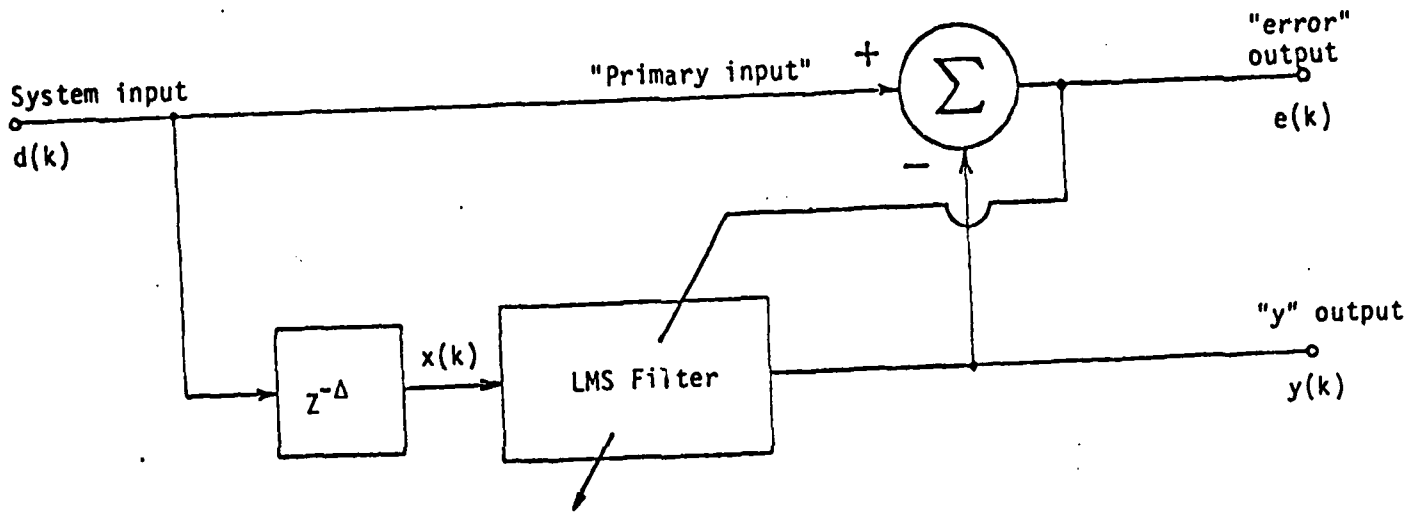

Figure 2-1. Adaptive Line Enhancer (ALE).

[Wid]. An LMS filter is a finite impulse response filter that tries to form the best least squares fit between its input signal (x(k) in the ALE) and the primary input (d(k) in the ALE). The "error" output, which is the difference between the primary input and the adaptive filter's output, measures how successful the filter has been in matching its input to the primary input. The "error" output is used as an auxiliary input to the LMS filter so that the adaptive algorithm can decide how to modify the transfer function of the filter to reduce the mean square error.

We can analyze the performance of the ALE without knowing how the LMS filter actually reduces the mean square error. For the sake of simplicity, assume that the input to the ALE consists of a sinusoid in white noise. The input to the adaptive filter, x(k), is a delayed version of the primary input, d(k). Therefore the "error" signal, e(k), is the sum of three terms: 1) noise in the primary input, 2) noise passing through the adaptive filter, and 3) a sinusoidal component. The significance of the delay between d(k) and x(k) is that the adaptive filter cannot match the noise in its input with the noise in the primary input, but can match the sinusoidal component by generating the appropriate gain and phase at the frequency of the sinusoid. To minimize the mean square error, the adaptive filter will try to pass as little noise as possible while also passing the sinusoid with the appropriate gain and phase.

A filter with a sinusoidal weight vector, at the same frequency as the input sinusoid, will have a bandpass characteristic at the frequency of the input sinusoid and minimum bandwidth. This is exactly

the form that the ALE requires, so we assume that the weight vector of the LMS filter is:

$$[W]_i = a \cos(\omega i + \phi) \qquad i = 0, 1, \ldots, n-1$$

where

ω is the angular frequency of the sinusoidal input

n is the number of filter weights

(Treicher [Tre] shows analytically that this is indeed the form of the weight vector). A filter with this weight vector has a gain of $\frac{n}{2}a$ and phase shift of ϕ at frequency ω, and a bandwidth of $2/n$. Thus if the power of the input sinusoid is P and the power of the input noise is σ^2, then the power at the "error" output is:

$$P_e = \sigma^2 + \sigma^2(\frac{n}{2}a)^2 \frac{2}{n} + P\left|1 - \frac{n}{2}a\ e^{j\phi}e^{-j\omega\Delta T}\right|^2 .$$

The LMS filter will converge to (a^*,ϕ^*) the values for which the error power is minimum

$$a^* = \frac{\frac{P}{\sigma^2}\frac{n}{2}}{1 + \frac{P}{\sigma^2}\frac{n}{2}} = \frac{\frac{n}{2}\,SNR}{1 + \frac{n}{2}\,SNR}$$

$$\phi^* = \omega\Delta T$$

where

$SNR = P/\sigma^2$ = signal to noise ratio

T = sampling period .

At low SNR, i.e. low signal power for fixed noise power, the gain ($\frac{n}{2}$ a) is low, but for high SNR the gain tends to one. Thus the ALE is a high-power pass APS because it passes strong signals better than weak signals. Figure 2-2 shows the transfer function of an ALE for several different SNR's. Incidentally, Treichler [Tre] has shown that the response to several sinusoidal inputs is the superposition of the response to the individual sinusoids provided that the frequencies of all the sinusoids differ by more than 1/nT Hz (where T is the sampling period).

A deficiency of the ALE is that the response depends upon the signal to noise ratio, not the signal power. Widrow and Treichler [Wid3] proposed adding noise to the input of the ALE, which would allow the designer to control the signal to noise ratio and thereby control the characteristics of the ALE. Of course this technique makes the output of the ALE more noisy and increases the variance of the LMS filter's weights, which modulates the output signal. However, since the characteristics of the injected noise are known, the effects of the noise upon the LMS algorithm can be computed. These effect can then be incorporated into the LMS algorithm [Gri, Wid4, Tre] which results, in the case of white noise added to the input, in the leaky LMS (LLMS) algorithm. The advantages of using the LLMS algorithm instead of injecting noise are a less noisy output, less weight variance, no need to build a noise generator and the LLMS algorithm can act as if noise with negative power were added to the input. For convenience we will refer to "algorithmic noise" when we mean the noise effects that are incorporated into the LLMS algorithm.

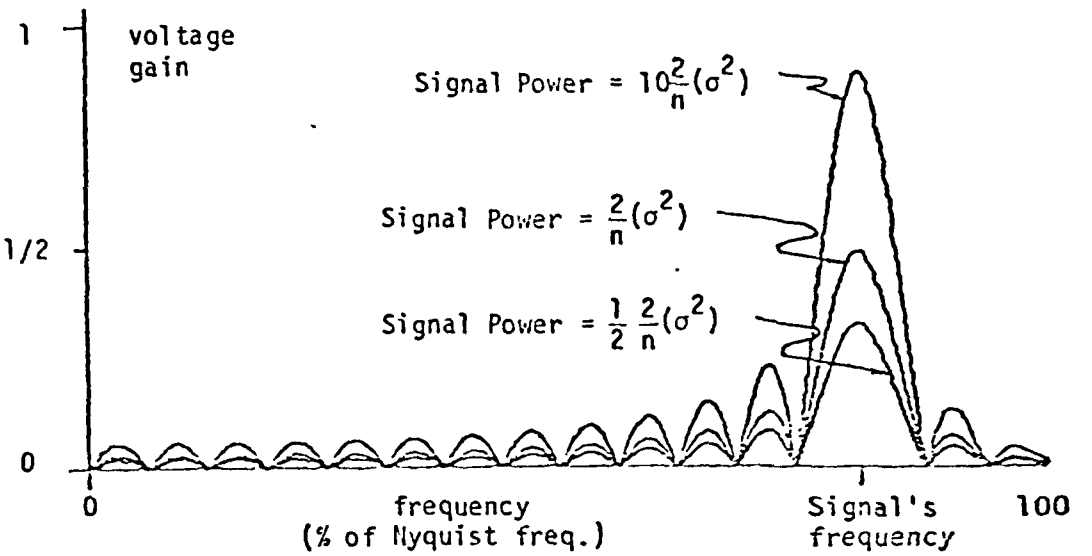

Figure 2-2. Transfer function of the ALE for three powers of an input signal.

By altering a parameter of the LLMS filter the designer can control the power of the "algorithmic noise." This permits the designer to control the effective SNR (effective SNR is the signal power divided by the sum of the actual input noise power and the "algorithmic noise" power), and thereby control the characteristics of the LALE. Thus the LALE is a high-power pass APS with a controllable characteristic.

The rest of this section is devoted to a more comprehensive and quantitative analysis of the LALE. This analysis is based on Treichler's [Tre] extensive analysis of the ALE with appropriate modifications to account for the changes between the LMS (Least Mean Square [Wid]) algorithm used in the ALE and the LLMS (Leaky LMS) algorithm used in the LALE. While the analysis is for the most part general, assumptions about the inputs are required to obtain insight into the solutions for the LALE weight vector. In particular, the LALE APS can be used to reject high-power, narrowband interference (where narrowband means a bandwidth significantly less than $\frac{1}{nT}$ where n is the number of LALE weights and T is the sampling interval). Therefore we assume that the input to the LALE consists of narrowband signals and white noise. Treichler [Tre] showed that under these conditions the input to the LALE can be modeled as one sinusoid per narrowband signal. Thus the input to the LALE is modeled as a number of sinusoids in white noise.

We start by defining various quantities in accordance with Figures 2-3 and 2-4:

$x(k)$ = adaptive filter input at time k

$X(k) = [x(k), x(k-1), \ldots, x(k-n+1)]^T$

= contents of tapped delay line at time k

$W(k)$ = vector of n filter weighting coefficients

$y(k) = X^T(k)W(k)$

= adaptive filter output

$e(k) = d(k)-y(k)$

= the "error" signal (drives the adaption)

$d(k) = x(k+\Delta)$

= desired (or reference) signal

Δ = decorrelation delay time

The LLMS algorithm for modifying the weight vector is:

$$W(k+1) = \nu W(k) + 2\mu e(k)X(k)$$

$$= [\nu I - 2\mu X(k)X^T(k)]W(k) + 2\mu d(k)X(k) \qquad (2\text{-}1)$$

where

ν = an arbitrary constant (leak factor)

$= 1 - 2\mu\gamma$

γ = power of "algorithmic noise"

μ = arbitrary constant which controls the rate of adaption and the stability of the algorithm

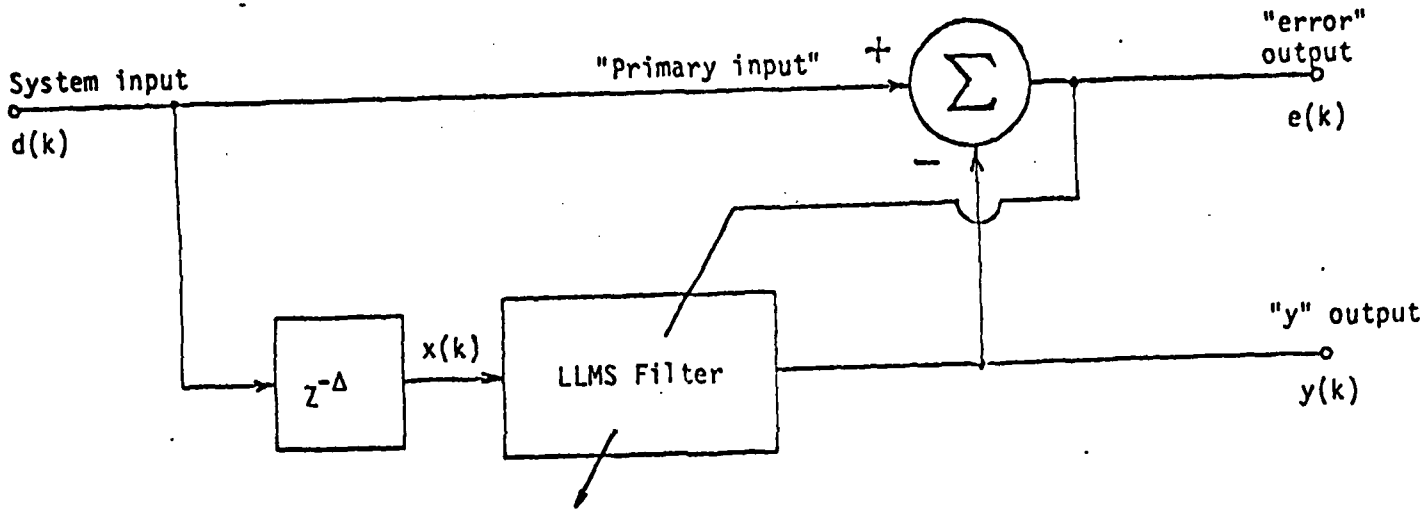

Figure 2-3. Leaky Adaptive Line Enhancer (LALE).

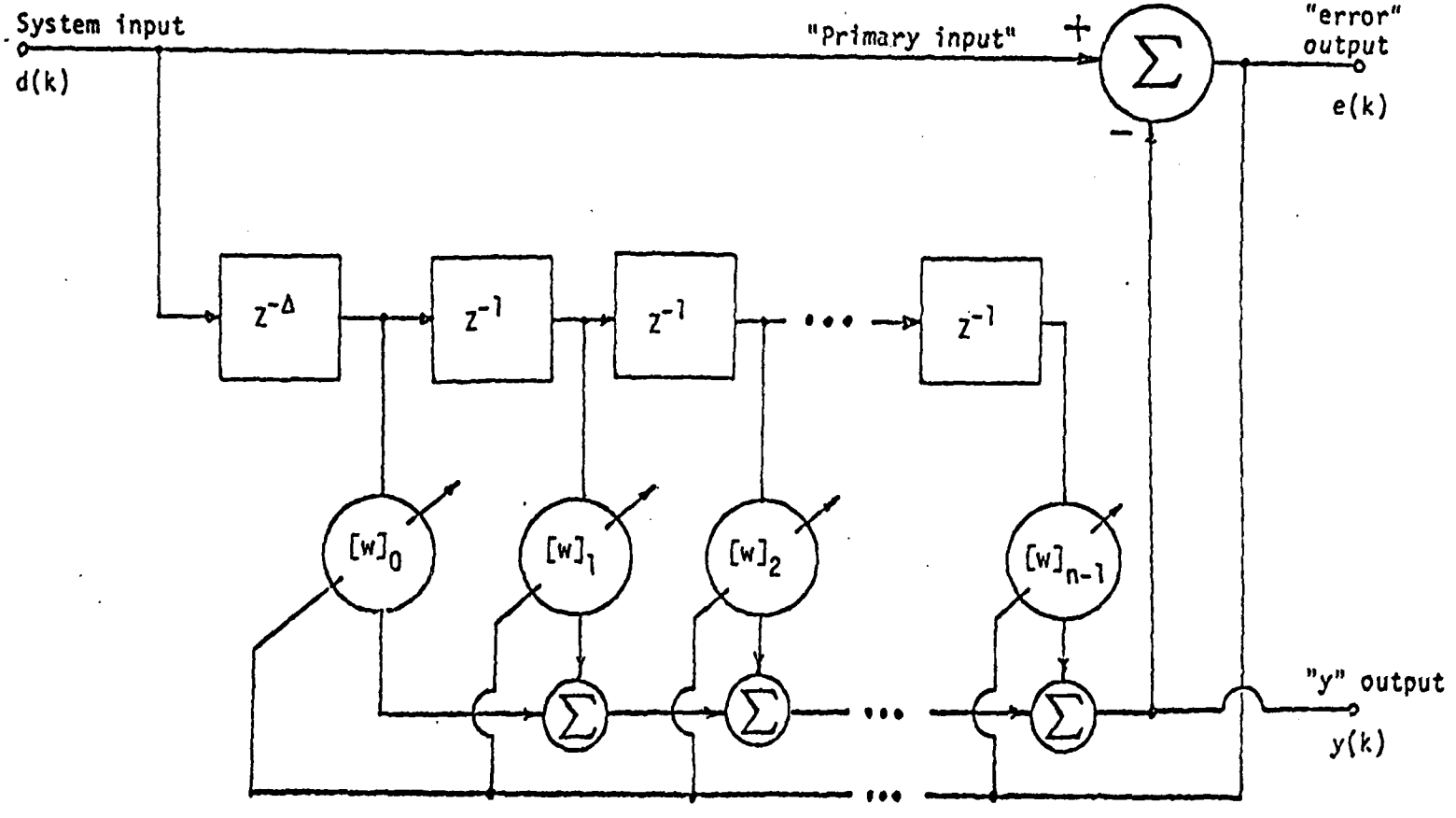

Figure 2-4. Diagram of the Leaky Adaptive Line Enhancer.

The average behavior of the LALE weight vector can be derived from equation 2-1 by taking the expected value of both sides of Eq. 2-1 and ignoring the covariance between $X(k)X^T(k)$ and $W(k)$ (this is an acceptable approximation if μ is small [Sen, Dan]):

$$E\{W(k+1)\} = [\nu I - 2\mu R(k)]\, E\{W(k)\} + 2\mu P(k) \qquad (2\text{-}2)$$

where

$$[R(k)]_{i,j} = E\{x(k-i)\, x(k-j)\}$$

$$= \text{input autocorrelation matrix.}$$

$$[P(k)]_i = E\{d(k)\, x(k-i)\}$$

$$= \text{desired-to-input cross correlation vector.}$$

If the input, $x(k)$, consists of one or more statistically independent, zero-mean and stationary components, then $R(k) = R_n + R_s$ and $P(k) = P_n + P_s$, where R_n is the autocorrelation matrix associated with the inputs whose correlation times are less than Δ and R_s is the autocorrelation matrix associated with the inputs whose correlation times are greater than Δ. If we assume that the incoherent components can be modeled as white noise with power σ^2, then $R_n = \sigma^2 I$. Finally, if $\Delta \geq 1$ then $P(k) = P_s$ since P_n is equal to zero (it is the autocorrelation of white noise for lags greater than Δ). Provided that all of these conditions hold, Eq. 2-2 can be written as:

$$E\{W(k+1)\} = [\nu I - 2\mu(\sigma^2 I + R_s)]\, E\{W(k)\} + 2\mu P_s \quad . \qquad (2\text{-}3)$$

Since R_s is the autocorrelation matrix of a real valued stochastic process, it is symmetric, Toeplitz, positive semi-definite and has a

full set of n orthonormal eigenvectors Q_0 through Q_{n-1} [Gra]. These eigenvectors can be used to form the modal matrix Q, where $Q = [Q_0, \ldots, Q_{n-1}]$. It is well known [Der] that the modal matrix has the following properties:

$$\bar{Q}^T R_s Q = \Lambda \tag{2-4a}$$

$$\bar{Q}^T Q = I \tag{2-4b}$$

where Λ is the diagonal matrix of the eigenvalues of R_s

$\bar{c}$ denotes the complex conjugate of c .

If a transformed weight vector is defined as $W'(k) = \bar{Q}^T W(k)$ and if both sides of Eq. 2-3 are premultiplied by $\bar{Q}^T$, then:

$$\begin{aligned} E\{W'(k)\} &= \bar{Q}^T E\{W(k)\} \\ &= \bar{Q}^T[\nu I - 2\mu(\sigma^2 I + R_s)]\, Q E\{W'(k)\} + 2\mu \bar{Q}^T P_s \quad . \end{aligned} \tag{2-5}$$

Equation 2-5 can be further simplified by using the relations given in Eq. 2-4 and by defining $C = \bar{Q}^T P_s$:

$$E\{W'(k)\} = [\nu I - 2\mu(\sigma^2 I + \Lambda)]\, E\{W'(k)\} + 2\mu C \quad . \tag{2-6}$$

The transition matrix of this recursion expression is diagonal since I and Λ are diagonal. Therefore the transformed weights, $W'(k)$, are uncoupled, so a separate scalar recursion expression can be written for each $[E\{W'(k)\}]_i$. The expression for the i^{th} uncoupled weight is:

$$[E\{W'(k)\}]_i = [\nu - 2\mu(\sigma^2 + \lambda_i)][E\{W'(k)\}]_i + 2\mu[C]_i \tag{2-7}$$

where λ_i is the i^{th} eigenvalue of R_s.

Incidentally, if $\nu = 1 - 2\mu\gamma$ is substituted into Eq. 2-6, the result is:

$$E\{W'(k)\} = [I - 2\mu([\sigma^2+\gamma]I + \Lambda)]\, E\{W'(k)\} + 2\mu C \quad . \qquad (2\text{-}8)$$

Equation 2-8 shows that γ affects the average weight vector in the same way as σ^2. Since the effects of γ are analagous to the effects of the white noise in the input, γ is called the "algorithmic noise" power. An LLMS filter with parameter γ will have the same average weight vector as a Wiener filter with noise of power γ added to its input signal. In a similar vein, the term "effective noise" power is used to mean $[\sigma^2 + \gamma]$, which is the sum of the actual input noise power and the "algorithmic noise" power.

Using the definition of γ, the scalar recursion for the uncoupled weights (Eq. 2-7) can be written as:

$$[E\{W'(k)\}]_i = [1 - 2\mu(\sigma^2+\gamma+\lambda_i)][E\{W'(k)\}]_i + 2\mu[C]_i \quad . \qquad (2\text{-}9)$$

If the adaption constant μ is chosen so that

$$0 < |1 - 2\mu(\sigma^2+\gamma+\lambda_i)| < 1 \qquad (2\text{-}10)$$

then each uncoupled recursion expression (Eq. 2-9) is stable, and $E\{W'(k)\}$ will converge to a value $E\{W'(\infty)\}$ which is independent of the starting conditions. The converged value is:

$$[E\{W'(\infty)\}]_i = \frac{[C]_i}{\sigma^2 + \gamma + \lambda_i} \quad i=0, 1, \ldots, n-1 \quad . \qquad (2\text{-}11)$$

Reversing the coordinate transformation yields:

$$E\{W(\infty)\} = \sum_{i=0}^{n-1} \frac{[C]_i}{\sigma^2 + \gamma + \lambda_i} Q_i \quad . \qquad (2\text{-}12)$$

Equation 2-12 defines the expected value of the converged weight vector. This definition is in terms of the eigenvectors of the input autocorrelation matrix, the power of the true input noise, the power of the equivalent noise and the power of the coherent signal component.

To determine the response of the LALE to particular inputs requires explicit solutions for the Q_i and $[C]_i$, and knowledge of σ^2 and γ. Since the input to the LALE can be modeled as multiple sinusoids in white noise, Treichler's results [Tre] are useful. Treichler showed that if the input consists of one or more sinusoids which meet the following criteria: 1) frequencies are between 20% and 80% of the Nyquist frequency (otherwise the two active eigenvalues degrade into a single active eigenvalue), and 2) all sinusoids are separated in frequency by at least $\frac{1}{nT}$ Hz (otherwise they interact instead of acting independently), then for each sinusoid of power p_i and frequency ω_i the following approximations hold:

$$Q_i \simeq \frac{1}{\sqrt{n}}\left[1 \; e^{j\omega_i T} \; \ldots \; e^{j(n-1)\omega_i T}\right]^T$$

$$Q_{n-i} \simeq \frac{1}{\sqrt{n}}\left[1 \; e^{-j\omega_i T} \; \ldots \; e^{-j(n-1)\omega_i T}\right]^T$$

$$[C]_i \simeq \frac{\sqrt{n}}{2} p_i \mathrm{Exp}(j\omega_i \Delta)$$

$$[C]_{n-i} \simeq \frac{\sqrt{n}}{2} p_i \mathrm{Exp}(j\omega_i \Delta)$$

$$\lambda_i \simeq \frac{n}{2} p_i \qquad (2\text{-}13)$$

These results can be substituted into Eq. 2-12 to determine the average weight vector of the LALE. Specifically, if the input to the LALE consists of a single sinusoid of power p and frequency ω in white noise of power σ^2, then

$$[E\{W(\infty)\}]_i = \frac{p}{\sigma^2 + \gamma + \frac{n}{2}p} \cos[(i+\Delta)\omega T] \qquad (2\text{-}14)$$

A filter with this weight vector has a bandpass characteristic with a maximum gain of $\frac{\frac{n}{2}p}{\sigma^2 + \gamma + \frac{n}{2}p}$ at the frequency of the sinusoid. Figure 2-5 shows the transfer function of the LALE for several input powers.

The operation of the LALE is more conveniently described as a gain characteristic (see Figure 2-6). The gain characteristic shows the converged gain of the adaptive system at the frequency of the input signal as a function of the signal's power. We see from Figure 2-4 that the LALE passes powerful signals and rejects weak signals and is thus a high-power pass APS. If a low-power pass APS is required, the "error" output of the LALE can be used instead of the "y" output. The "error" output gain characteristic is shown in Figure 2-7.

The threshold power of an APS hereby defined as the input signal power for which the gain of the APS is $\frac{1}{2}$. In the case of the LALE the threshold power is $\frac{2}{n}(\sigma^2+\gamma)$. Now the input noise power σ^2, is beyond the designer's control, but γ is controllable since it depends on μ and ν which are both parameters of the LLMS filter. Thus the threshold power of the LALE is easily controllable. However, the transition from high gain to low gain is gradual so the LALE is said to have a soft

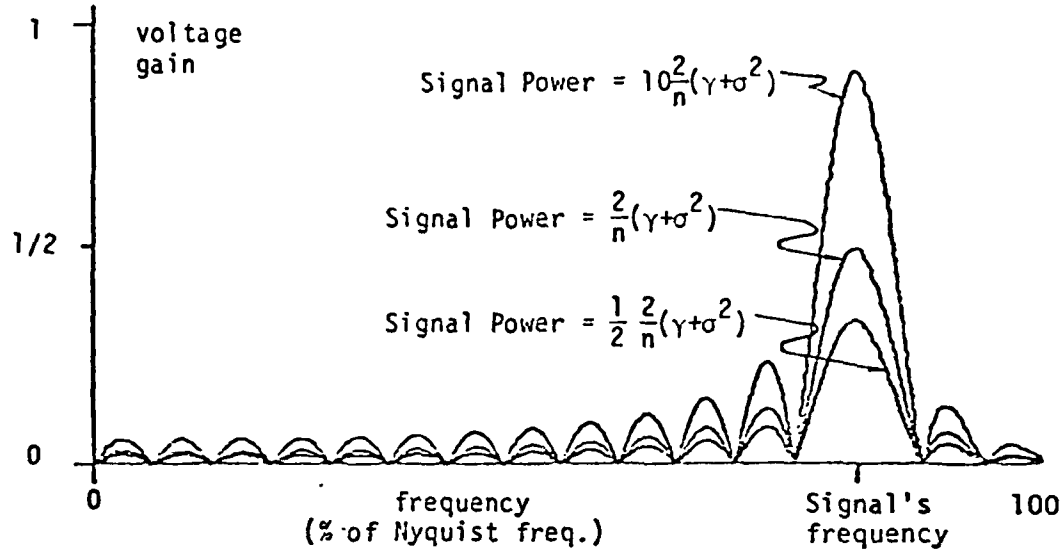

Figure 2-5. Transfer function of the LALE for three powers of an input signal.

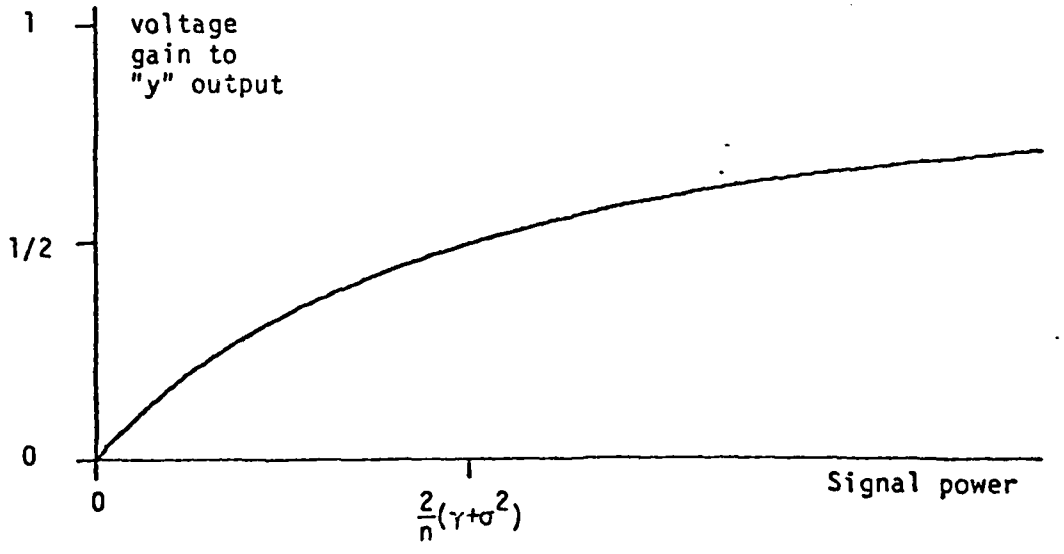

Figure 2-6. "y"-gain characteristic of LALE (High-power pass APS).

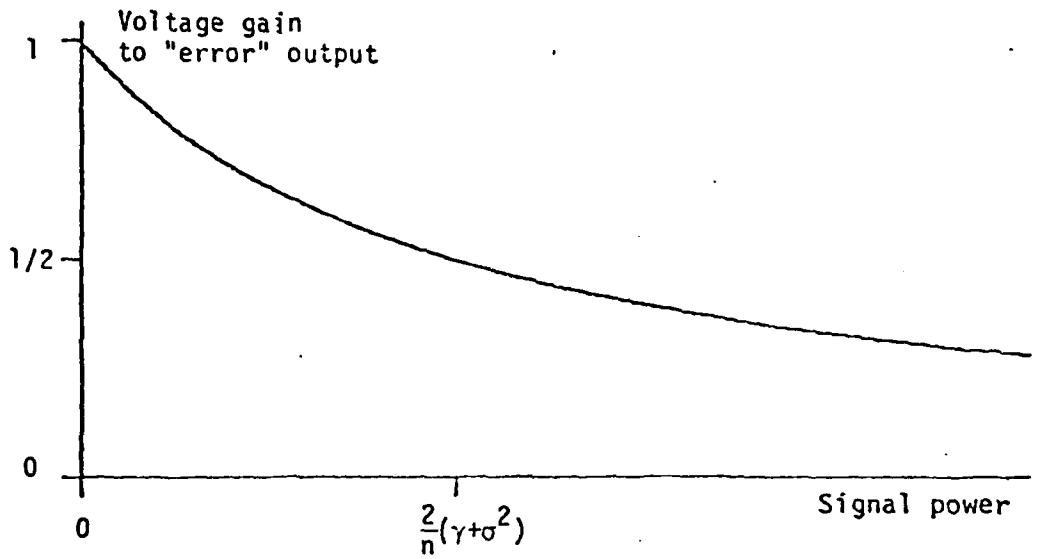

Figure 2-7. "error"-gain characteristic of LALE (Low-power pass APS).

threshold or broad transition region. Because of the soft threshold a LALE based APS cannot decisively discriminate between two signals with nearly the same power.

3 -- PRACTICAL SPECIFICATIONS FOR AN ADAPTIVE POWER SEPARATOR.

Figure 3-1 shows the gain characteristic of leaky adaptive line enhancer superimposed on the gain characteristic of an ideal APS. The gain characteristic of the ideal APS has unit gain for input power less than some threshold power and zero gain for input power greater than the same threshold. In contrast, the gain characteristic of the LALE (leaky adaptive line enhancer) has no sharp discontinuity and is never zero. Thus the LALE cannot reject signals, it can only attenuate them. However, the LALE has a gain of nearly one for low power inputs and a gain of nearly zero for high power inputs. Thus the LALE is similar to the ideal APS because it passes low power signals more strongly than it passes high power signals. The purpose of this chapter is to define specifications which quantify the difference between a practical APS (such as the LALE) and the ideal APS.

One approach to defining a practical gain specification is to allow a range of gains which are near to the ideal gain. For example, instead of requiring that the gain be one if the input power is less than some threshold, require that the gain be between $1-\delta_1$ and $1+\delta_1$ if the input power is less than the threshold. Figure 3-2 shows a gain tolerance scheme which is based on this idea. A mathematical description of the allowable gains is:

$$\begin{aligned} 1 - \delta_1 \leq 1 + \delta_1 \quad & \text{for } p \leq p_1 \\ g \leq 1 + \delta_1 \quad & \text{for } p_1 < p < p_2 \\ g \leq \delta_2 \quad & \text{for } p_2 \leq p \end{aligned} \tag{3-1}$$

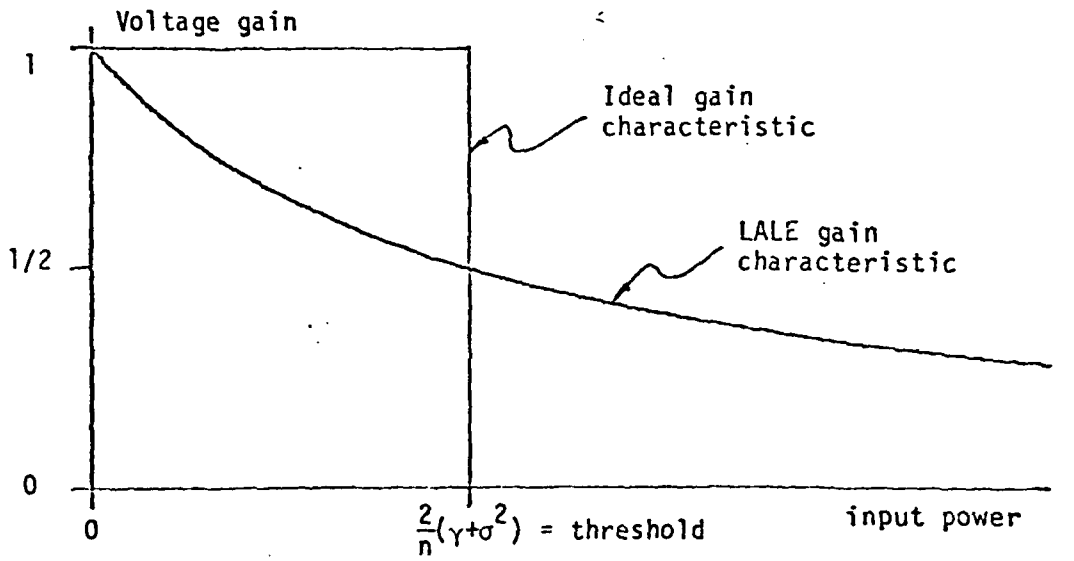

Figure 3-1. Comparison of ideal gain characteristic with LALE gain characteristic.

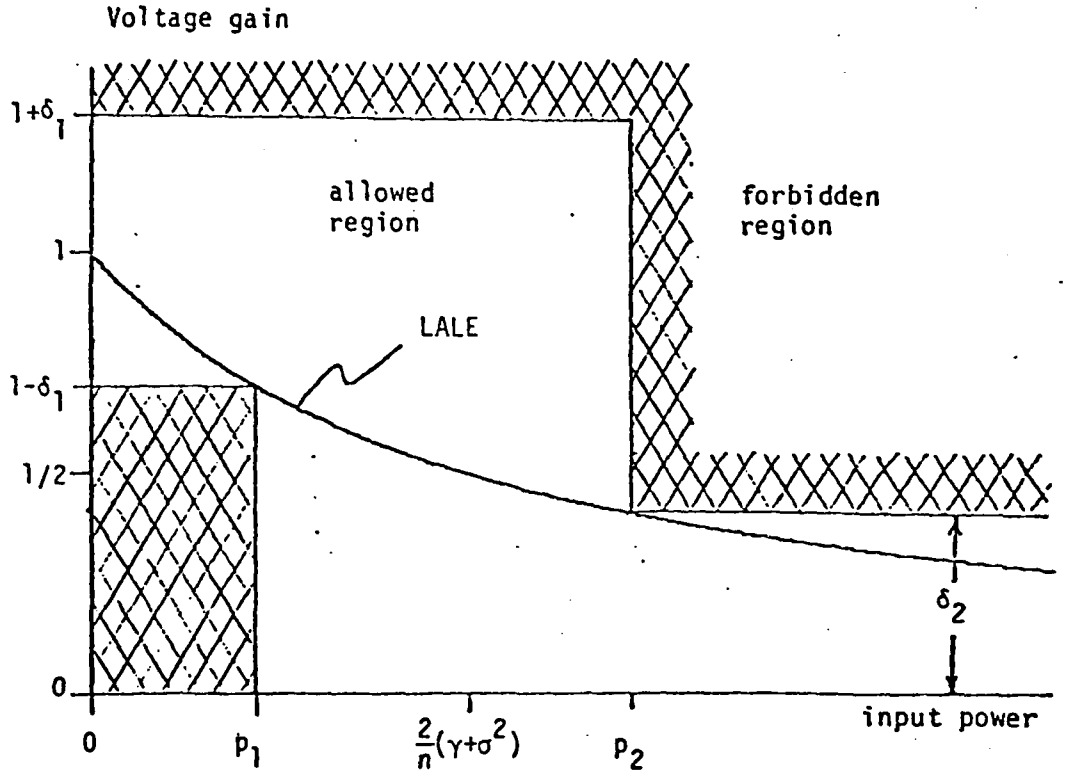

Figure 3-2. Tolerance scheme one for the gain of an APS.

We will refer to this tolerance scheme as tolerance scheme one (TS1). If $\delta_1 = 0$, $\delta_2 = 0$ and $p_1 = p_2$, then TS1 describes the ideal APS gain characteristic.

An alternative is to consider the APS entirely from the power domain. Figure 3-3 shows a power-out vs. power-in curve for an ideal APS. The power-out vs. power-in formulation suggests bounding of the output power rather than the filter gain.

A practical power-out vs. power-in specification can be derived by permitting tolerances about the ideal curve. Figure 3-4 shows a practical power-out vs. power-in tolerance scheme. This tolerance scheme will be called tolerance scheme two (TS2). TS1 and TS2 differ because TS2 controls the response to high power inputs more tightly than TS1. If TS1 is converted into a power-out vs. power-in specification (see Figure 3-5), it is clear that TS1 permits high power inputs to have high output power. TS2, on the other hand, guarantees that signals with input power greater than p_2 will have less output power than signals with an input power between p_3 and p_1.

A mathematical description of TS2 is:

$$\begin{aligned} 1 - \rho_1 \le g \le 1 + \rho_1 \quad &\text{for} \quad p \le p_1 \\ g \le 1 + \rho_1 \quad &\text{for} \quad p_1 < p \le p_2 \\ g \le \rho_2 \sqrt{\frac{p_2}{p}} \quad &\text{for} \quad p_2 < p \end{aligned} \tag{3-2}$$

If $\rho_1 = 0$, $\rho_2 = 0$ and $p_1 = p_2$, then TS2 describes the ideal APS characteristic. Also, if $\delta_1 = \rho_1$ and $\delta_2 = \rho_2$ then TS2 is equivalent

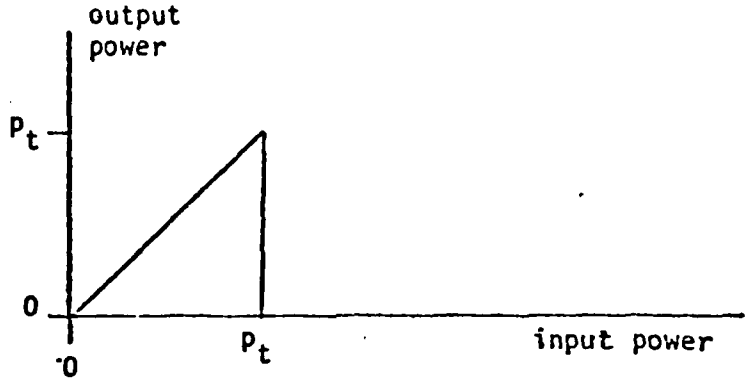

Figure 3-3. Power-out vs. Power-in characteristic of the ideal APS.

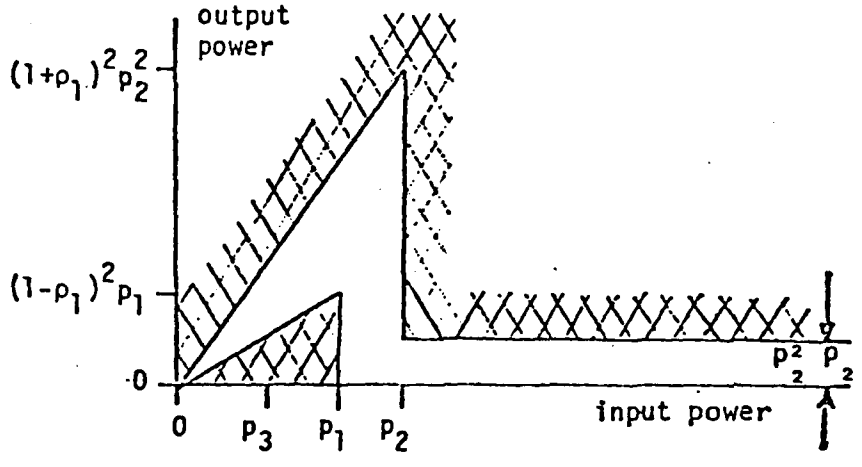

Figure 3-4. Tolerance scheme two for power-out vs. power-in.

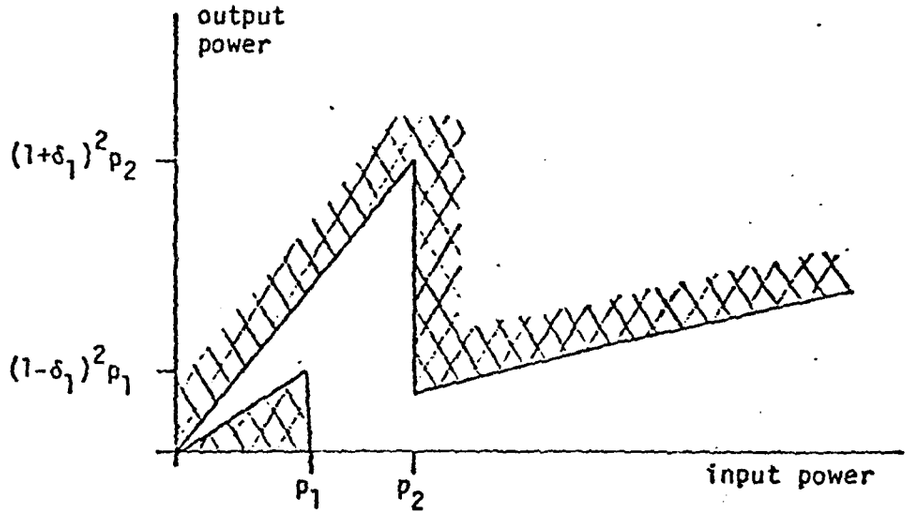

Figure 3-5. Tolerance scheme one as power-out vs. power-in.

to TS1 for input power less than p_2 (but TS2 is more stringent than TS1 for input powers greater than p_2).

The two tolerance schemes presented in this chapter can be used to describe a practical APS. By using these schemes to characterize different power separators we will be able to identify the strengths and weaknesses of the different power separators with the goal of developing improved practical power separators.

4 -- APS2: A DFT BASED ADAPTIVE POWER SEPARATOR

A straightforward approach to adaptive power separation is to evaluate the power spectrum of the input signal and then to use the spectrum to design a filter which has zero gain at frequencies where the power spectral density exceeds a chosen threshold and unit gain elsewhere. When the input signal is applied to the resulting filter (see Figure 4-1), the output will contain only the weak input components which do not spectrally overlap the strong input components. This is a general structure for an APS.

The power spectrum of a signal can be evaluated by the digital Fourier transform (DFT). This technique, which is called the Welch-periodogram method [Opp], creates a power spectral estimate by averaging the squared magnitude of the DFT of the input data. An associated filtering technique multiplies the outputs of the DFT (which correspond to spectral components) by zero or one and then takes an inverse DFT to obtain the output time series. Figure 4-2 shows the block diagram of an adaptive power separator which is based on these ideas. This APS is called the APS2.

The input signal is applied to the APS2 as a series of data samples, and the APS2 computes the DFT of the last n data samples:

$$[G(k)]_m = \sum_{i=0}^{n-1} x(k-i)\ \mathrm{Exp}(2\pi\frac{im}{n}) \qquad m = 0, 1, \ldots, n-1 \qquad (4\text{-}1)$$

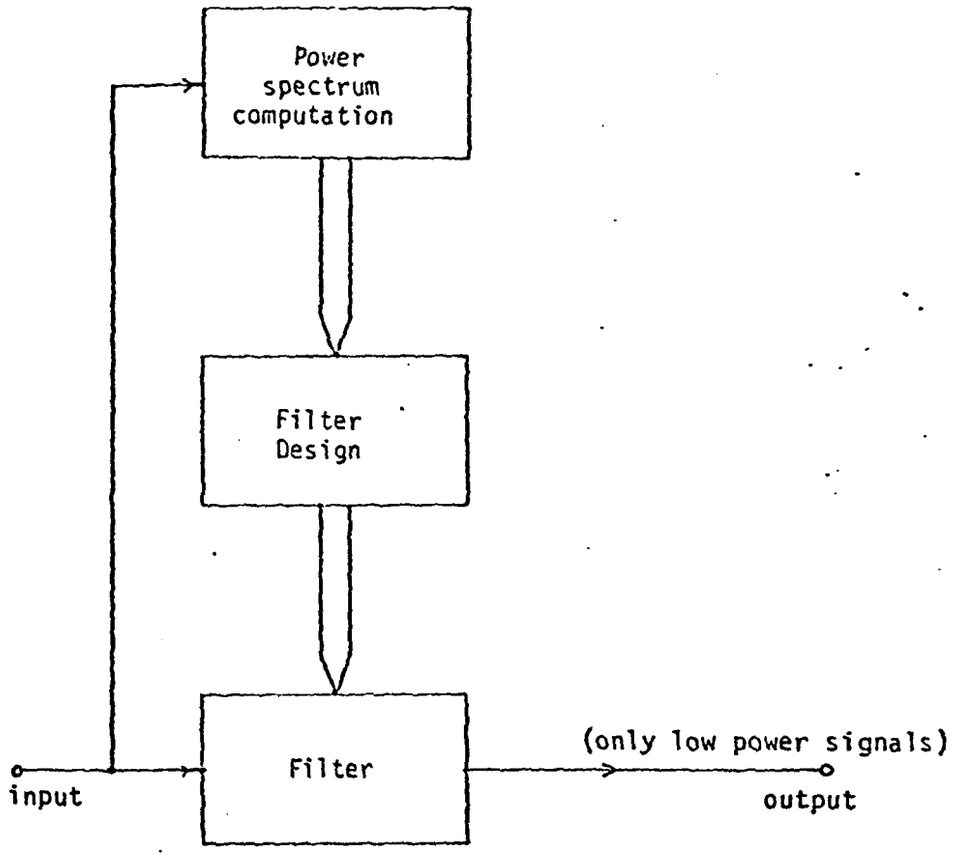

Figure 4-1. General structure of the APS.

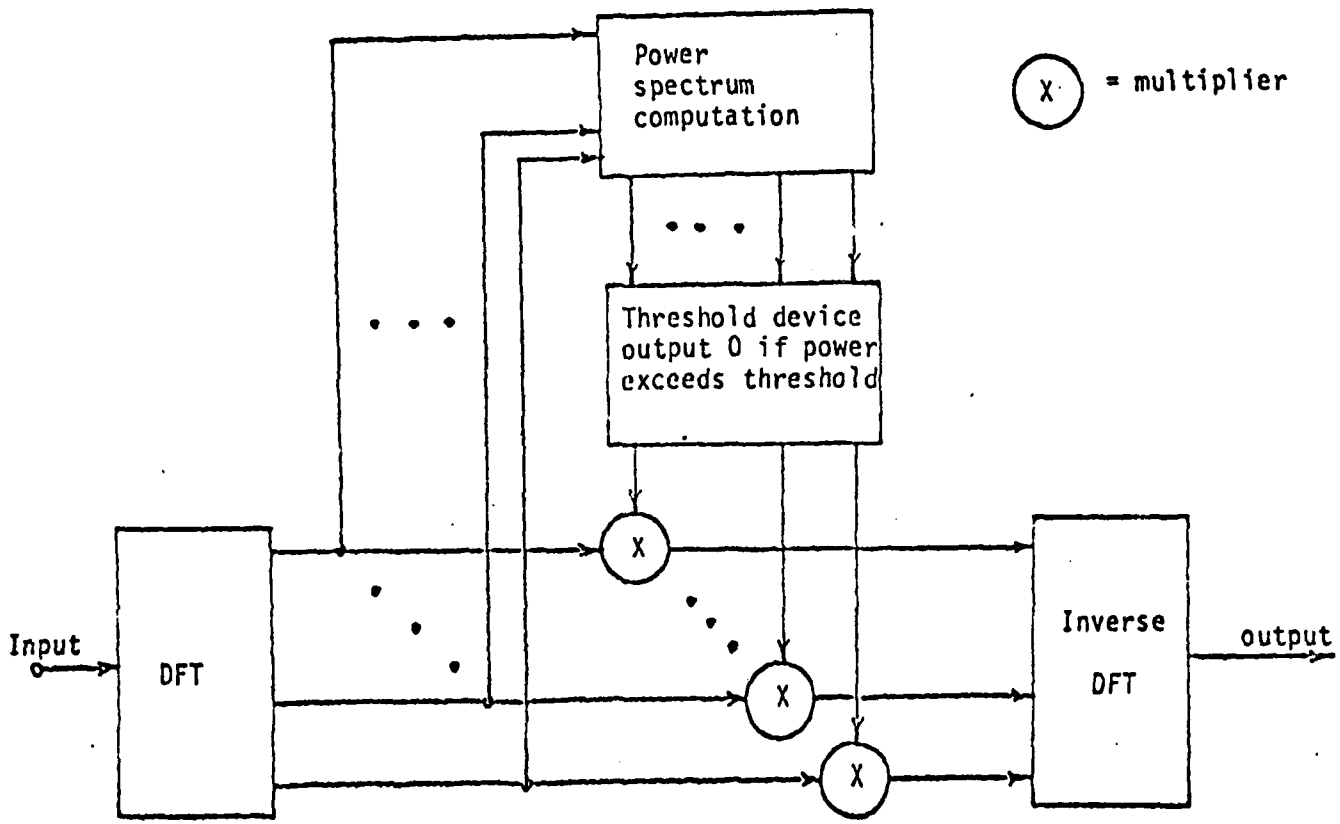

Figure 4-2. Block diagram of DFT/threshold based power separator (APS2).

where

$G(k)$ = vector of DFT values at time k

m = spectral bin number

= n f T

T = sampling period

f = frequency .

Each DFT value $[G(k)]_m$ is the output of a finite impulse response (FIR) filter with transfer function:

$$H(Z,m) = \sum_{i=0}^{n-1} \text{Exp}(j2\pi\frac{im}{n})Z^{-i}$$

$$= \frac{1 - Z^{-n}}{1 - \text{Exp}(j2\pi\frac{m}{n})Z^{-1}} \qquad m = 0, 1, \ldots, n-1 \quad . \qquad (4\text{-}2)$$

Thus the DFT of the input sequence can be computed by a bank of n FIR filters with transfer functions given by Eq. 4-2 [Pap]. Figure 4-3 shows an implementation of the DFT which is based on Eq. 4-2. While a more efficient way to compute the DFT is by one of the fast algorithms such as the fast fourier transform, great insight can be obtained by viewing the DFT as a bank of bandpass filters. Thus we will analyze the APS2 as if it were made from a bank of bandpass filters.

The APS2 filtering technique multiplies the outputs of the DFT by zero or one and then inverse DFT's the resulting filtered signal to obtain a time series. If the DFT is modeled as a bank of bandpass filters, as shown in Figure 4-3, then the APS2 filtering technique can be modeled as multiplying the outputs of the bandpass filters by zero or

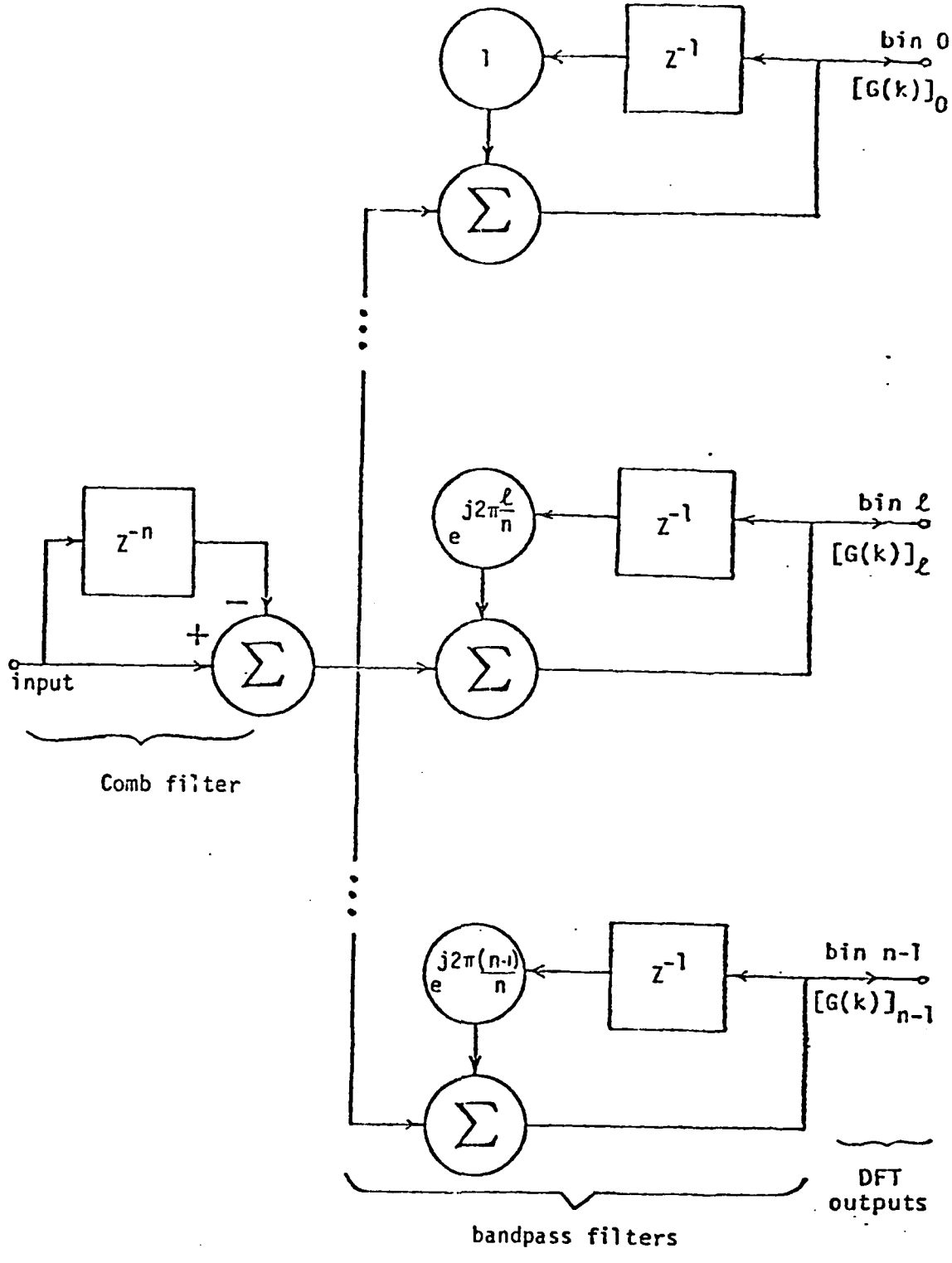

Figure 4-3. Filter equivalent of the DFT.

one and then summing the weighted outputs. This is shown in Figure 4-4 where the threshold devices have an output of 1 if the input power at a given spectral bin is less than the threshold power and 0 if the input power is greater than the threshold power. We will use this model to analyze the two phases of the APS2's operation: spectral estimation and filter design.

Recall that the APS2 uses the average squared magnitude of the DFT as an estimate of the power spectrum. Also, the m^{th} DFT output is the output of a filter with transfer function given by Eq. 4-2. This filter has n zeros, equally spaced on the unit circle at frequencies which are integer multiples of $\frac{1}{nT}$, and a pole at $Exp(j2\pi\frac{m}{n})$ which cancels the zero at frequency $\frac{m}{nT}$. The transfer function of such a filter is shown in Figure 4-5 (m = 4, n = 16 for this filter). If the input consists of sinusoids at integer bin numbers* (i.e. their frequencies are integer multiples of $\frac{1}{nT}$), then the output power of the m^{th} filter will be proportional to the power of the sinusoid at frequency $\frac{m}{nT}$ because the zeros of the comb filter will cancel all of the sinusoids except the sinusoid at frequency $\frac{m}{nT}$ where there is a pole zero cancellation. Thus, provided that the input consists of on-bin sinusoids, the power in the DFT output is the true power spectrum. However, if the input has off-bin sinusoids, then the APS2 will not estimate the true power spectrum. Consider the case of a sinusoid at frequency f_u (see Figure 4-5). This sinusoid is in a sidelobe of every DFT filter and so will pass through

*In digital filtering, signal frequencies are often expressed in terms of spectral bin numbers where:

bin number = f x T x number of points in the DFT .

For convenience, signals with integer bin numbers are called on-bin signals and those with non-integer bin numbers are called off-bin signals.

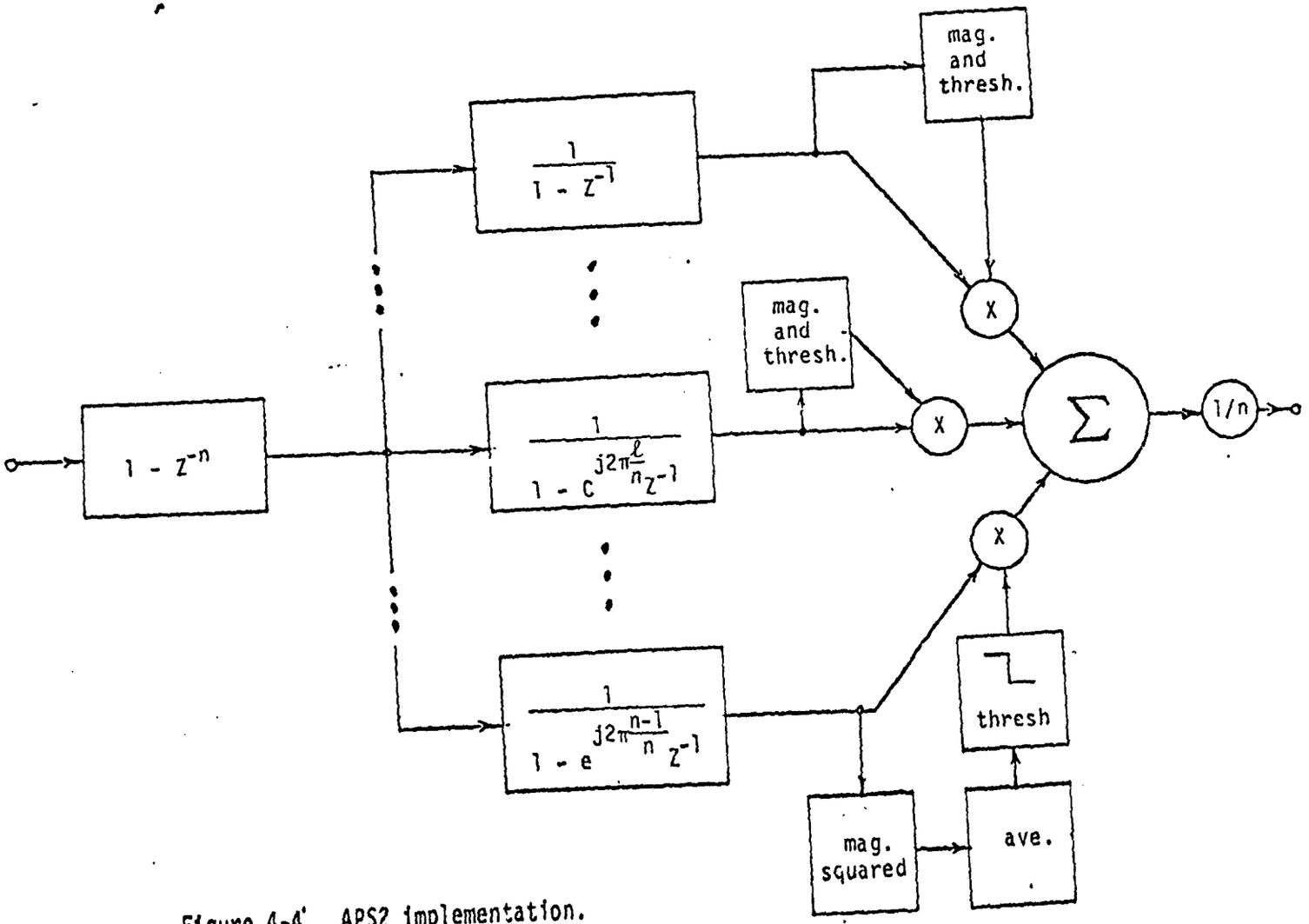

Figure 4-4. APS2 implementation.

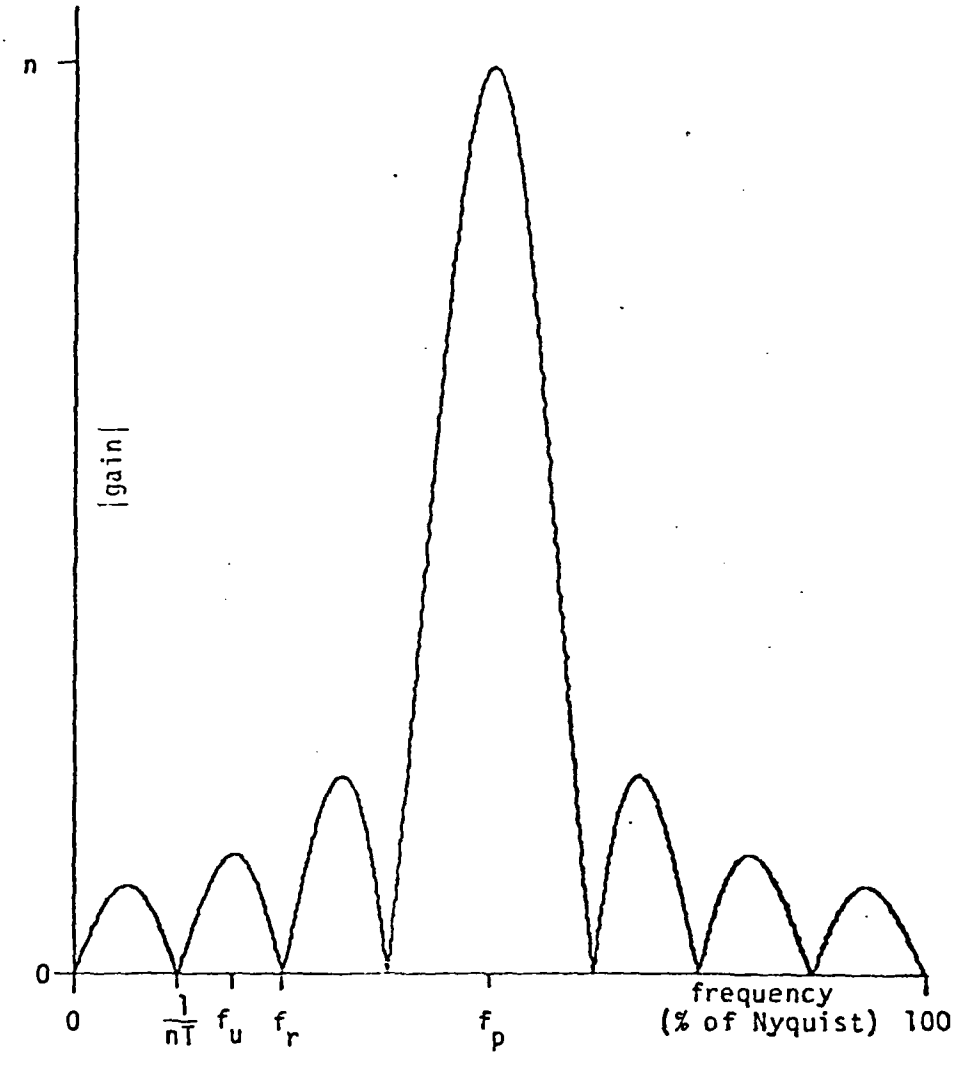

Figure 4-5. Typical bandpass filter used in the DFT.

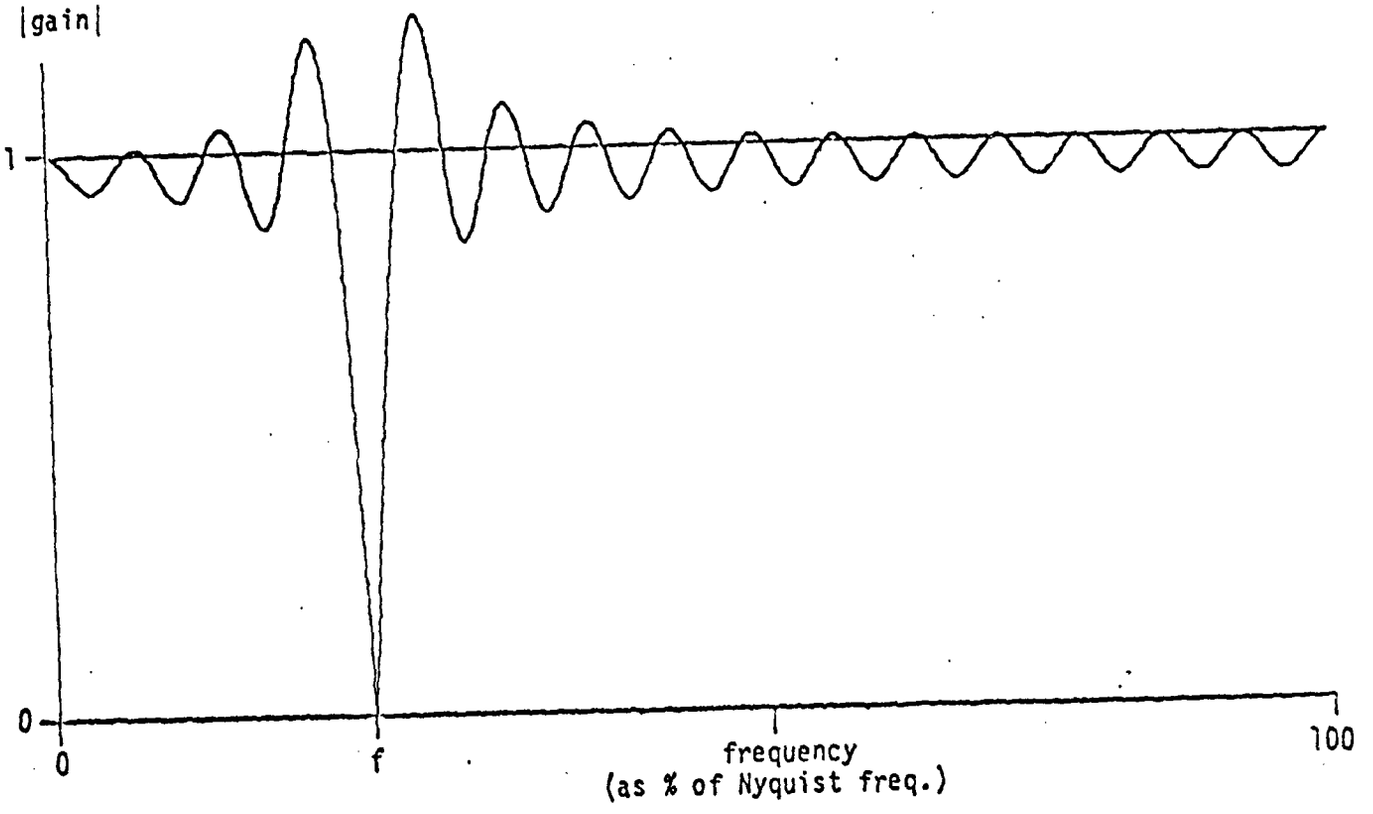

Figure 4-6. Transfer function of the APS2 when the output of one DFT bin is blocked.

In summary, the APS2 functions ideally for any number of sinusoidal inputs provided that their frequencies all correspond to integer bin numbers. Sinusoidal inputs which are not on-bin can cause undesirable effects. First, the DFT based power spectrum estimator will exhibit leakage. This causes the power spectral estimate to show more power than is really present at some frequencies, so the APS2 may block weak signals because the power spectral estimate falsely indicates that they are strong. Similarly, the power spectral estimate may show less power at some frequencies than is actually present. Second, the filter design used by the APS2 to reject powerful signals unfortunately creates relatively large gains in portions of the rejection region. Consequently the APS2 will only partially reject powerful off-bin signals.

Simulation of the APS2

An APS2 based on a 32 point DFT was simulated. The first test input to the APS2 was the sum of two sinusoids. Sinusoid one was at 25% of the Nyquist frequency (bin number = 4) and sinusoid two was at 56.25% of the Nyquist frequency (bin number = 9). During the simulation the power of the first sinusoid was varied from 0.1 to 100 and the power of the second sinusoid was held constant at 0.1. The threshold power was 1.

Figures 4-7A and B show the gain characteristic of the APS2 at the frequency of each sinusoid. Since both of the signals were on-bin the DFT did not suffer from leakage and the APS2 functioned perfectly. Figure 4-7A shows that the gain at the frequency of sinusoid one was unity when the power was less than the threshold and zero when the power exceeded the threshold. Figure 4-7B shows that the gain at the frequency of the sinusoid two remained unity for all powers of sinusoid one.

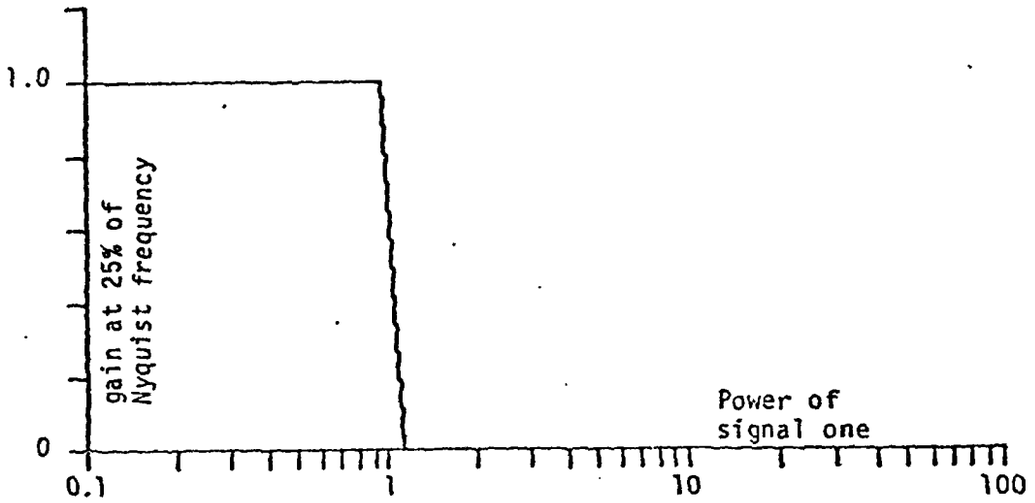

Figure 4-7A. Gain characteristic at the frequency of sinusoid one.

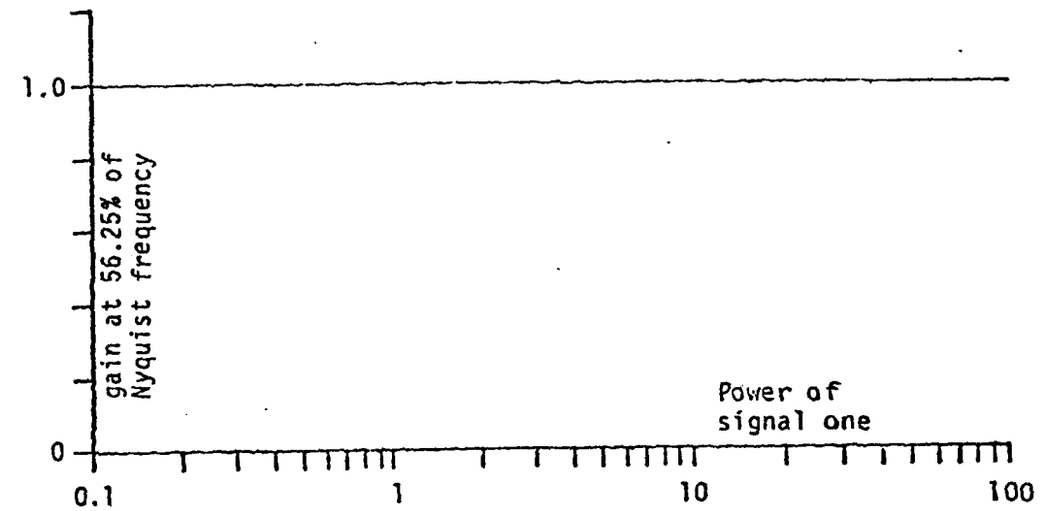

Figure 4-7B. Gain characteristic of the APS2.

Figures 4-8 shows the transfer function of the APS2 for several powers of signal one. From this figure we see that the APS2 cancels the powerful signal by creating a notch at its frequency.

Figures 4-9A and B show the gain of the APS2 for the another test input. Again the test input was the sum of two sinusoids. Sinusoid one was at 28.125% of the Nyquist frequency (bin number - 4.5) and sinusoid two was at 56.25% of the Nyquist frequency (bin number - 9). During the simulation the power of sinusoid one was varied from 0.1 to 100 and the power of sinusoid two was held constant at 0.1. The threshold power was 1. The major weaknesses of the APS2 are apparent from this figure: (A) Because the gain of a DFT bandpass filter is not unity for off-bin signals, the gain at the frequency of sinusoid one remained unity when the power of the sinusoid was between 1 and 2, even though the threshold power was 1. (B) Because of poor filter design, when the gain at sinusoid one's frequency did change, it first increased and then slowly dropped towards zero, rather than immediately becoming zero. (The only reason that the gain drops as the signal power increases is that leakage causes more and more of the poles to be removed.) (C) The gain at the frequency of the second sinusoid dropped to zero even though the power at that frequency was always less than the threshold power. This is the result of leakage from sinusoid one.

The effects of leakage can also be seen in Figure 4-10 which shows the transfer function of the APS2 for several powers of signal one. Figure 4-10 show that the APS2 is an allpass filter when the power of signal one is 0.1. When the power of signal one is 2.5, the APS2 develops a notch near the frequency of signal one. However, sidelobe

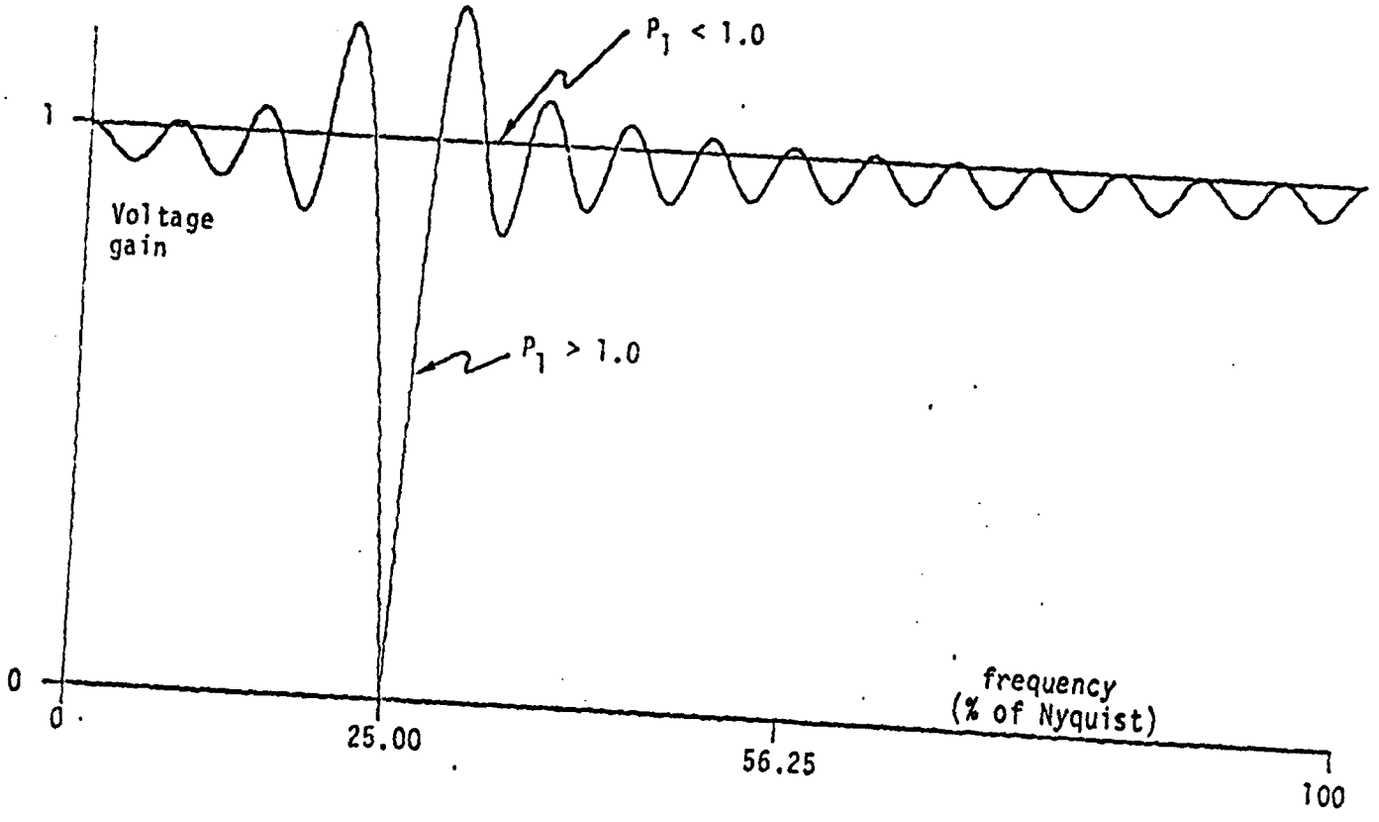

Figure 4-8. Transfer function of APS2 for various input powers.

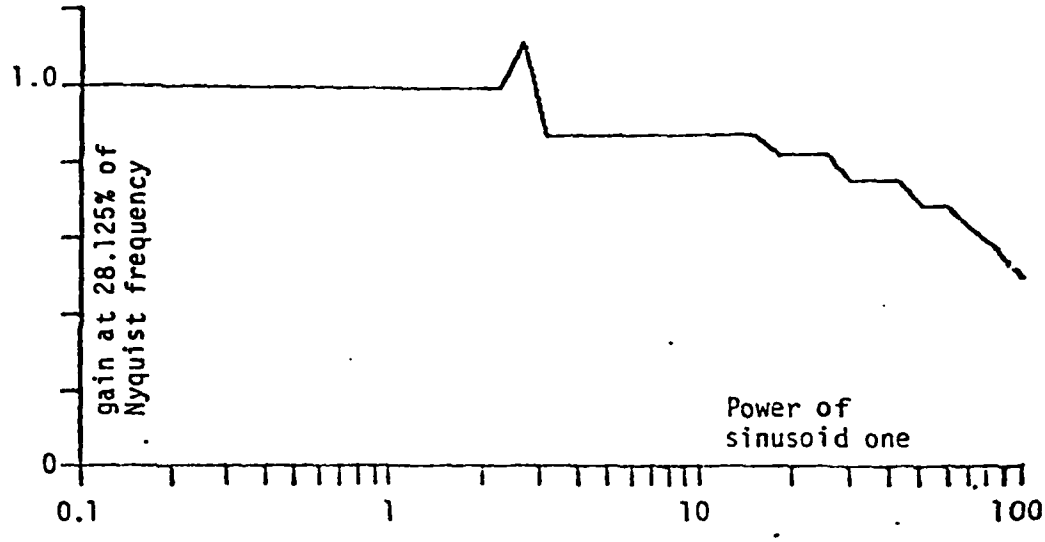

Figure 4-9A. Gain characteristic at frequency of sinusoid one.

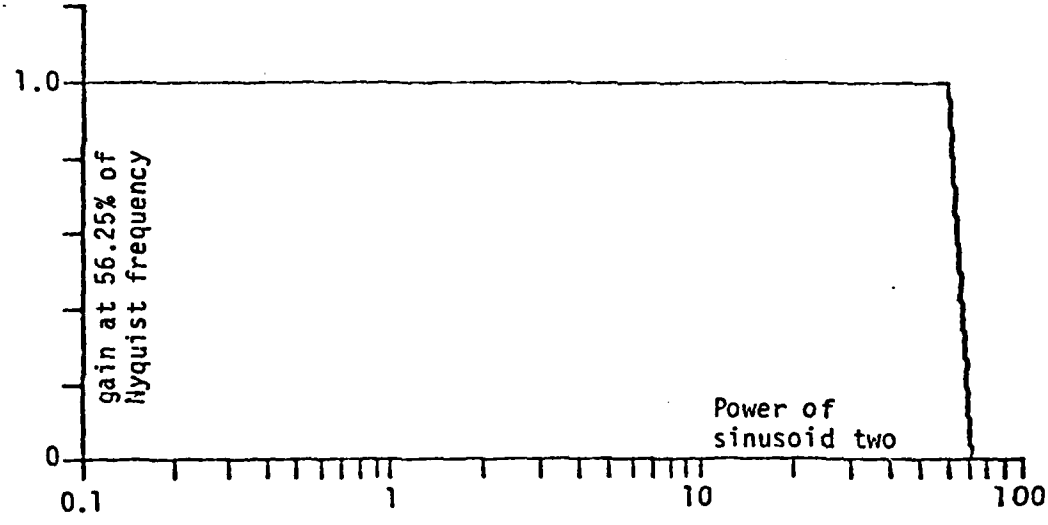

Figure 4-9B. Gain characteristics of the APS2.

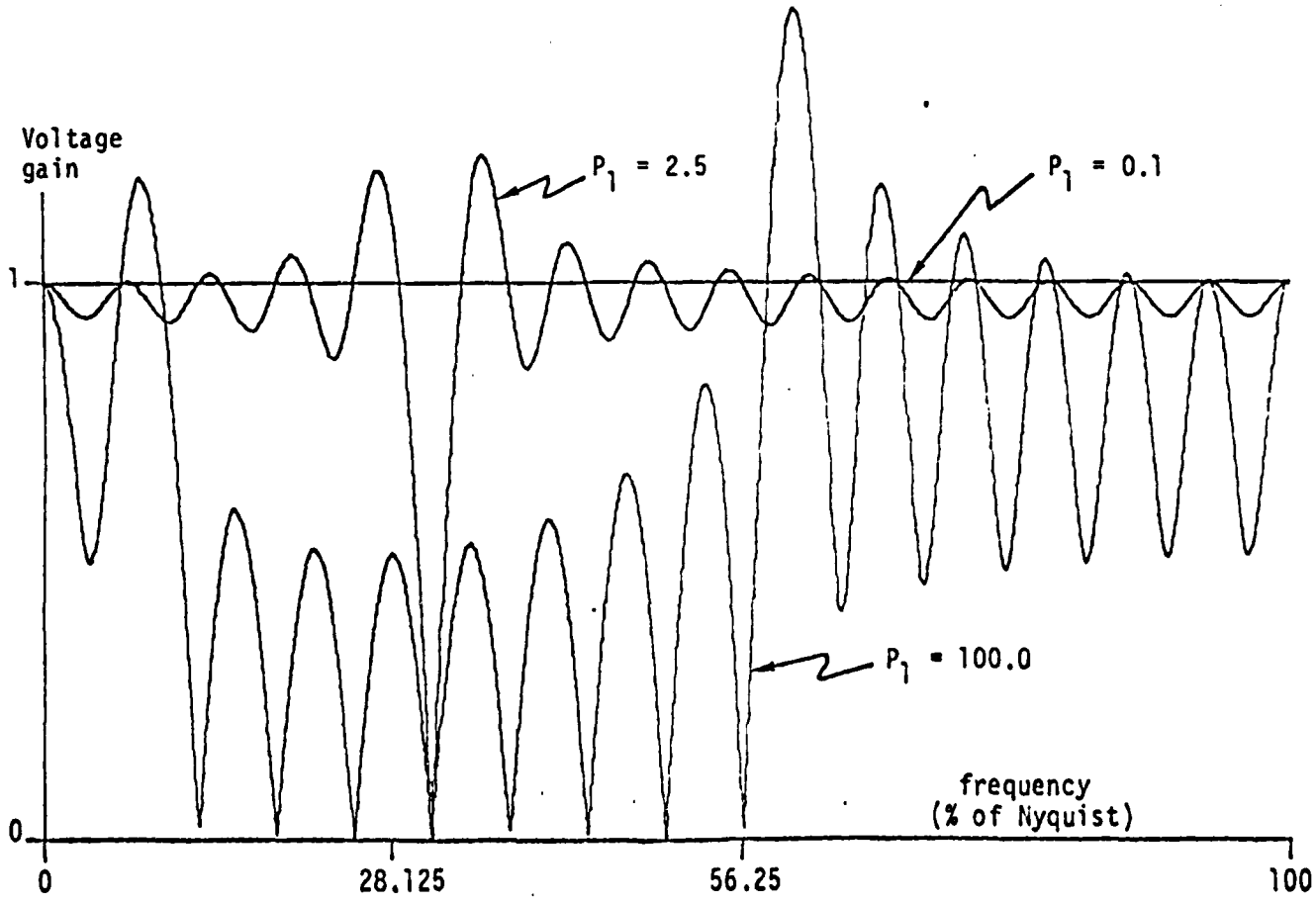

Figure 4-10. Transfer function of APS2 for various input powers.

effects cause the gain at the frequency of signal one to be greater than one. When the power of signal one is 100 the APS2 notches a wide range of frequencies, including the frequency of signal two. This wide notch is caused by leakage from signal one.

5 -- APS3: AN LALE-DFT BASED ADAPTIVE POWER SEPARATOR

Introduction

This chapter proposes and examines an APS which uses the LALE and a DFT for spectral analysis, and a DFT based filter design technique called frequency sampling [Rab] to design bandstop filters. This adaptive power separator will be called the APS3 to distinguish it from the purely DFT based APS2 that was analyzed in Chapter 4. The reason for using a LALE and a DFT for spectral estimation is that the LALE reduces leakage effects and is not sensitive to the frequency of the signals (i.e. the signals do not have to be 'on-bin'). The advantage of the frequency sampling filter design technique is that it is simple, fast, and by increasing the filter length can create arbitrarily good filters. Thus the APS3 improves on the two weaknesses of the APS2: poor power spectral estimation and poor filter design.

The APS3 is based on the same simple idea as the APS2. Estimate the power spectrum of the input and then design a filter that passes the frequencies which have low power signals and rejects the frequencies which have high power signals. Figure 5-1 shows a block diagram of the APS3. The theory of operation is: 1) the LALE forms a filter with a gain that is related to the signal-to-noise ratio (SNR). The larger the signal power the larger the SNR and consequently the larger the filter gain. 2) The DFT of the weight vector of the LALE measures the gain of the LALE, which is a modified power spectral estimate. 3) The

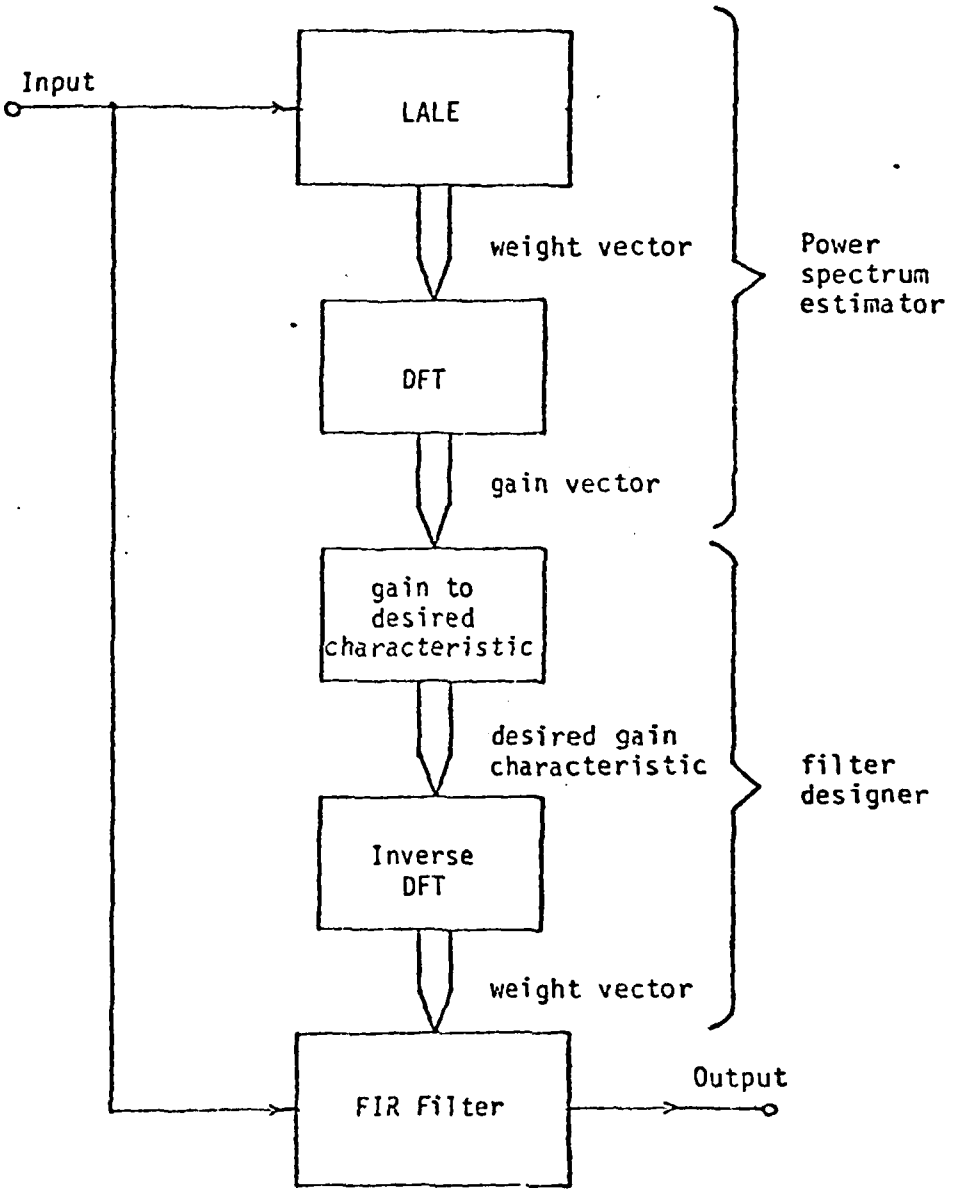

Figure 5-1. Block Diagram of the APS3.

modified power spectral estimate is used to create a desired filter characteristic, which is then realized as a practical filter. 4) The resulting filter is used to filter the input, and by design the output of this filter will contain only the weak signals.

The next few sections are devoted to analyzing the modified power spectral estimate that is derived from the LALE. We show that this modified power spectral estimate has less leakage than a DFT based power spectral estimate. Thus the LALE power spectral estimate can detect small signals that are near powerful off-bin signals better than a DFT power spectral estimate. (Note: the use of windows with the DFT will reduce the effects of leakage, but very powerful off-bin signals will still swamp small signals.) Thus the LALE power spectral estimate can be used to obtain arbitrarily good switching characteristics, so the APS3 can have a lower power threshold p_1 that is arbitrarily close to the upper power threshold p_2 (see the descriptions of tolerance scheme one and two which are given by Eq. 3-1 and 3-2).

The last sections of this chapter analyze the filter design technique used in the APS3. We prove that the filter design technique used in the APS3 can design arbitrarily good (in an integral squared error sense) filters. Thus we show that the APS3 fits gain tolerance scheme one (Eq. 3-1).

LALE-DFT Based Power Spectral Estimate

In this section we will use the analysis of the mean LALE weight vector, which was presented in Chapter 2, to show that the DFT of the LALE weight vector is a modified power spectral estimate. The performance of the LALE-DFT power spectral estimate will be analyzed and

compared to the conventional Welch periodogram power spectral estimate. Again, the analysis in this section follows Treichler's [Tre] analysis with only small modifications to account for the use of a LALE as opposed to an ALE.

The discrete power spectrum of a signal x(k) may be found by taking the DFT of n samples of the autocorrelation function of x(k). If the autocorrelation of x(k) is r(t), then samples of the autocorrelation function can be grouped to form the vector:

$$\Gamma = [r(\Delta),\ r(\Delta+1),\ \ldots,\ r(\Delta+n-1)]^T \quad .$$

The discrete power spectrum, S, corresponding to this autocorrelation vector is:

$$S = F \cdot \Gamma \tag{5-1}$$

where F is an m by n matrix formed from the basis vectors of the DFT. The elements of the F matrix are:

$$[F]_{i,\ell} = \mathrm{Exp}\{j2\pi(\frac{i\ell}{m} + \phi)\} \tag{5-2}$$

where the starting phase, ϕ, is arbitrarily set to correspond to the decorrelation delay Δ.

The ALE spectral estimate, which is derived from the DFT of the expected LALE weight vector, can be written as:

$$\begin{aligned} \hat{S}_{LALE} &= F \cdot E\{W\} \\ &= F \sum_{i=0}^{n-1} \frac{[C]_i}{\sigma^2 + \gamma + \lambda_i} Q_i \quad . \end{aligned} \tag{5-3}$$

If the input can be modeled as K sinusoids with powers $p_1, \ldots, p_K$ and frequencies $\omega_1, \ldots, \omega_K$, and if all of the sinusoids are separated by at least $\frac{1}{nT}$ Hz and all of the frequencies are between 20% and 80% of the Nyquist frequency, then the autocorrelation matrix has eigenvectors of a simple form (Eq. 2-13). Under these conditions Eq. 5-3 becomes:

$$\hat{S}_{LALE} = F \sum_{i=1}^{K} \frac{1}{\sigma^2 + \gamma + \frac{n}{2} p_i} \Gamma_i \qquad (5\text{-}4)$$

where Γ_i is the autocorrelation vector associated with the i^{th} sinusoid.

Substituting the definition of the discrete power spectrum (Eq. 5-8) into Eq. 5-4 yields:

$$\hat{S}_{LALE} = \sum_{i=1}^{K} \frac{1}{\sigma^2 + \gamma + \frac{n}{2} p_i} S_i \qquad (5\text{-}5)$$

where S_i is the power spectrum associated with the i^{th} sinusoid.

Thus Eq. 5-5 shows that the LALE-DFT power spectral estimate contains the true power spectrum, but with a considerable (but desirable) distortion of the estimated power. If we define a shape vector for the power spectrum of a sinusoid as:

$$U = \frac{2}{n} F\Gamma$$

$$= \frac{1}{\frac{2}{n} p} S \qquad (5\text{-}6)$$

where Γ is the autocorrelation vector of a sinusoid

p is the power of the sinusoid .

Then for a sinusoid at frequency ω,

$$|[U]_i| = \frac{\mathrm{Sin}\{\frac{n}{2}(2\pi\frac{i}{n} - \omega T)\}}{n\mathrm{Sin}\{\frac{1}{2}(2\pi\frac{i}{n} - \omega T)\}} + \frac{\mathrm{Sin}\{\frac{n}{2}(2\pi\frac{i}{2} + \omega T)\}}{n\mathrm{Sin}\{\frac{1}{2}(2\pi\frac{i}{n} + \omega T)\}} \quad . \tag{5-7}$$

The LALE-DFT power spectral estimate is, in terms of the shape vector,

$$\hat{S}_{LALE} = \sum_{i=1}^{K} \frac{\frac{n}{2}\,ESNR_i}{1 + \frac{n}{2}\,ESNR_i} U_i \tag{5-8}$$

where

$ESNR_i$ = effective SNR of the i^{th} sinusoid

$$= \frac{p_i}{\sigma^2 + \gamma} \quad .$$

For comparison, the Welch spectral estimate is:

$$S = \sum_{i=1}^{K} \frac{n}{2} p_i U_i \quad . \tag{5-9}$$

Thus the LALE-DFT produces an amplitude distorted power spectral estimate when compared to the Welch spectral estimate. However, the amplitude distortion can be compensated for in the APS3 by adjusting threshold power p_t. Since the amplitude of the LALE-DFT power

spectral estimate is a monotonic function of the signal power, an amplitude threshold a_t can be found for any given power threshold p_t:

$$a_t = \frac{\frac{n}{2} p_t}{\alpha^2 + \gamma + \frac{n}{2} p_t} \qquad (5\text{-}10)$$

such that if the amplitude of the LALE-DFT power spectral estimate is greater than a_t then the power of the input signal must be greater than p_t. Thus the LALE-DFT power spectral estimate can be used by the APS3 to distinguish between weak signals and strong signals.

Compared to the Welch spectrum, the LALE-DFT spectrum provides better detectability of relatively weak signals that are close in frequency to powerful signals. This advantageous behavior is a result of the biased amplitude in the LALE-DFT spectrum. Recall that the LALE-DFT spectrum is composed of a sum of scaled shape functions (Eq. 5-8). These shape functions, U, have a maximum amplitude of 1 and sidelobes whose amplitudes are inversely proportional to the difference between the frequency of the sidelobe and the mainlobe. The maximum scale factor is unity, so the largest possible peak in the LALE-DFT spectrum has an amplitude of unity. Therefore, since the largest sidelobe of the shape function is typically less than 0.25 for a reasonably sized DFT, the largest sidelobe in the LALE-DFT spectrum is smaller than 0.25. If γ is appropriately chosen so that a_t, the amplitude threshold, is greater than 0.25, then no sidelobe can exceed a_t thus no sidelobe can be falsely treated as a powerful signal. (However, sidelobes can add and thereby cause a weak signal to appear strong or a strong signal to appear weak. This effect is relatively minor and only of concern when there are closely spaced input signals, consequently

the superposition of sidelobes can usually be ignored if all of the input signals are separated by at least 1.5/nT Hz.) In contrast the Welch spectrum is also composed of scaled shape functions, but the scaling factor is proportional to the signal power. Thus a powerful signal will have large sidelobes which would be falsely treated as powerful signals.

Figure 5-2 illustrates the difference between the LALE-DFT spectrum and the Welch spectrum. The input consisted of the sum of two sinusoids. One sinusoid was at 25% of the Nyquist frequency with a power of 1, and the other was at 32.8125% of the Nyquist frequency with a power of 10. These spectral estimates were computed with a 256 point DFT of a 32 weight LALE (224 zeros are appended to the 32 values of the LALE weights to generate a 256 point vector for the DFT) and a 256 point DFT of a 64 point autocorrelation function, since a 64 point autocorrelation function is as easy to compute as a 32 weight LALE. (Note: the DFT of a 64 point autocorrelation function has better frequency resolution than the DFT of a 32 point autocorrelation function, thus this comparison is not biased in favor of the LALE.) The LALE power spectrum clearly shows the peak due to the smaller signal, whereas the smaller signal is swamped in the Welch spectrum. Thus for any fixed computational complexity, the LALE-DFT power spectral estimate has less leakage than the Welch spectrum.

We have established that the LALE-DFT power spectrum can be used to determine the frequencies at which the signal power exceeds a predetermined threshold. However, if a simple threshold device is used to distinguish between low power and high power signals, noise in the spectral estimate could cause serious problems. For example, if the

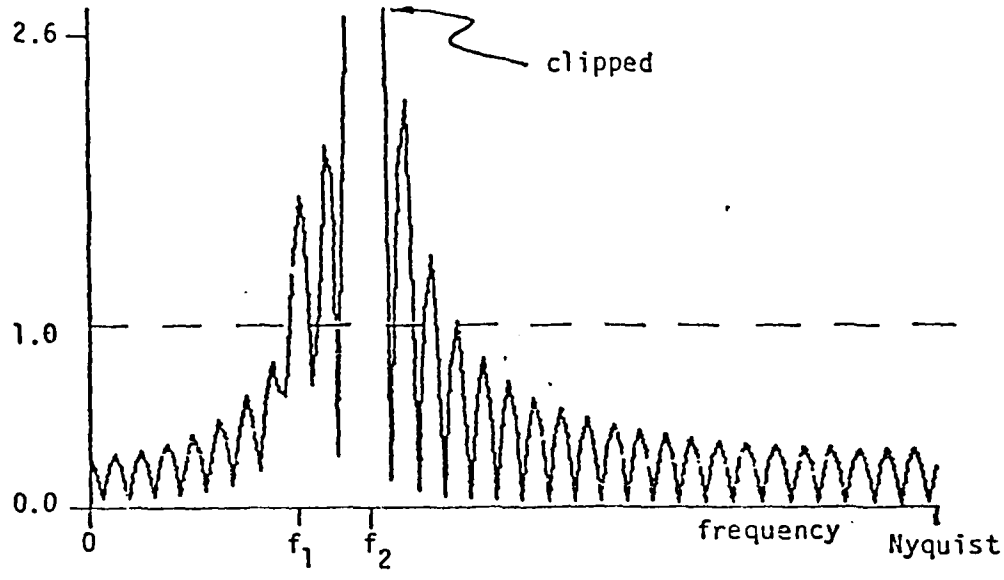

Welch spectrum

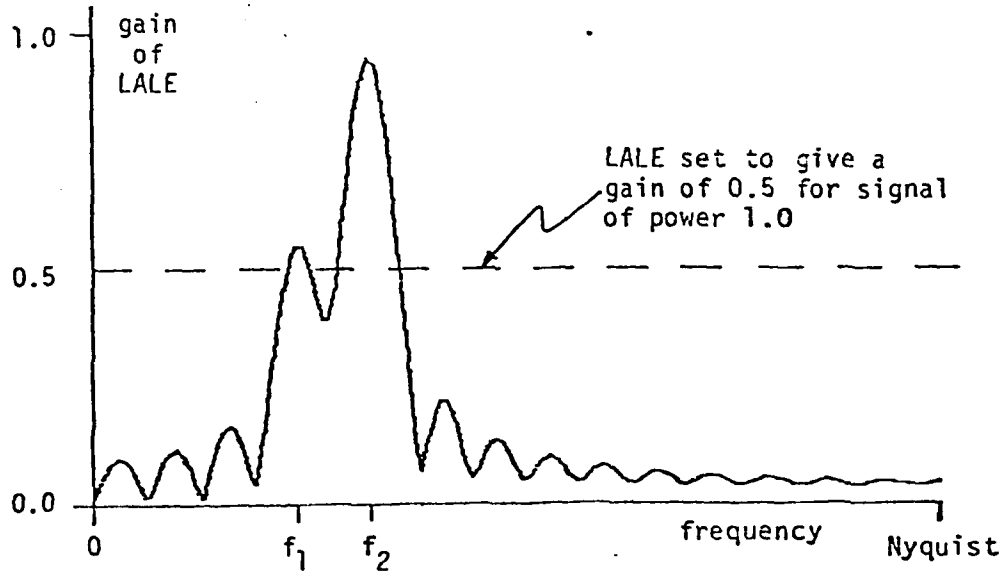

LALE spectrum

Power of signal at frequency f_1 = 1.0

Power of signal at frequency f_2 = 10.0

Figure 5-2. Comparison of Welch and LALE power spectra.

expected spectrum is near the threshold value then noise could cause the threshold device to switch repeatedly as the actual spectral estimate varied about the expected value. Switching by the threshold devices would cause the APS3 to redesign its bandstop filter, and this would, in turn, modulate the output which is often undesirable. Thus we need to analyze the noise in the power spectral estimate.

Variance of the LALE weight vector

The variance of the LALE-DFT power spectral estimate depends on the variance of the LALE weight vector, so in this section we analyze the variance of the LALE weight vector. As in Chapter 2, this analysis follows Treichler's [Tre] analysis with only those modifications required to account for the change in adaptive algorithm.

Define the weight vector noise to be:

$$\Delta W(k) = W(k) - E\{W(k)\} \tag{5-11}$$

then the weight vector covariance is:

$$E\{\Delta W(k)\Delta W^T(k)\} = \Pi(k) \quad . \tag{5-12}$$

The evolution of $\Delta W(k)$ is complicated, so we study instead the evolution of $V(k)$ where:

$$V(k+1) = [\nu I - 2\mu R(k)]V(k) + 2\mu[d(k)X(k) - P_s] \quad . \tag{5-13}$$

The evolution of $V(k)$ closely models the average behavior of $\Delta W(k)$, especially if μ is small and the LALE is near convergence. Since $V(k)$ closely approximates $\Delta W(k)$, the converged covariance of V will approximates $W(k)$, the converged covariance of V will approximate the converged covariance of ΔW.

The covariance of V can be written as:

$$\text{Cov}\{V(k+1)\} = E\{V(k+1)V^T(k+1)\}$$

$$= [\nu I - 2\mu R(k)]\text{Cov}\{V(k)\}\,[\nu I - 2\mu R(k)]$$

$$+ 4\mu^2[E\{B(k,0)\} + \sum_{i=1}^{k}([\nu I - 2\mu R(k-i)]^i$$

$$+ E\{B^T(k,i)\}[\nu I - 2\mu R(k,i)]^i)] \quad . \qquad (5\text{-}14)$$

where the matrix $B(k,i)$ is defined as:

$$B(k,i) = [d(k)X(k) - P_s]\,[d(k-i)X(k-i) - P_s]^T \quad . \qquad (5\text{-}15)$$

Equation 5-15 is a function of the specific input signals and very complicated. However, if the input consists of white noise of power σ^2 and a sinusoid of power p and angular frequency ω then Treichler [Tre] showed that:

$$[E\{B(k,i)\}]_{\ell,m} = \frac{p}{2}^2 \text{Cos}[\omega T(\ell - m - 2i)]$$

$$+ p\text{Cos}[\omega T(\ell - m)]\sigma^2\delta(\ell - m + i)$$

$$+ p\text{Cos}[\omega T(\ell - m + i)]\sigma^2\delta(i)$$

$$+ \sigma^4\delta(i)\delta(\ell - m + i) \quad .$$

By transforming Eq. 5-14 with the modal matrix Q, and defining $V(k) = QV'(k)$, $\Pi = Q\Pi'\bar{Q}^T$, and assuming that μ and γ are small enough so that $[\nu I - 2\mu R]^{n+\Delta} \simeq I$, then:

$$E\{V'(k+1)V'^T(k+1)\} = [\nu I - 2\mu(\sigma^2 + \Lambda)]E\{V'(k)V'^T(k)\}$$

$$+ [\nu I - 2\mu(\sigma^2 + \Lambda)]$$

$$+ 4\mu^2(2\sigma^2\Lambda + \sigma^4 I) \quad . \qquad (5\text{-}16)$$

Both the transition matrix and the driving term of Eq. 5-16 are diagonal, so the converged value of Π' is diagonal. Thus Eq. 5-16 can be solved for the converged value of Π':

$$[\Pi'(\infty)]_{i,i} = \frac{\mu\sigma^2(2\lambda_i+\sigma^2)}{(\gamma+\sigma^2+\lambda_i) - \mu(\gamma+\sigma^2+\lambda_i)^2}$$

$$\simeq \mu\sigma^2\left(1 + \frac{\lambda_i - \gamma}{\gamma + \sigma^2 + \gamma_i}\right) \quad . \qquad (5\text{-}17)$$

Equation 5-17 can be solved for $\Pi(\infty)$ by reversing the coordinate transformation:

$$\Pi(\infty) = \mu\sigma^2\left(I + \sum_{i=0}^{n-1} \frac{\lambda_i}{\gamma + \sigma^2 + \lambda_i} Q_i \bar{Q}_i^T\right) \quad . \qquad (5\text{-}18)$$

Equation 5-18 is valid if the input consists of multiple sinusoids in white noise. As a check, if the input has low SNR, i.e. $\sigma^2 >> \frac{n}{2}\lambda_i$, then $\Pi(\infty) \simeq \mu\sigma^2 I$ which is the result derived in [Wid] for stochastic inputs.

Variance of the LALE-DFT power spectral estimate

Denote the actual LALE-DFT spectral estimate as $\hat{S}_{LALE}$ and the mean spectral estimate as $\hat{S}_{LALE} = F \cdot E\{W\}$. Using these definitions the covariance of $\hat{S}_{LALE}$ is:

$$\mathrm{Cov}\{\hat{S}_{LALE}\} = E\{(\hat{S}_{LALE}-S_{LALE})(\hat{S}_{LALE}-S_{LALE})^T\}$$

$$= F\, E\{(W-E\{W\})(W-E\{W\})^T\}\bar{F}^T \quad . \qquad (5\text{-}19)$$

From Eq. 5-18,

$$\Pi = E\{(W-E\{W\})(W-E\{W\})^T\}$$

$$\simeq \mu\sigma^2(I+R_e) \qquad (5\text{-}20)$$

where:

$$R_e = \sum_{i=0}^{n-1} \frac{\lambda_i}{\gamma + \sigma^2 + \lambda_i} Q_i \bar{Q}_i^T$$

= coherent input equivalent autocorrelation matrix

Substituting Eq. 5-20 into 5-19 yields:

$$Cov\{\hat{S}_{LALE}\} = \mu\sigma^2(nI+FR_e\bar{F}^T) \qquad (5\text{-}21)$$

The variance of the spectral estimate is the main diagonal of $Cov\{\hat{S}_{LALE}\}$. Solving for the variance yields:

$$[Var\{\hat{S}_{LALE}\}]_m = \sum_{i=0}^{n-1}\sum_{\ell=0}^{n-1} [\Pi]_{i,\ell} \, Exp(2\pi jm\frac{i-\ell}{n})$$

$$= \mu\sigma^2\left[1 + \sum_{t=-(n-1)}^{n-1} \frac{n-|t|}{n} r_e(t) Exp(2\pi jm\frac{t}{n})\right]$$

(5-22)

where

$r_e(t)$ = the coherent component equivalent autocorrelation function

Equation 5-22 shows that the variance of the spectral estimate is a constant plus a curve which is determined by the DFT of a Bartlett-windowed version of the equivalent coherent autocorrelation function $r_e(t)$. An important property of the variance is that it is proportional to μ. Thus by decreasing μ, the variance of the spectral estimate can be reduced to any desired value.

A simple example serves to illustrate the properties of the variance. Suppose that the input is a sinusoid of frequency $\frac{m_0}{nT}$ (an on-bin signal) and power p, then:

$$[\mathrm{Var}\{\hat{S}_{LALE}\}]_m =$$

$$n\mu\sigma^2\left[1 + \frac{p}{\gamma + \sigma^2 + \frac{n}{2}p} \sum_{t=-(n-1)}^{n-1} \frac{n - |t|}{n} \cos\left(2\pi\frac{m_0 T}{n}\right) \mathrm{Exp}\left(2\pi j m\frac{t}{n}\right)\right]$$

$$= \begin{cases} n\mu\sigma^2 & m \neq m_0 \text{ or } n-m_0 \qquad (5\text{-}23A) \\ n\mu\sigma^2\left(1 + \dfrac{\frac{n}{2}\,\mathrm{ESNR}}{1 + \frac{n}{2}\,\mathrm{ESNR}}\right) & m = m_0 \text{ or } n-m_0 \qquad (5\text{-}23B) \end{cases}$$

For the design of the APS3, Eqs. 5-23A and 5-23B can be reduced to one simple design rule:

$$n\mu\sigma^2 \leq \mathrm{Var}\{\hat{S}_{LALE}\} \leq 2n\mu\sigma^2 \qquad (5\text{-}24)$$

In summary, we have found that if the input could be modeled as a sum of sinusoids in white noise then the LALE-DFT spectrum has the same shape as the ideal power spectrum, but that the power estimate is

biased (Eq. 5-15). Furthermore, we have shown that the variance of the spectral estimate can be bounded by a simple expression (Eq. 5-24). In the next section we will use these results to show that the LALE-DFT power spectrum, in conjunction with a hysteresis threshold device, fits the power switching requirements of both gain tolerance schemes that were presented in Chapter 2.

How the LALE-DFT fits the gain tolerance schemes

In this section we will show how the LALE-DFT power spectral estimate can be used in the APS3, and how the APS3 will meet the switching requirements of both gain tolerance schemes. This is an importnat step towards a useful adaptive power separator.

Both gain tolerance schemes have two power thresholds, p_1 and p_2. A switching device that obeys the tolerance schemes should indicate "pass" if the input signal power is less than p_1, "stop" if the signal power is greater than p_2 and either "pass" or "stop" otherwise. From Eq. 5-10 we find that the amplitude of the LALE-DFT spectrum is a monotonic function of the input signal power. Thus a unique spectrum amplitude is associated with each input power. Assume that an amplitude threshold a_t is found (using Eq. 5-18) which corresponds to an input power of $\frac{(p_1+p_2)}{2}$. Then if the amplitude of the LALE-DFT spectrum is greater than a_t the input power must be greater than $\frac{(p_1+p_2)}{2}$. Thus if n threshold devices with equations:

$$\text{output} = \begin{cases} \text{"stop"} & \text{if input} > a_t \\ \text{"pass"} & \text{if input} \leq a_t \end{cases} \qquad (5\text{-}25)$$

are used on the output of the LALE-DFT they will indicate which frequencies should be passed and which should be stopped.

Noise in the spectral estimate will adversely affect the threshold devices. For example, because of noise the amplitude of the spectral estimate may be less than a_t even though the signal power is greater than $\frac{(p_1+p_2)}{2}$. This will cause the threshold device to output a "pass" when it should indicate "stop." Thus with a noisy spectral estimate there is a possibility of a false output from the threshold devices. Since the statistics of the spectral noise are known, these effects can be quantified.

In accordance with the gain tolerance schemes, we say there is an error (false output) when the threshold devices indicate "pass" even though the input power is greater than p_2 or when the threshold devices indicate "stop" even though the input power is less than p_1. The probability of an error is:

$$P\{error\} = P\{(\hat{S}_{LALE} > a_t \text{ and } p \le p_1) \text{ or } (\hat{S}_{LALE} < a_t \text{ and } p \ge p_2)\} \quad ($$

$$= P\{(\hat{S}_{LALE} > \frac{n(p_1+p_2)}{n(p_1+p_2) + 4(\gamma+\sigma^2)} \text{ and } S_{LALE} \le \frac{np_1}{np_1 + 2(\gamma+\sigma^2)}) \text{ or}$$

$$(\hat{S}_{LALE} < \frac{n(p_1+p_2)}{n(p_1+p_2) + 4(\gamma+\sigma^2)} \text{ and } S_{LALE} \ge \frac{np_2}{np_2 + 2(\gamma+\sigma^2)})\}$$

$$= P\{\hat{S}_{LALE} - S_{LALE} \ge \frac{2n(\gamma+\sigma^2)(p_2-p_1)}{[n(p_1+p_2) + 4(\gamma+\sigma^2)][np_1+2(\gamma+\sigma^2)]} \text{ or}$$

$$\hat{S}_{LALE} - S_{LALE} \le \frac{-2n(\gamma+\sigma^2)(p_2-p_1)}{[n(p_1+p_2) + 4(\gamma+\sigma^2)][np_2+2(\gamma+\sigma^2)]}\}$$

$$\le P\{|\hat{S}_{LALE} - S_{LALE}| \ge \frac{2n(\gamma+\sigma^2)(p_2-p_1)}{[n(p_1+p_2) + 4(\gamma+\sigma^2)][np_2+2(\gamma+\sigma^2)]}\} \quad . \qquad (5\text{-}26)$$

Equation 5-26 is Chebyshev's inequality [Dud] so,

$$P\{error\} \le \frac{Var\{S_{LALE}\}}{\delta^2} \qquad (5\text{-}27)$$

where

$$\delta = \frac{2n(\gamma+\sigma^2)(p_2-p_1)}{[n(p_1+p_2) + 4(\gamma+\sigma^2)][np_2+2(\gamma+\sigma^2)]} \quad .$$

From Eq. 5-24 $Var\{S_{LALE}\} \le 2n\mu\sigma^2$ so:

$$P\{error\} \le 2n\mu \frac{\delta^2}{\delta^2} \quad . \qquad (5\text{-}28)$$

Thus, provided that $p_1 \neq p_2$, the probability of an error is finite and can be made as small as desired by making μ small. Therefore the LALE-DFT spectral estimator fits both tolerance schemes in a probability of an error have to be balanced against convergence time.

Earlier we discussed the possibility that a signal with power near the threshold power could cause the output of the threshold devices to repeatedly change state. This could be undesirable since it would cause the APS3 to repeatedly redesign its bandstop filter which would, in turn, modulate the signals that pass through the filter. A measure of this behavior is the expected design cycle time, where the design cycle time is the time it takes for the output of a threshold device to change state and then return to the original state. If the design cycle time is large then the filter is infrequently redesigned and will not continually modulate the signals. Thus we will analyze the APS3 threshold devices to find the design cycle time T_c.

The output of a threshold device can be viewed as a Markov process. The output has two states, "pass" and "stop," and for each input power there are probabilities associated with each state. We define P_p as the probability that the output is a "pass" and P_s as the probability that the output is a "stop." The state diagram for the threshold device is shown in Figure 5-3. The expected design cycle time can be computed [Cin]:

$$E\{T_c\} = E\{\text{time from pass to stop}\} + E\{\text{time from stop to pass}\}$$

$$= \frac{1}{P_p} + \frac{1}{P_s} \quad . \tag{5-29}$$

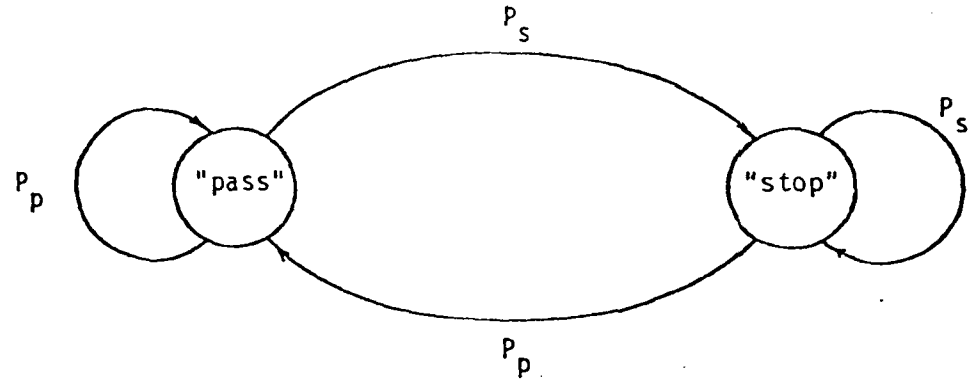

Figure 5-3. State diagram of a simple threshold device.

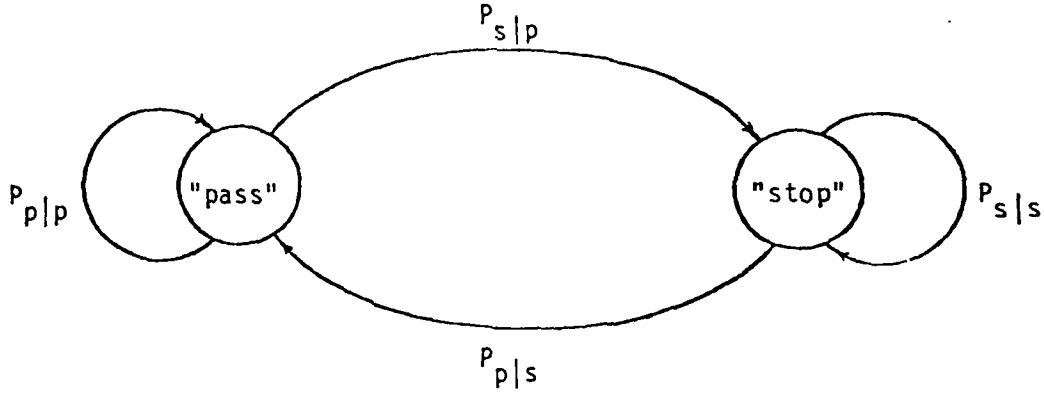

Figure 5-4. State diagram of a hysteresis threshold device.

AD-A118 554 STANFORD UNIV CA INFORMATION SYSTEMS LAB F/G 17/4
RESEARCH ON ADAPTIVE ANTENNA TECHNIQUES. IV.(U)
AUG 80 B WIDROW, T SAXE, K DUVALL, W NEWMAN N00019-79-C-0331
UNCLASSIFIED NL

2 OF 2
AD A
118554

END
DATE FILMED
09-82
DTIC

If the signal power is exactly the threshold power, $P_p = P_s = 0.5$, and so $E\{T_c\} = 4$ iterations. If this time is too short, a more complicated threshold device will have to be used because there is no way to control P_p and P_s with a simple threshold device.

A threshold device with hysteresis will allow the designer to control P_p and P_s. By making P_s or P_p small, $E\{T_c\}$ can be made as large as desired. To see how a hysteresis device provides control over P_s and P_p we define:

$\phi(k)$ = output of the threshold device at time k

$i = \hat{S}_{LALE}$ = input to the threshold device

a_ℓ = lower threshold

a_h = higher threshold .

Using these definitions the law for the hysteresis threshold device is:

$$\phi(k+1) = \begin{cases} \text{"pass"} & i \leq a_\ell \\ \text{"pass"} & a_\ell < i < a_h \text{ and } \phi(k) = \text{"pass"} \\ \text{"stop"} & a_h \leq i \\ \text{"stop"} & a_\ell < i < a_h \text{ and } \phi(k) = \text{"stop"} \end{cases} \quad (5\text{-}30)$$

The probabilities of changing state are conditioned on the current state, $\phi(k)$:

$$P_{s|p} = P\{\phi(k+1) = \text{"stop"} | \phi(k) = \text{"pass"}\} = P\{i \geq a_h\}$$

$$P_{p|p} = P\{\phi(k+1) = \text{"pass"} | \phi(k) = \text{"pass"}\} = P\{i < a_h\}$$

$$P_{s|s} = P\{\phi(k+1) = \text{"stop"} | \phi(k) = \text{"stop"}\} = P\{i > a_l\}$$

$$P_{p|s} = P\{\phi(k+1) = \text{"pass"} | \phi(k) = \text{"stop"}\} = P\{i \leq a_l\} \quad . \quad (5\text{-}31)$$

The state diagram for the hysteresis device is shown in Figure 5-4. For this device the expected cycle time is:

$$E\{T_c\} = \frac{1}{P_{s|p}} + \frac{1}{P_{p|s}} \quad . \quad (5\text{-}32)$$

THEOREM 5-1: If $a_h \neq a_l$ then $E\{T_c\}$ can be made as large as desired.

PROOF: If either $P_{s|p}$ or $P_{p|s}$ can be made as small as desired then $E\{T_c\}$ can be made as large as desired, so we will show that either $P_{s|p}$ or $P_{p|s}$ can be made as small as desired.

Let $\delta = \text{Max}(E\{i\}-a_\ell, a_h-E\{i\})$. Assume for convenience that $\delta = E\{i\}-a_\ell$, then:

$$\begin{aligned} P_{s|p} &= P\{i \leq a_\ell\} \\ &= P\{E\{i\}-i \geq \delta\} \\ &\leq P\{|i-E\{i\}| \geq \delta\} \\ &\leq \frac{\text{Var}\{\hat{S}_{LALE}\}}{\delta^2} \quad . \end{aligned}$$

Equation 5-24 shows that $\text{Var}\{\hat{S}_{LALE}\}$ can be made as small as desired by making the value of μ small. Therefore $P_{s|p}$ can be

made as small as desired, and consequently $E\{T_c\}$ can be as large as desired since:

$$E\{T_c\} \geq \frac{1}{P_{s|p}} + 1 \quad .$$

An analagous demonstrations can be used to show that $P_{p|s}$ can be made as small as desired by defining $\delta = a_h - E\{i\}$.

This completes the proof of theorem 5-1.

The expected design cycle time can be bounded using the same type of arguments that were presented in the proof of theorem 5-1. A lower bound on $E\{T_c\}$ is:

$$E\{T_c\} \geq \frac{a_h - a_\ell}{2VAR\{\hat{S}_{LALE}\}}$$

$$\geq \frac{a_h - a_\ell}{4n\mu\sigma^2} \qquad (5\text{-}33)$$

When a hysteresis device is used in the APS3, the probability of an incorrect state or error is:

$$P\{error\} \leq P\{(i \geq a_h \text{ and } p<p_1) \text{ or } (i \leq a_\ell \text{ and } p>p_2)\}$$

$$\leq P\{|i-E\{i\}| \geq Min(a_h-a_{min}, a_{max}-a_\ell)\}$$

$$\leq \frac{Var\{\hat{S}_{LALE}\}}{Min(a_h-a_{min}, a_{max}-a_\ell)^2} \qquad (5\text{-}34)$$

where

$$a_{min} = \frac{\frac{n}{2}p_1}{\frac{n}{2}p_1 + \gamma + \sigma^2}$$

$$a_{max} = \frac{\frac{n}{2}p_2}{\frac{n}{2}p_2 + \gamma + \sigma^2} \quad .$$

Since $VAR\{\hat{S}_{LALE}\}$ can be made as small as desired, the probability of an error can be made as small as desired. Therefore, by using threshold devices with hysteresis the switching characteristics of the APS3 will meet both gain tolerance schemes and still have as long a design cycle time as desired.

Frequency sampling filter design

In the previous sections we have analyzed the power spectral estimation technique used by the APS3. We have shown that the DFT of the LALE weight vector in conjunction with hysteresis threshold devices can indicate with any desired accuracy which frequencies should be blocked and which should be passed. In the following section we will show that the frequency sampling filter design technique can use the output of the threshold devices to design a filter that will block, to any desired accuracy, the high power signals and pass, with nearly unit gain, the low power signals.

One technique for designing finite impulse response (FIR) filters is the frequency sampling technique [Opp, Rab, Rab2]. Frequency sampling uses an inverse DFT to obtain a weight vector from samples of the ideal frequency response. This technique is fast, computationally

efficient and not iterative. Since the APS3 will be a real-time signal processor speed is important. Also, frequency sampling can be used to design filters with linear phase which may be desirable in communication systems. Therefore the frequency sampling technique is used in the APS3 to design the bandstop filter that rejects the strong input signals.

In the APS3 the ideal frequency response is derived from the DFT of the LALE weight vector n threshold devices process the outputs of an n point DFT to produce samples of the ideal frequency response. The frequency sampling technique uses the following equation (inverse DFT) to obtain a weight vector from the sampled frequency response:

$$[W]_i = \frac{1}{n} \sum_{\ell=0}^{n-1} [H]_\ell \mathrm{Exp}(2\pi j \frac{\ell i}{n}) \quad i = 0, 1, \ldots, n-1 \qquad (5\text{-}35)$$

where

W = the weight vector of the FIR filter
= the pulse response of the FIR filter
H = the vector of gain specifications
= samples of the ideal frequency response
$[H]_\ell$ = ideal gain at frequency $\frac{\ell}{nT}$
n = number of weights in FIR filter
= number of frequency samples
T = sampling period of FIR filter .

Since we stipulate that W must be real, the following symmetry condition has to be imposed on H:

$$[H]_\ell = \mathrm{Conjugate}\{[H]_{n-\ell}\} \qquad (5\text{-}36)$$

The transfer function of an FIR filter designed by Eq. 5-35 is [Opp]:

$$H(Z) = \frac{1 - Z^{-n}}{n} \sum_{\ell=0}^{n-1} \frac{[H]_\ell}{1 - \text{Exp}(j2\pi\frac{\ell}{n})Z^{-1}} \quad . \qquad (5\text{-}37)$$

The frequency response of the FIR filter is found by substituting $Z = \text{Exp}(j\omega)$ into Eq. 5-37:

$$H(e^{j\omega}) = \frac{1}{n} \text{Exp}(-j\omega\frac{n-1}{2}) \sum_{\ell=0}^{n-1} (-1)^\ell [H]_\ell \text{Exp}(j\pi\frac{\ell}{n}) \frac{\text{Sin}[\frac{n}{2}(\omega-2\pi\frac{\ell}{n})]}{\text{Sin}[\frac{1}{2}(\omega-2\pi\frac{\ell}{n})]} \qquad (5\text{-}38)$$

substituting $\omega = \pi\frac{\ell}{n}$ into Eq. 5-38 shows that:

$$|H(e^{j\pi\frac{\ell}{n}})| = |[H]_\ell| \qquad \ell = 0, 1, \ldots, n-1 \quad .$$

Thus the gain of the FIR filter has the correct magnitude at the sample frequencies (integer multiples of $\frac{1}{nT}$). What about the phase? Eq. 5-37 shows that the frequency response consists of a linear phase term, $\text{Exp}(-j\omega\frac{n-1}{2})$, and a complex term. One of the design requirements is that the FIR filter have linear phase. This will be true if the complex term is purely real which requires that:

$$[H]_\ell = [G]_\ell \, e^{-j\pi\frac{\ell}{n}} \qquad (5\text{-}39)$$

where $[G]_\ell$ is a real value, the magnitude of the ideal frequency response. Also, since H has to obey Eq. 5-36:

$$[G]_\ell = -[G]_{n-\ell} \quad . \qquad (5\text{-}40)$$

If H has the form specified in Eqs. 5-39 and 5-40, then the FIR filter will have a real weight vector, linear phase and the same magnitude as the ideal filter at the specification frequencies (integer multiples of $\frac{1}{nT}$ Hz). However, there will be zeros in any passband, as can be seen by rewriting Eq. 5-38 as:

$$H(e^{j\omega}) = e^{-j\omega\frac{n-1}{2}} \sum_{\ell=0}^{n-1} (-1)^{\ell}[G]_{\ell} \frac{\mathrm{Sin}[\frac{n}{2}(\omega-2\pi\frac{\ell}{n})]}{n\mathrm{Sin}[\frac{1}{2}(\omega-2\pi\frac{\ell}{n})]} \quad . \qquad (5\text{-}41)$$

This shows that the magnitude of H(Z) is the sum of n bandpass filters. The peak amplitude of the filters is $[G]_{\ell}$ at frequency $\pi\frac{\ell}{n}$. In a passband, where $[G]_{\ell-1} = [G]_{\ell} = 1$, the sign alternations in $H(e^{j\omega})$ caused by the term $(-1)^{\ell}$ will cause the gain to be zero somewhere between frequency $\frac{\ell-1}{nT}$ and $\frac{\ell}{nT}$. This follows from the intermediate value theorem [Ros]. Since this behavior is undesirable, an additional condition is imposed:

$$[G]_{\ell}(-1)^{\ell} \geq 0 \quad . \qquad (5\text{-}42)$$

With the added restriction of Eq. 5-42 the magnitude of H(Z) will approximate quite closely the magnitude of the ideal frequency response. Figure 5-5 shows the magnitude of H(Z) for a typical bandstop filter designed by frequency sampling. The frequency response has ripples which increase in magnitude near discontinuities in the derivative of the ideal frequency response.

The magnitude of the ripples in the actual frequency response can be reduced by smoothing the ideal frequency response. A common technique

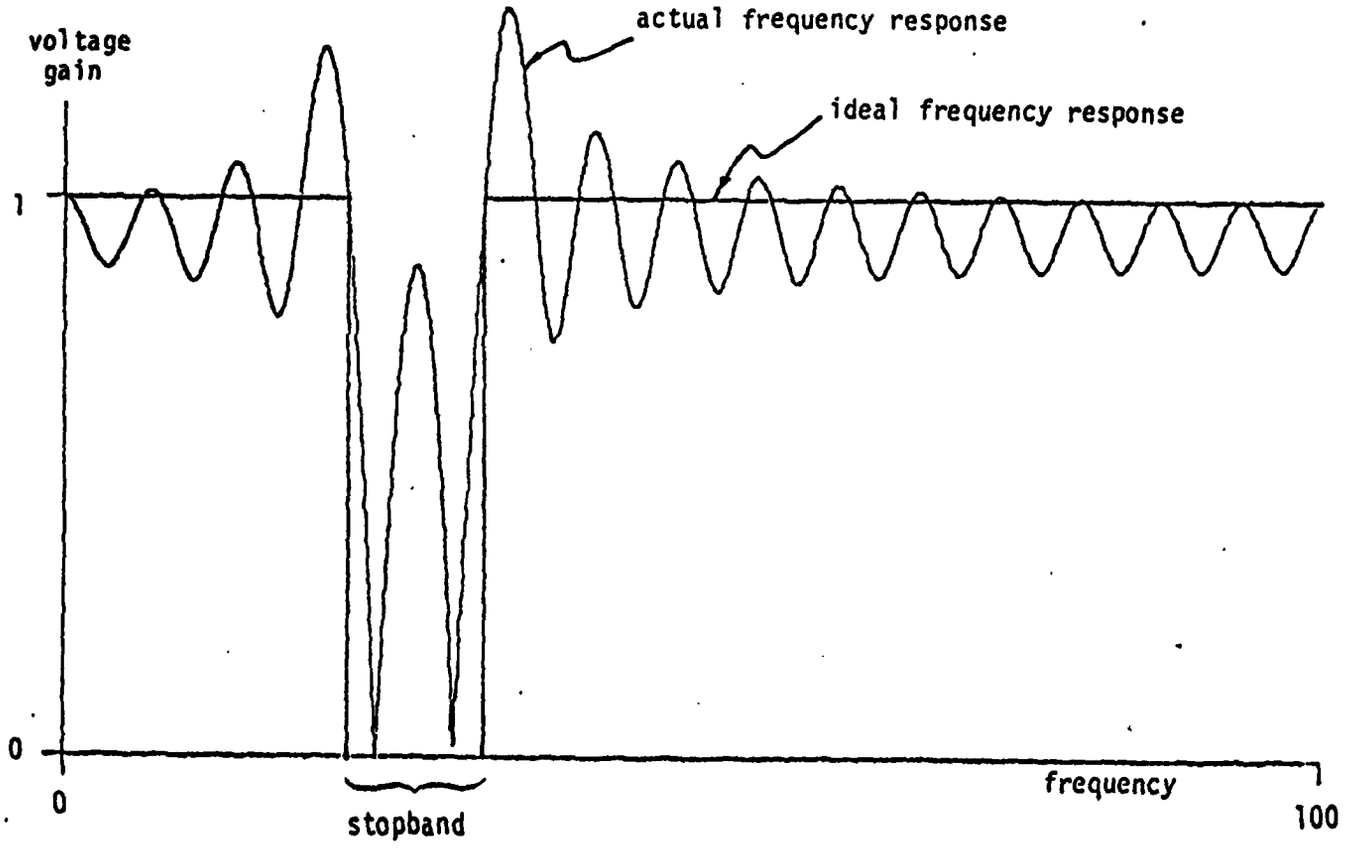

Figure 5-5. Frequency sampling designed bandstop filter.

for smoothing the ideal response is to vary a few of the ideal gains near a discontinuity. Usually the gains are varied until the ripple is minimized [Opp, Rab, Rab2]. This procedure is complicated and may be too slow for real-time filter design. Thus the APS3 uses fixed smoothing of the ideal filter characteristic. Wherever there is a transition from a desired gain of one to a desired gain of zero, the APS3 will alter the gain of one to a gain of 0.4 (0.4 was chosen by examining a table of optimal values [Rab2] and selecting a compromise value).

Some reduction in the complexity of the APS3 can be obtained by using the symmetry of Eqs. 5-39 and 5-40 and the fact that:

if

$$W = \text{inverse DFT}(H) \qquad (5\text{-}43A)$$

then

$$W' = \text{inverse DFT}(H') \qquad (5\text{-}43B)$$

where

$$[W']_i = [W]_{i + \frac{n}{2} \bmod n}$$

$$[H']_i = (-1)^i [H]_i \quad .$$

Figure 5-6 shows a block diagram for one possible implementation of the filter design portion of the APS3. Notice how symmetry eliminates the need for half of the threshold devices and half of the smoothers. Also, the symmetry conditions required for linear phase dictate that the n/2 input must be zero since $[G]_{\frac{n}{2}} = -[G]_{\frac{n}{2}}$ from Eq. 5-40. Finally, the

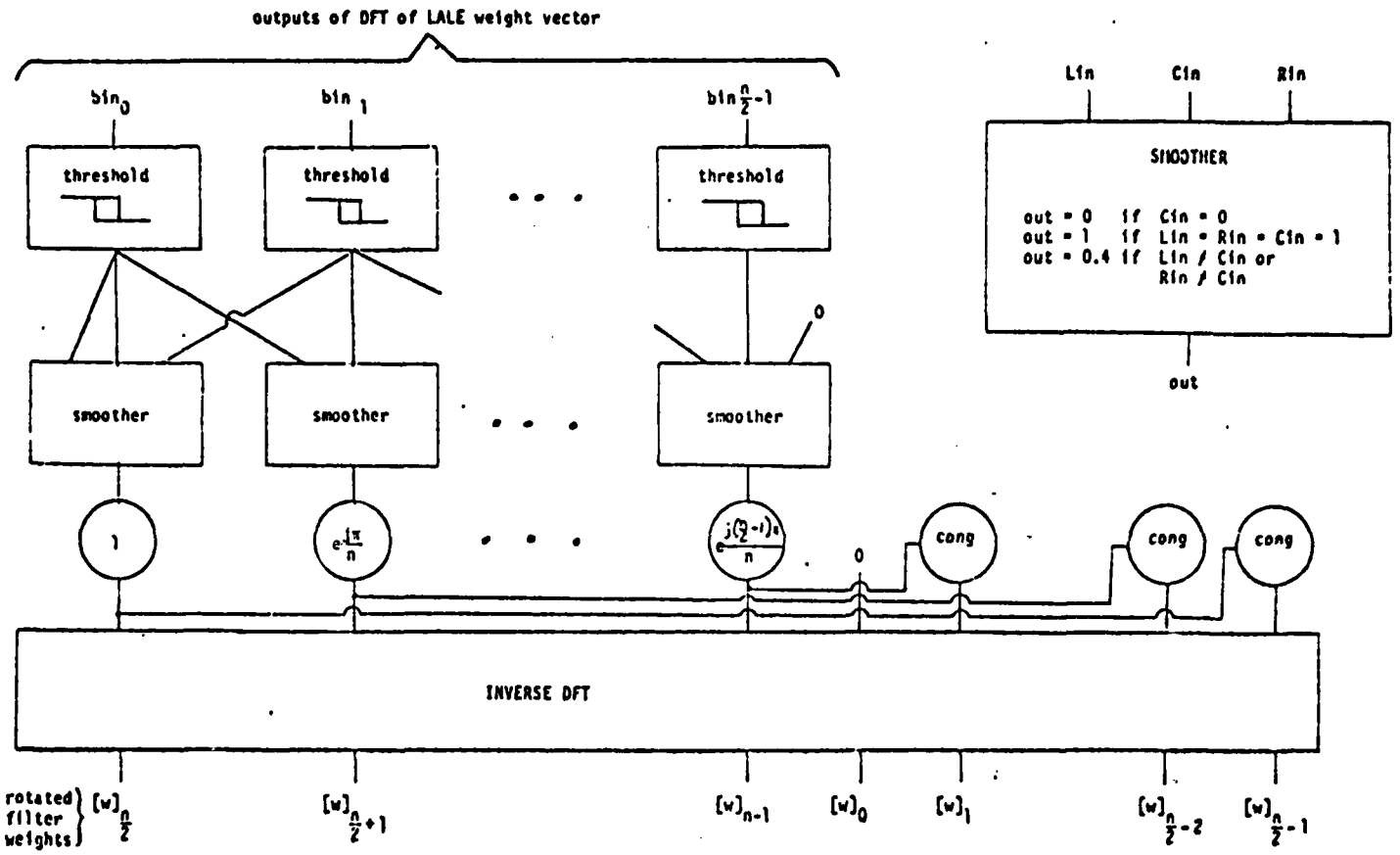

Figure 5-6. Filter design in the APS3.

output of the inverse DFT is 'rotated', which by Eqs. 5-43A and B has the same effect as Eq. 5-42.

This completes the derivation of the frequency sampling technique for filter design. In the next section we will show that the frequency response of filters designed by the APS3 can be made as nearly ideal as desired.

Quality of frequency sampling designed filters

The quality of a filter can be defined in many ways. One measure of the quality of a filter is defined as the integral of the square of the difference between the ideal transfer function and the actual transfer function. The following theorem uses the integral squared error [Trt, Oga] criterium to characterize a frequency sampling filter.

THEOREM 5-2: The integral squared error between the transfer function of a filter designed by frequency sampling and the ideal transfer function can be reduced to any desired value by making the filter length large enough.

A useful corollary to Theorem 5-2 is:

COROLLARY 5-2: Given a signal with a finite power spectral density and a frequency sampling designed FIR filter, the output power due to the difference between the actual transfer function and the ideal transfer function can be made as small as desired.

Before we prove Theorem 5-2 we will prove two lemmas.

LEMMA 1: The impulse response of a frequency sampling designed FIR filter is an aliased or folded version of the impulse response of the ideal filter [Rab2].

PROOF: (The technique used in this proof is due to Papoulis [Pap].)

The transfer function $H(\omega)$, of a digital filter is periodic with a period of $\frac{1}{T}$. This implies that $H(\omega)$ can be expanded in a Fourier series:

$$H(\omega) = \sum_{k=-\infty}^{\infty} c_k \text{Exp}(-j2\pi kT\omega)$$

where the c_k are the Fourier coefficients and also the pulse response of the ideal filter.

Frequency sampling uses samples of the ideal transfer function. Let n be an arbitrary integer and define:

$$\omega_1 = \frac{1}{nT}$$

then the samples of the ideal transfer function used by frequency sampling are:

$$H(m\omega_1) \qquad m = 0, 1, \ldots, n-1 \quad .$$

In terms of the Fourier coefficients these samples are:

$$H(m\omega_1) = \sum_{k=-\infty}^{\infty} c_k \text{Exp}(-j2\pi kTm\omega_1)$$

$$= \sum_{k=-\infty}^{\infty} c_k \text{Exp}(-j2\pi k\frac{m}{n}) \qquad m = 0, 1, \ldots, n-1 \quad .$$

Note that k can be written as:

$$k = i + rn \quad \text{for} \quad i = \frac{-n}{2}, \ldots, \frac{n}{2} - 1 \quad \text{and} \quad r = \ldots, -1, 0, 1, \ldots$$

so

$$\text{Exp}[-j2\pi k\frac{m}{n}] = \text{Exp}[-j2\pi(i+rn)\frac{m}{n}] = \text{Exp}[-j2\pi i\frac{m}{n}]$$

since

$$\text{Exp}[j2\pi] = 1 \quad .$$

Therefore,

$$H(m\omega_1) = \sum_{i=\frac{-n}{2}}^{\frac{n}{2}-1} \sum_{r=-\infty}^{\infty} c_{i+rn}\text{Exp}[-j2\pi(i+rn)\frac{m}{n}]$$

$$= \sum_{i=\frac{-n}{2}}^{\frac{n}{2}-1} \text{Exp}[-j2\pi i\frac{m}{n}] \sum_{r=-\infty}^{\infty} c_{i+rn}$$

$$= \sum_{i=\frac{-n}{2}}^{\frac{n}{2}-1} c'_i\text{Exp}[-j2\pi i\frac{m}{n}]$$

where

$$c'_i = \sum_{r=-\infty}^{\infty} c_{i+rn} \qquad \frac{-n}{2} \leq i \leq \frac{n}{2} - 1 \quad .$$

This equation for $H(m\omega_1)$ is the DFT of the sequence c'_i. Thus the weight coefficients or pulse response derived by the frequency

sampling technique are the c'_i which are "aliased" Fourier series coefficients. QED

LEMMA 2: Given a sequence c_k of Fourier coefficients and an arbitrary number, ε, then a value of n can be found such that if $m \geq n$ then

$$\sum_{i=\frac{-m}{2}}^{\frac{m}{2}-1} \left| \sum_{|r|>0} c_{i+rn} \right|^2 < \varepsilon \quad .$$

PROOF: By a form of Parseval's theorem [Trt]

$$\sum_{\ell=-\infty}^{\infty} |c_k|^2 = \frac{1}{T} \int_{\frac{-1}{2T}}^{\frac{1}{2T}} |H_i(\omega)|^2 d\omega = a$$

where

$H_i(\omega)$ is the ideal frequency response

a is some constant

now

$$\sum_{k=\frac{-m}{2}}^{\frac{m}{2}-1}\left|\sum_{|r|>0} c_{k+rn}\right|^2 \leq \sum_{k=\frac{-m}{2}}^{\frac{m}{2}-1}\sum_{|r|>0} |c_{k+rn}|^2$$

$$\leq \sum_{k\geq\frac{m}{2}} |c_k|^2$$

$$k\leq\frac{-m}{2}-1$$

$$\leq \sum_{|k|\leq\frac{m}{2}} |c_k|^2 .$$

$$= a - \sum_{|k|<\frac{m}{2}} |c_k|^2$$

since $\sum_{k=-\infty}^{\infty} |c_k|^2$ is a convergent series [Ros] there must exist, for any arbitrary ε, some n such that

$$a - \sum_{|k|<\frac{n}{2}} |c_k|^2 < \varepsilon$$

which implies that

$$\sum_{k=\frac{-n}{2}}^{\frac{n}{2}-1}\left|\sum_{|r|>0} c_{k+rn}\right|^2 < \varepsilon$$

QED

PROOF of THEOREM 5-2: the integral squared error is defined as:

$$e^2 = T\int_{\frac{-1}{2T}}^{\frac{1}{2T}} |H_i(\omega)-H_a(\omega)|^2 d\omega$$

where

$H_i(\omega)$ is the ideal transfer function

$H_a(\omega)$ is the actual transfer function

also, if the c_k are the Fourier series coefficients of $H_i(\omega)$, then

$$H_i(\omega) - H_a(\omega) = \sum_{k=-\infty}^{\infty} c_k \text{Exp}[-j\omega kT] - \sum_{k=\frac{-n}{m}}^{\frac{n}{2}-1} \left| \sum_{r=-\infty}^{\infty} c_{k+rn} \right| \text{Exp}[-j\omega kT]$$

by LEMMA 1.

Parseval's theorem [Trt] is:

$$\frac{1}{T}\int_{\frac{-1}{2T}}^{\frac{1}{2T}} |H_i(\omega)|^2 d\omega = \sum_{k=-\infty}^{\infty} |c_k|^2$$

where the c_k are the Fourier series coefficients of $H_i(\omega)$ so

$$e^2 = \sum_{k<\frac{-n}{2}} |c_k|^2 + \sum_{k=\frac{-n}{2}}^{\frac{n}{2}-1} \Big| \sum_{|r|>0} c_{k+rn} \Big|^2$$

$$k>\frac{n}{2}-1$$

$$= \sum_{k=-\infty}^{\infty} |c_k|^2 - \sum_{k=\frac{-n}{2}}^{\frac{n}{2}-1} |c_k|^2 + \sum_{k=\frac{-n}{2}}^{\frac{n}{2}-1} \Big| \sum_{|r|>0} c_{k+rn} \Big|^2$$

$$= \frac{1}{T}\int_{\frac{-1}{2T}}^{\frac{1}{2T}} |H_i(\omega)|^2 d\omega + \sum_{k=\frac{-n}{2}}^{\frac{n}{2}-1} |c_k|^2 + \sum_{k=\frac{-n}{2}}^{\frac{n}{2}-1} \Big| \sum_{|r|>0} c_{k+rn} \Big|^2$$

Given an arbitrary ε there exists an n_1 such that if $m > n_1$ then

$$\frac{1}{T}\int_{\frac{-1}{2T}}^{\frac{1}{2T}} |H_i(\omega)|^2 d\omega - \sum_{k=\frac{-m}{2}}^{\frac{m}{2}-1} |c_k|^2 < \frac{\varepsilon}{2}$$

also, by LEMMA 2 an n_2 can be found such that if $m > n_2$ then

$$\sum_{k=\frac{-m}{2}}^{\frac{m}{2}-1} \Big| \sum_{|r|>0} c_{k+rn} \Big|^2 < \frac{\varepsilon}{2}$$

thus if $n = MAX(n_1, n_2)$ then for any $m > n$

$$e^2 < \frac{\varepsilon}{2} + \frac{\varepsilon}{2} = \varepsilon \quad .$$

QED

PROOF of COROLLARY to THEOREM 5-2: The error output power is:

$$P_e = \int_{\frac{-1}{2T}}^{\frac{1}{2T}} S_e(\omega)d\omega = \int_{\frac{-1}{2T}}^{\frac{1}{2T}} |E(\omega)|^2 S(\omega)d\omega$$

where

$S(\omega)$ = Power Spectral Density of input signal

$S_e(\omega)$ = Power Spectral Density of signal which is due to the error between the ideal filter and the actual filter .

Therefore,

$$P_e \leq \int_{\frac{-1}{2T}}^{\frac{1}{2T}} V|E(\omega)|^2 d\omega = Ve^2$$

where

V = $\text{Max}[S(\omega)]$

e^2 = integral squared error between the ideal and actual transfer function. e^2 can be made as small as desired (Theorem 5-2)

this completes the proof.

NOTE: A signal with zero bandwidth, such as a sinusoid, does not have a finite power spectral density. Consequently this proof does not hold for sinusoids. However, it is conjectured that Gibbs phenomena

[Car] may appear at discontinuities in the transfer function. So if the input has a sinusoid at the frequency of a discontinuity, then the Gibbs phenomenon will cause the error power to be finite for all values of n.

Theorem 5-2 supports the intuitive notion that increasing the number of weights in an FIR filter should allow the transfer function to become closer to the ideal transfer function. The corollary lets us know that in principle frequency sampling filters can attenuate any finite bandwidth signal to any desired level. This means that the filters designed by the APS3 fit gain tolerance scheme one. (In practice this may not be true due to problems such as finite precision arithmetic).

Figures 5-7 through 5-10 show a series of frequency sampling designed bandstop filters. All of the filters have a stopband between 12.5% and 25% of the Nyquist frequency. The transition gains, which are at 12.5% and 25% of the Nyquist frequency, are 0.4. Figure 5-7 shows the frequency response of a 32 weight filter. Figures 5-8, 5-9 and 5-10 show the frequency response of a 64 weight filter, a 128 weight filter and a 256 weight filter respectively. The improvement in the frequency response is evident.

Summary and conclusions

This chapter has presented a scheme for an adaptive power separator which is based on a LALE, a DFT and an inverse DFT. We have shown that the adaptive power separator, called the APS3, fits tolerance scheme one. This means that the designer can select two power thresholds, p_1 and p_2 (with $p_1 < p_2$) and guarantee that all signals with power less than p_1 will be passed and all signals with power greater than p_2 will be

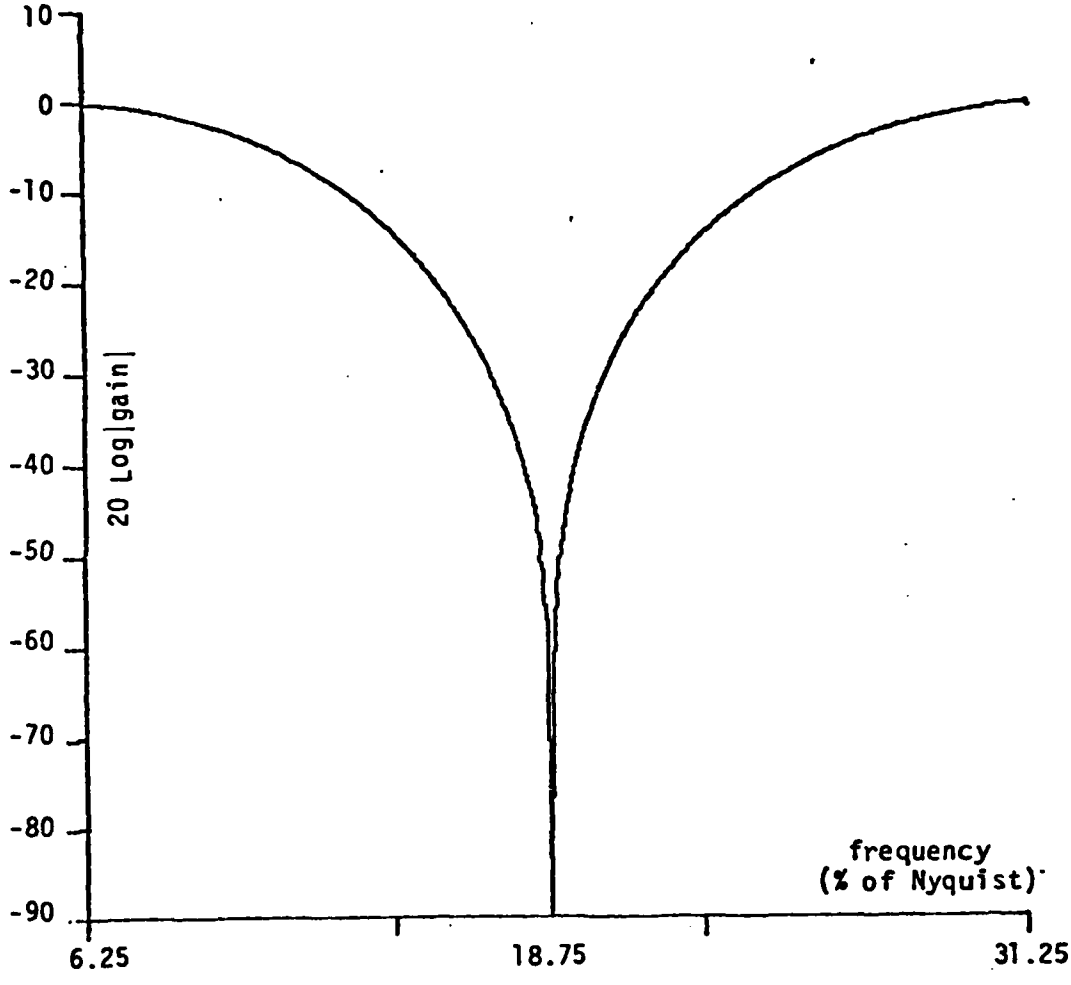

Figure 5-7. Stop region of a 32 weight bandstop filter.

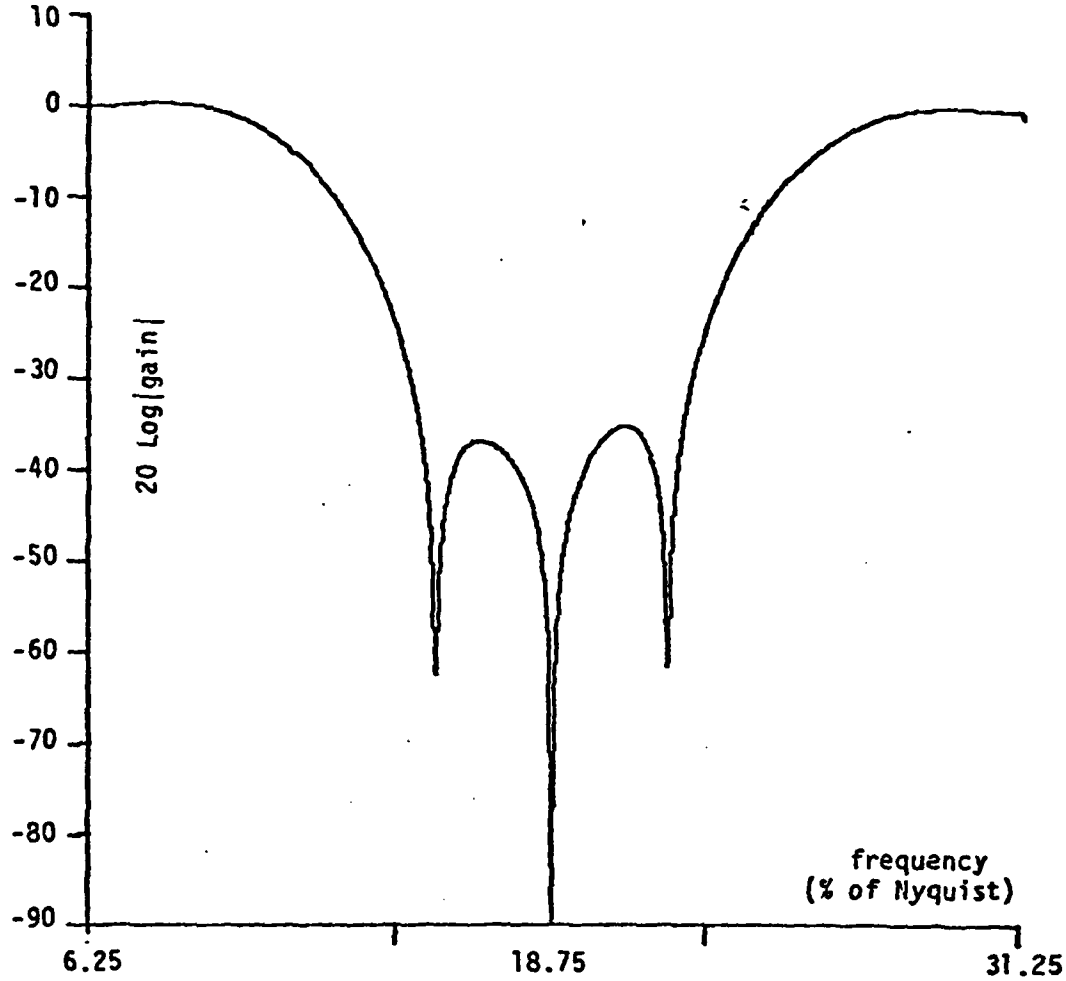

Figure 5-8. Stop region of a 64 weight bandstop filter.

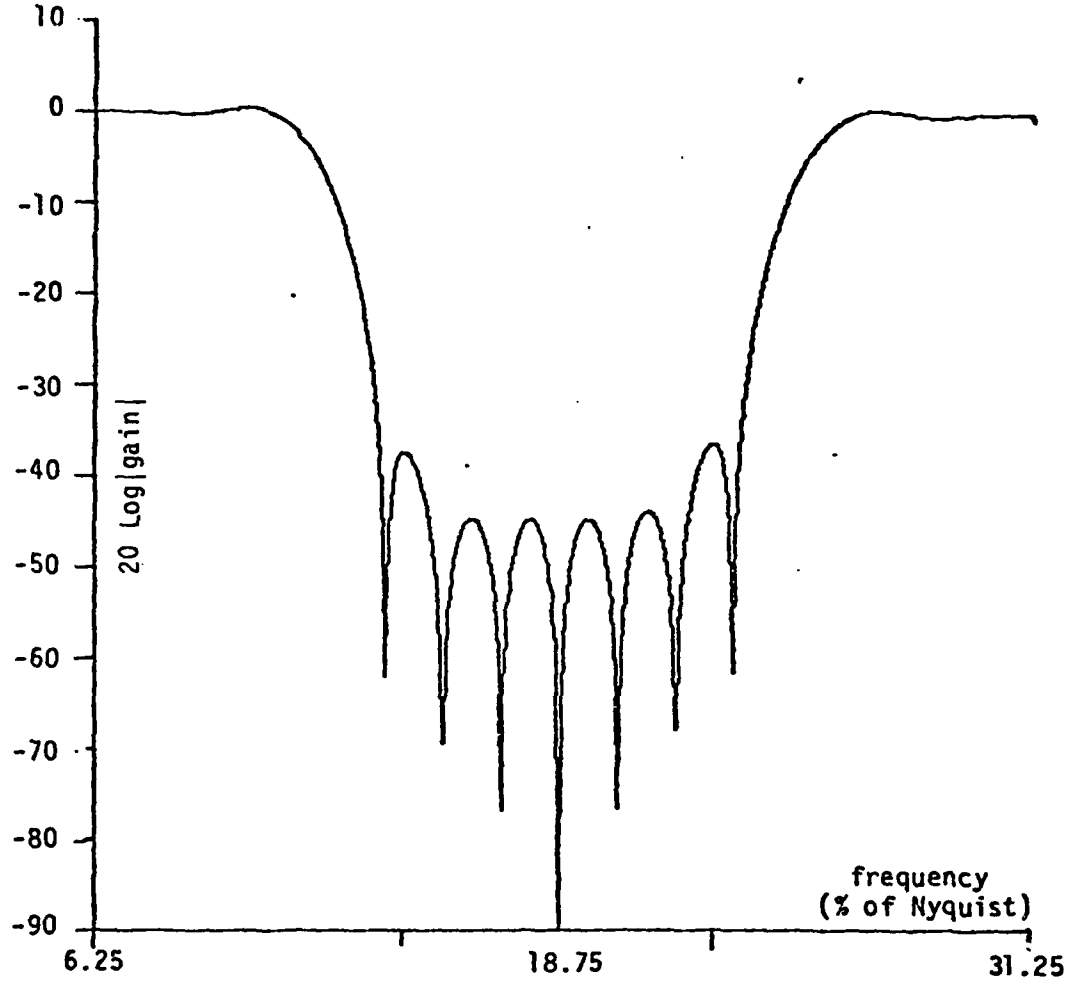

Figure 5-9. Stop region of a 128 weight bandstop filter.

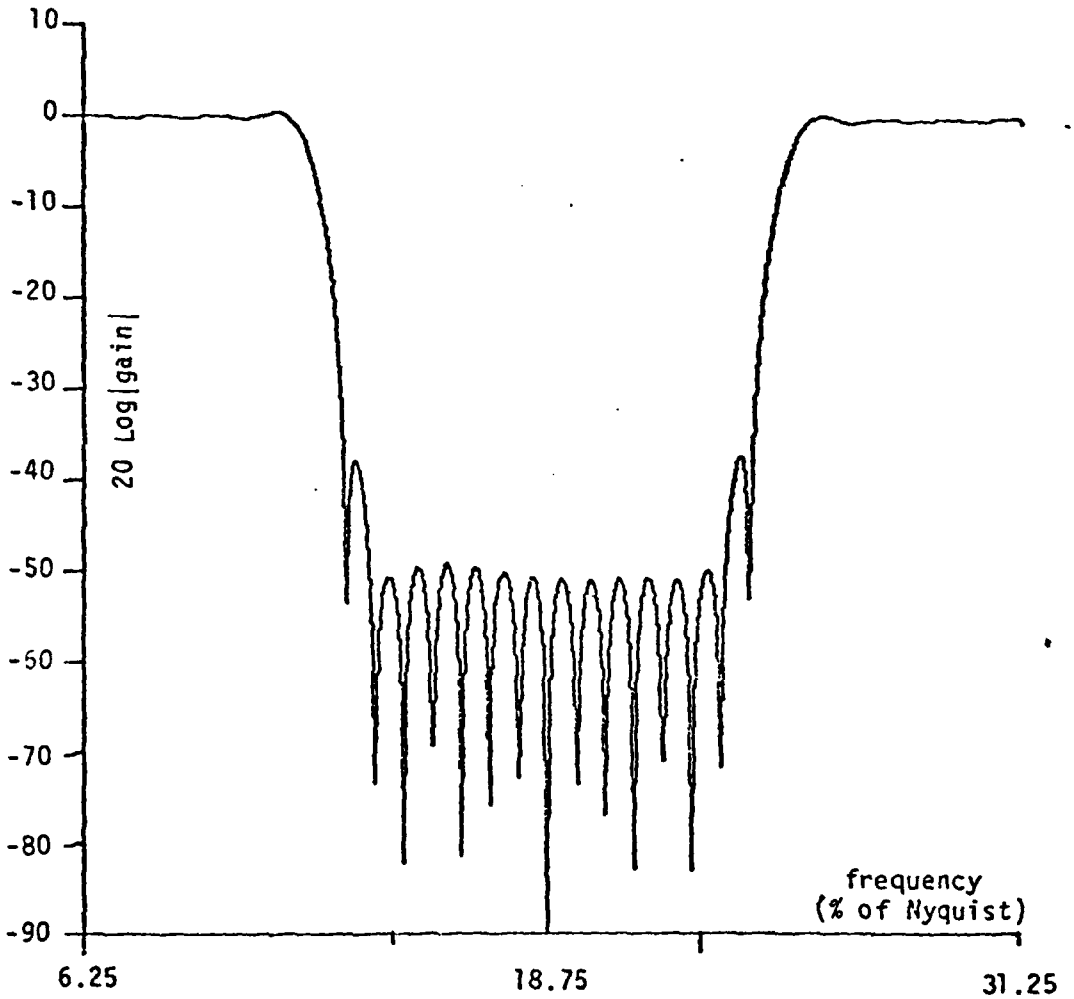

Figure 5-10. Stop region of a 256 weight bandstop filter.

stopped. In the context of the APS3, and gain tolerance scheme one, the signals that are stopped will be multiplied by some gain g which is between zero and some arbitrarily small value δ_2 which is selected by the designer.

6 -- APS4: THE ADDITION OF NOISE CANCELLING TO THE APS3

This chapter proposes and examines an adaptive power separator (APS) which uses an adaptive noise canceller to improve the performance of the APS3. The new APS has more components than the APS3, but the performance fits tolerance scheme two. Because of the significant improvement in performance, the new APS is called the APS4 to distinguish it from the APS3.

The previously explained APS, the APS3, designs a bandstop filter that will reject the strong signals. However, the bandstop filter is not perfect, so a small fraction of the strong signal may still be in the output of the APS3. Consequently, if the strong signal is powerful enough the output power can be very large. We would like to find a scheme for cancelling the residues of strong signals.

Noise cancelling is a common application for adaptive filters [Wid, Glo]. The usual situation for noise cancelling is shown in Figure 6-1. The adaptive filter forms a best fit between the noise signal at the reference input and the noise in the primary input. Thus the output consists of the signal and whatever noise the filter could not match. In the case of the APS4, the primary input to the canceller is the output of the APS3, and the reference input to the canceller is the output of a bandpass filter which passes only the strong signals.

Figure 6-2 shows the structure of the APS4. The LALE and the bandstop filter form the APS3. The new bandpass FIR filter, which has pass regions wherever the bandstop filter has rejection regions

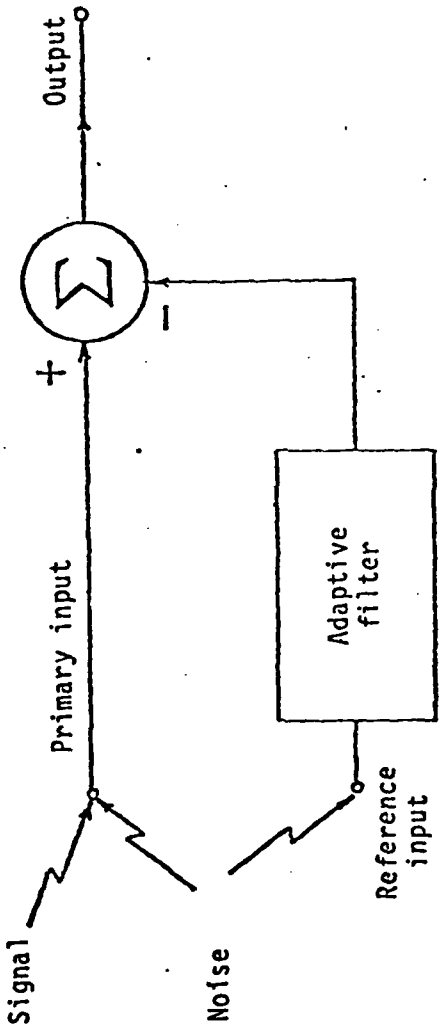

Figure 6-1. Noise cancelling.

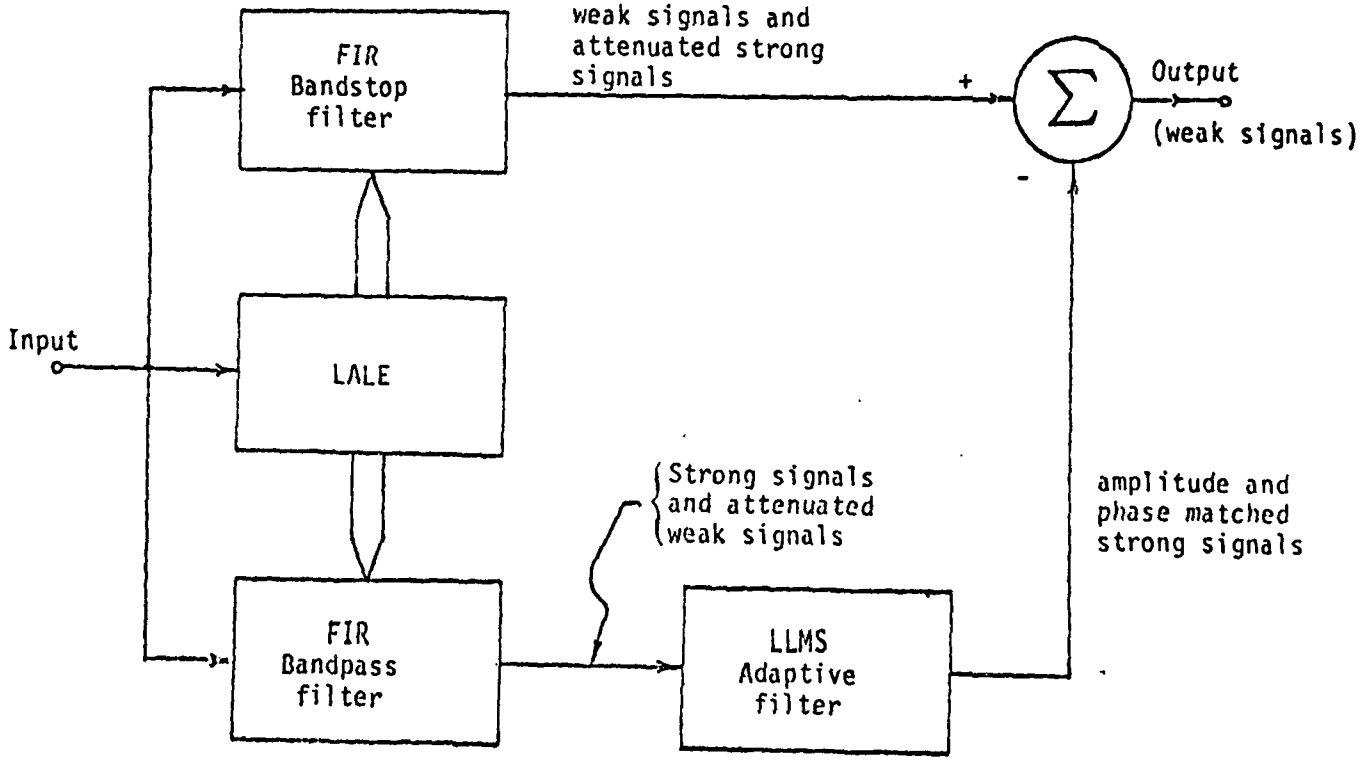

Figure 6-2. Structure of the APS4.

(see Fig. 6-3), passes only the strong signals. The strong signals are used as the reference input to a leaky LMS canceller which cancels the residues of the strong signals from the APS3 output. (An LLMS canceller is used because greatly attenuated versions of the weak signals will pass through the bandpass filter (due to ripple), and an LMS filter would use these to cancel the weak signals in the APS3 output.) The output of the noise canceller is the output of the APS4.

The bandpass filter used in the APS4 is the complement of the bandstop filter which is used in the APS3. A simple way to design the bandpass filter is to use the frequency sampling technique. The ideal transfer function is derived from the ideal transfer fucntion of the bandstop filter by replacing all gains of zero by gains of one and all gains of one by gains of zero. The resulting bandpass filter (see Fig. 6-3) will pass all of the signals which the bandstop filter rejects -- these are the strong signals.

The analysis of the noise cancelling stage divides into two cases. The first case is the analysis of weak signals and the second case is the analysis of strong signals.

If a signal is weak then the bandstop filter will pass the signal with a gain of nearly one, and the bandpass filter will pass the signal with a gain of nearly zero. We will denote the gain of the bandstop filter at the signal's frequency as $1-f_1$ and the gain of the bandpass filter at the signal's frequency g_1. Figure 6-4 shows the canceller in this situation. The signal power at the "error" output is:

$$\text{power} \simeq \sigma^2 + (1-f_1-g_1 g)^2 p_s \qquad (6\text{-}1)$$

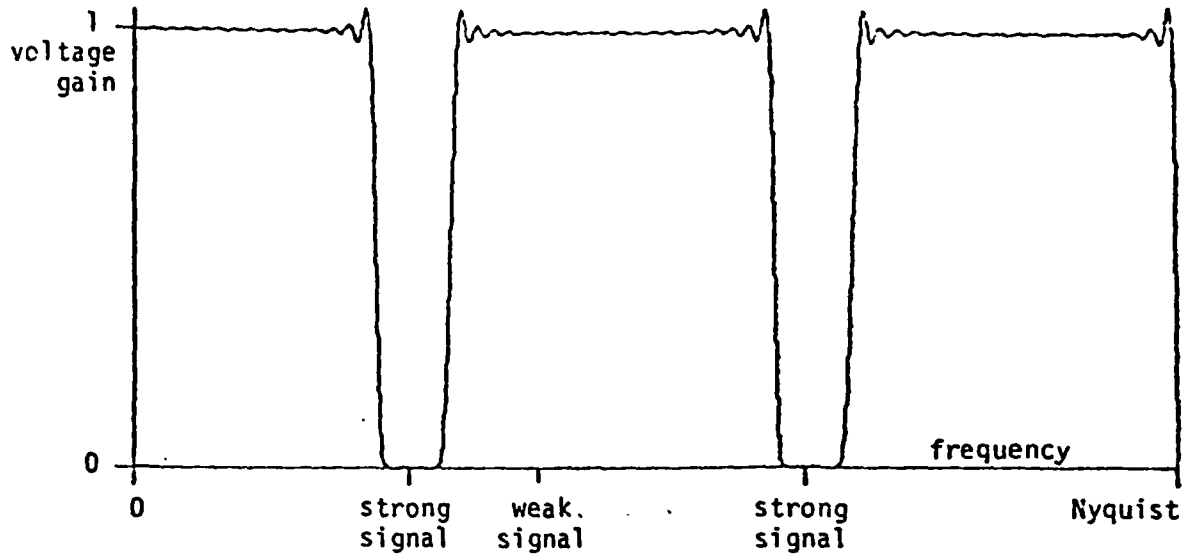

Bandstop filter designed by the APS4

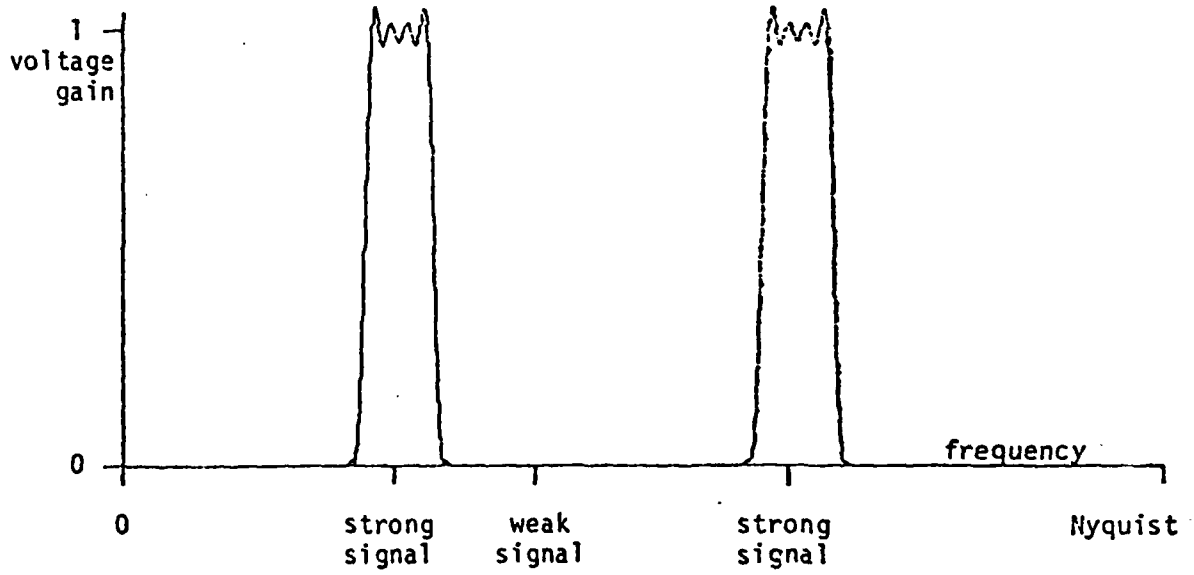

Figure 6-3. Bandpass filter designed by the APS4 to derive a reference input for cancelling strong signals.

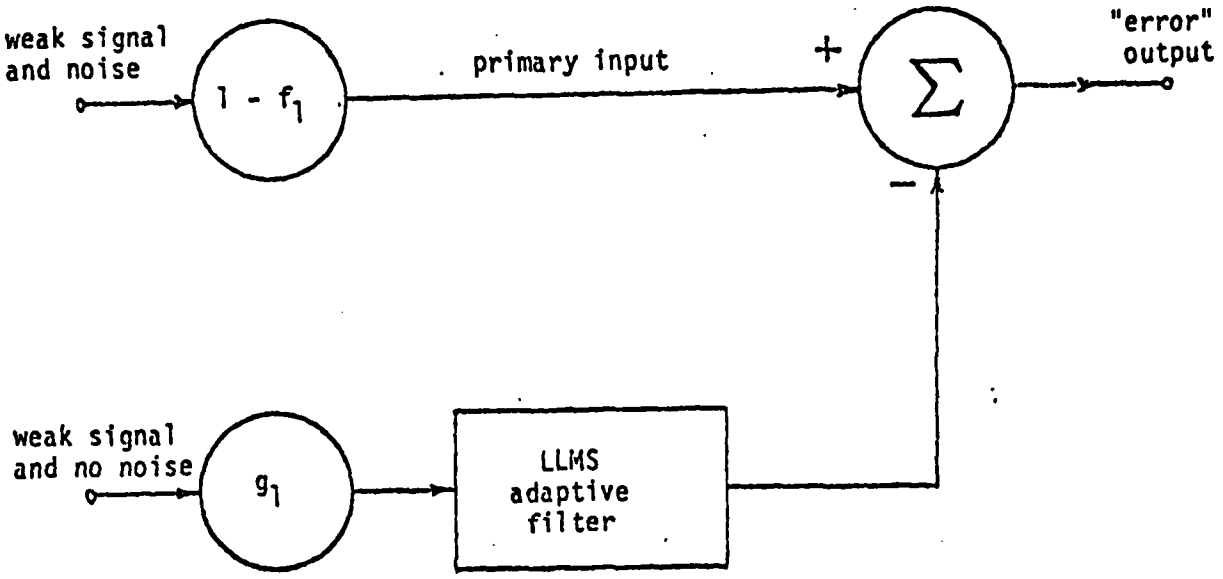

Figure 6-4. Noise canceller and input gains for a weak input signal.

where

g is the gain of the LLMS filter at the weak signal's frequency

σ^2 is the noise power in the APS input (we ignore any power reduction due to notches and ripples in the bandstop filter, also we ignore the noise passing through the bandpass filter)

p_s is the power of the weak signal .

The LLMS algorithm acts as if there were white noise with power γ_2 added to the reference input. Thus the LLMS filter minimizes the effective "error" power which is given by:

$$\text{effective error power} = \sigma^2 + (1-f_1-g_1 g)^2 p_s + \gamma_2 g^2 \frac{2}{n_2} \qquad (6\text{-}2)$$

where

n_2 = the number of weights in the LLMS filter

$\gamma_2 g^2 \frac{2}{n_2}$ = the noise power which the LLMS filter believes is passing through it

γ_2 = a parameter of the LALE

= power of "algorithmic noise"

The value of g which minimizes the effective "error" power is:

$$g^* = \frac{(1-f_1) g_1 \frac{p_s}{\gamma_2}}{g \frac{2 p_s}{\gamma_2} + \frac{2}{n_2}} = \frac{(1-f_1) g_1 \text{ESNR}}{g_1^2 \text{ESNR} + \frac{2}{n_2}} \qquad (6\text{-}3)$$

where

$$\text{ESNR} = \frac{P_s}{\gamma_2}$$

$$= \text{effective signal to noise ratio} \quad .$$

The gain for the weak signal from the primary input to the "error" output is:

$$g_e = (1-f_1) - g_1 g^* = \frac{(1-f_1)\frac{2}{n_2}}{g_1^2 \text{ESNR} + \frac{2}{n_2}} \quad . \qquad (6\text{-}4)$$

This is the gain which will apply to a weak signal in the APS4.

If a signal is strong, then the bandstop filter will reject the signal with a gain of nearly zero, and the bandpass filter will pass the signal with a gain of nearly one. We will denote the gain of the bandstop filter as f_2 and the gain of the bandpass filter as $1 - g_2$. The analysis parallels the analysis in the weak signal case and we find that the gain which applies to the strong signal is:

$$g_e = \frac{f\frac{2}{2n_2}}{(1-g_2)^2 \text{ESNR} + \frac{2}{n_2}} \quad . \qquad (6\text{-}5)$$

The reason for adding the canceller to the APS3 was to limit the output power due to strong input signals. Theorem 6 shows that this is possible.

THEOREM 6: If $\gamma_2 \leq p_t(1-g_2)^2 \frac{n_2}{2}$, then the output power due to a signal with power $p \geq p_t$ will be less than or equal to the output power due to a signal with power p_t, where p_t is the threshold power of the APS3, g_2 is the passband ripple in the bandpass filter and n_2 is the length of the LLMS filter.

PROOF: The gain of the APS4 is:

$$g = \frac{f_2 \frac{2}{n_2}}{(1-g_2)^2 \frac{p}{\gamma_2} + \frac{2}{n_2}}$$

for signals whose power, p, is greater than or equal to the threshold power p_t.

The output power due to strong signals is therefore:

$$p_{out} = g^2 p = \frac{f_2^2\left[\frac{2}{n_2}\right]^2}{\left[(1-g_2)^2 \frac{p}{\gamma_2} + \frac{2}{n_2}\right]^2} \quad p \quad .$$

The slope of the output power with respect to the input power is:

$$\frac{\partial p_{out}}{\partial p} = \frac{f_2^2\left[\frac{2}{n_2}\right]^2 \left[(1-g_2)^2 \frac{p}{\gamma_2}\right] - 2f_2^2\left[\frac{2}{n_2}\right]^2 p \frac{(1-g_2)^2}{\gamma_2}}{\left[(1-g_2)^2 \frac{p}{\gamma_2} + \frac{2}{n_2}\right]^3}$$

Since p, n_2 and γ_2 are greater than zero, the slope of the power-out versus power-in curve will be negative if:

$$2f_2^2\left[\frac{2}{n_2}\right]^2 \frac{p}{\gamma_2} - f_2^2\left[\frac{2}{n_2}\right]\left[(1-g_2)^2 \frac{p}{\gamma_2} + \frac{2}{n_2}\right]$$

$$\Rightarrow (1-g_2)^2 \frac{p}{\gamma_2} \geq \frac{2}{n_2}$$

$$\Rightarrow p \geq \frac{2}{n_2(1-g_2)^2} \gamma_2 \quad .$$

Thus the slope of the power-out versus power-in curve is negative if:

$$p \geq \frac{2}{n_2(1-g_2)^2} \gamma_2 \quad .$$

This is the condition that makes the theorem true. For if the power-out versus power-in curve has a negative slope then an increase in input power will cause a decrease in output power. Thus the theorem requires that the slope of the power-out versus power-in curve be negative for all powers $p \geq p_t$. This implies that:

$$p_t \geq \frac{2}{n_2(1-g_2)^2} \gamma_2$$

$$\Rightarrow \gamma_2 \leq p_t(1-g_2)^2 \frac{n_2}{2} \quad .$$

This demonstrates that the condition:

$$\gamma_2 \leq p_t(1-g_2)^2 \frac{n_2}{2}$$

is sufficient to guarantee that any signal with power $p > p_t$ will have less output power than a signal with power p_t.

QED

As the power of a weak signal increases the gain of the APS4 decreases. The gain variation for weak signals is minimized if γ_2 is maximized. Since the APS4 should have a minimum gain variation for weak signals, the best choice of γ_2 is:

$$\gamma_2 = p_t(1-g_2)^2 \frac{n_2}{2} \tag{6-6}$$

since this is the largest possible value for γ_2 that will still guarantee, by Theorem 6, that the output power due to strong signals will decrease as the input power increases. By using this value for γ_2 we find that the minimum gain for weak signals is:

$$\frac{(1-f_1)\frac{2}{n_2}}{\frac{g_1^2}{\gamma_2} p_t + \frac{2}{n_2}} = 1 - \rho_1 \tag{6-7}$$

which implies that

$$\rho_1 = \frac{g_1^2 + f_1(1-g_2)^2}{g_1^2 + (1-g_2)^2} \tag{6-8}$$

where

ρ_1 is the gain deviation in the weak signal region (see Eq. 3-2, the definition of tolerance scheme two)

g_1 is the stopband ripple of the bandpass filter

g_2 is the passband ripple of the bandpass filter

f_1 is the passband ripple of the bandstop filter

Since g_1, g_2 and f_1 can be made as small as desired (Theorem 5-2), ρ_1 can be made as small as desired, thus the APS4 meets the gain specifications of tolerance scheme 2 (Eq. 3-2) in the weak signal region.

The maximum gain for strong signals is:

$$\frac{f_2}{2} = \rho_2 \tag{6-9}$$

where

$\rho_2^2 p_t$ is the maximum allowed output power due to a strong signal (see the definition of tolerance scheme two, Chapter 3)

f_2 is the stopband ripple for the bandstop filter .

Since f_2 can be made as small as desired (Theorem 5-2), ρ_2 can be made as small as desired, thus the APS4 meets the gain specifications of tolerance scheme 2 in the strong signal region.

The switching characteristics of the APS4 are controlled by the APS3 part of the APS4. Since the switching characteristic of the APS3 with hysteresis devices fits tolerance scheme two, the switching characteristics of the APS4 also fits tolerance scheme two. Since the gain characteristics of the APS4 filters fit tolerance scheme two, the APS4 fits tolerance scheme two. Thus, any desired quality of adaptive power separator, as measured by tolerance scheme two, can be implemented with the APS4.

Summary and Conclusions

This chapter has presented the APS4, which consists of the APS3 with an adaptive noise cancelling stage. The APS4 uses more computations than the APS3, but the gain characteristic of the APS4 fits tolerance scheme two. Because the APS4 controls output power, rather than gain, it is suited to applications where the power of the strong signals can be many times larger than the threshold power. For this reason, the APS4 is the best of the adaptive power separators discussed in this work.

7 -- SYNTHESIS OF AN APS

In this chapter we show how to design an APS given a problem specification. The problem to be solved is: design a system that will reject jamming signals and pass communication signals given a received signal that consists of narrowband communications signals with powers between 0.1 and 2.0, narrowband jammers with power greater than 3.0, and white noise with power 0.5. Conventional filters cannot be used because the frequencies of the various signals are unknown, and the LALE cannot be used because it cannot suppress the jammers without also suppressing the communication signals.

Because the problem definition is incomplete, we have to make several assumptions. First, we assume that the jammer powers are less than 20 and design the APS3 accordingly. Second, we assume that the jammer powers at the output of the APS should be less than 0.01. Third, we assume that there will be at most 20 signals at any time and that the frequencies of the signals are between 2 MHz and 8 MHz. Finally, we assume that the jammer powers can be as large as 20 000 and show how to design an APS4 to accommodate this case.

The design of the adaptive power separator consists of a number of steps:

1) Selection of n, the number of LALE weights.

   Since an n weight LALE can handle up to n/2 sinusoids, n must be greater than 40. Also, the FFT, which is an efficient implementation of the DFT, requires that n be an integral power of 2, so n is chosen to be 64.

2) Selection of T, the sampling period.

The LALE will give good spectral estimates only if the frequencies of all the signals are between 20% and 80% of the Nyquist frequency. Thus T has to be 50nS ($\frac{1}{20}$ MHz). The sampling rate, in conjunction with the number of LALE weights, determines the bin width of the LALE (313 kHz). Any signal with bandwidth less than a tenth the bin width can be reasonably approximated as a sinusoid, so the APS will treat all signals with bandwidth less than 30 kHz as narrowband signals and behave as predicted. Signals with wide bandwidth cause unpredictable operation of the APS.

3) Selection of γ, the "algorithmic noise" power.

The gain of the LALE is related to γ, the sum of the true noise power and the signal power. To prevent the spectral sidelobes of powerful signals from causing errors requires that a large LALE gain correspond to a signal at the threshold power. However, for good switching performance the gain should have a high sensitivity to power changes, which implies that a small LALE gain correspond to the threshold power. Accordingly, a compromise is reached by choosing a LALE gain of 0.5 to correspond to the threshold power. For simplicity the threshold power is taken to be $p_t = 2.5$ (the average of the maximum signal power and the minimum jammer power). Using this information we can solve for γ:

$$0.5 = \text{gain at the threshold power}$$

$$= \frac{\frac{n\ P_t}{2\gamma + \sigma^2}}{1 + \frac{n\ P_t}{2\gamma + \sigma^2}}$$

$$= \frac{32\frac{2.5}{\gamma + 0.5}}{1 + 32\frac{2.5}{\gamma + 0.5}}$$

$$\Rightarrow \gamma = 79.5 \quad . \qquad (7\text{-}1)$$

4) Selection of n', the length of the FIR filter.

Selection of n' controls the maximum gain in the stopband of the FIR filter and also the quality of the power spectral estimate. The APS3 uses the LALE gain as a power spectral estimate. However, the APS3 uses a finite length DFT to determine the gain of the LALE. The outputs of the DFT are samples of the LALE gain, and these samples may not coincide with the peaks in the LALE gain that are caused by signals. If the DFT samples bracket a peak, then the APS3 will act as if there are two smaller signals. This effect is a combination of leakage and the "picket-fence" effect [Ber]. The picket-fence effect is caused by the gain characteristics of the bank of bandpass filters that constitute the DFT (see Chapter 4, Eq. 4-2). If the signal is on-bin, the bandpass filter passes it with a gain of one, but if the signal is between bins then the gain of the bandpass filter is 0.64. The LALE gain can be sampled more frequently if the LALE weight vector is padded with $n'-n$ zeros and an n'-point DFT is used to evaluate the

gain [Ber]. This technique of "zero-filling" reduces the picket-fence effect. The minimum gain for an n' point DFT of an n weight LALE is $\frac{\mathrm{Sin}(x)}{x}$ where $x = \frac{\pi}{2\frac{n'}{n}}$. Thus if a signal is present that causes the LALE gain to peak with a value g, as n' point DFT will return a peak value between g and $2n'\frac{\mathrm{Sin}(\frac{\pi n}{2n'})}{n\pi}$ g. To find the minimum allowable DFT gain we first determine that the peak gain of the LALE for a communication signal with power 2.0 (largest power to keep) is 0.444, and that the peak gain for a jammer of power 3.0 (smallest power to discard) is 0.545. Since $0.444 = 0.80 \times 0.545$, the minimum gain of the DFT must be greater than 0.80 to avoid confusing weak jammers with strong communication signals. From Table 7-1 we select $n' = 4n$ because the extra gain gives us room for a large deadband in the hysteresis threshold device (which will reduce the error rate).

The other constraint was that the FIR filter have a low enough maximum stopband gain. It turns out that a 4n FIR filter has a maximum stopband gain of about -35 dB, and the requirement is for a maximum stopband gain of $\frac{0.01}{20.0} = 5 \times 10^{-4}$ or -33 dB. Thus the 4n filter fits all of the constraints, so n' is chosen to be 256.

5) Selection of a_ℓ and a_h, the low threshold and high threshold of the hysteresis device.

Once the minimum DFT gain has been determined it is possible to find the minimum DFT output amplitude that corresponds to a jammer:

n'	Minimum DFT Gain
n	0.6366
.2n	0.9003
4n	0.9745
8n	0.9936
16n	0.9984
32n	0.9996
64n	0.9999

Table 7-1.

$$\text{Min}[a_j] = \text{Min}[\text{DFT gain}] \times \text{LALE gain for weakest jammer}$$
$$= 0.531 \quad .$$

Also, the maximum DFT output due to a communication signal is:

$$\text{Max}[a_s] = 0.444 \quad .$$

In the absence of other information it seems reasonable to select the two threshold values as 1/4 of the difference between $\text{Min}[a_j]$ and $\text{Max}[a_s]$ (see Fig. 7-1):

$$a_\ell = 0.466$$
$$a_h = 0.509 \quad .$$

6) Selection of μ.

From Eq. 5-34 the probability of error for the threshold device is:

$$P\{\text{error}\} = \frac{\text{VAR}\{\hat{S}_{LALE}\}}{\text{Min}\{a_h - \text{Max}[a_s],\ \text{Min}[a_j] - a_\ell\}^2} \qquad (7\text{-}2)$$

From Eq. 5-24, $\text{VAR}\{\hat{S}_{LALE}\} \leq 2n\mu\sigma^2$, so Eq. 7-2 becomes:

$$P\{\text{error}\} \leq 7\ 600\mu \quad . \qquad (7\text{-}3)$$

If we want $P\{\text{error}\} < 1\%$, then:

$$\mu \leq 1.3 \times 10^{-6} \quad . \qquad (7\text{-}4)$$

This value of μ also guarantees the stability of the adaptive process.

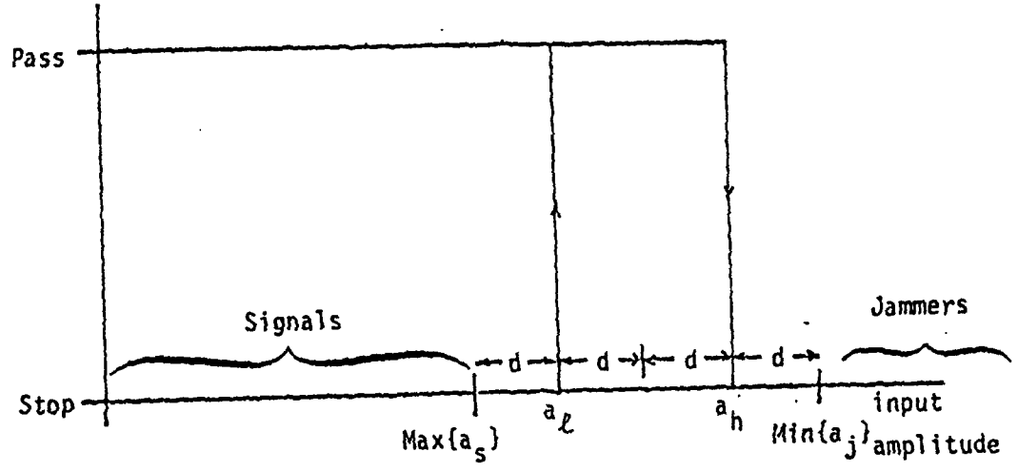

Figure 7-1. Characteristic of hysteresis threshold device.

Another constraint on μ is the expected design cycle time. Using Eq. 5-33, we can find $E\{T_c\} \geq 2\,500$, which is acceptable. If the expected design cycle time was unacceptable, μ would have to be reduced.

This completes the design of the APS3. The design parameters for the APS3 are summarized in Table 7-2.

Now assume that the jammer powers can range from 3 to 20 000. In this case the APS3 will not be sufficient to reject the jammers because the stopband ripple is too large. To obtain the desired performance we will add a noise cancelling stage to the APS3 and thus design an APS4. The APS3 portion of the APS4 will have the same parameters as in Table 7-2, except that μ will be 1.5×10^{-7} to guarantee that the small μ assumptions used in the analysis of the LALE remain valid (this μ is a tenth of the stability limit). The LLMS filter used for noise cancelling will have as many weights as the LALE (i.e. 64), and a μ of 1.5×10^{-7}. γ_2 is computed from Eq. 6-6 to be 96.

This completes the design of the APS4.

Simulations of the APS3 and APS4

Both the APS3 and the APS4 were simulated on a digital computer. Figures 7-2 through 7-5 show characteristic curves of both power separators for a single sinusoidal input. Figure 7-2 shows output-power versus input-power as the input power ranges from 0.1 to 10 000, and Fig. 7-3 gives an expanded view of the transition region. Figure 7-4 shows gain versus input-power as the input power ranges between 0.1 and 10 000, and Fig. 7-5 gives an expanded view of the transition region.

number of LALE weights	$n = 64$
equivalent LALE noise power	$\gamma = 79.5$
adaption constant	$\mu = 1.3 \times 10^{-6}$
low amplitude threshold	$a_\ell = 0.466$
high amplitude threshold	$a_n = 0.509$
number of FIR Filter weights	$n' = 256$
sampling frequency	$f_s = 20$ MHz

Table 7-2. Parameters of the APS3.

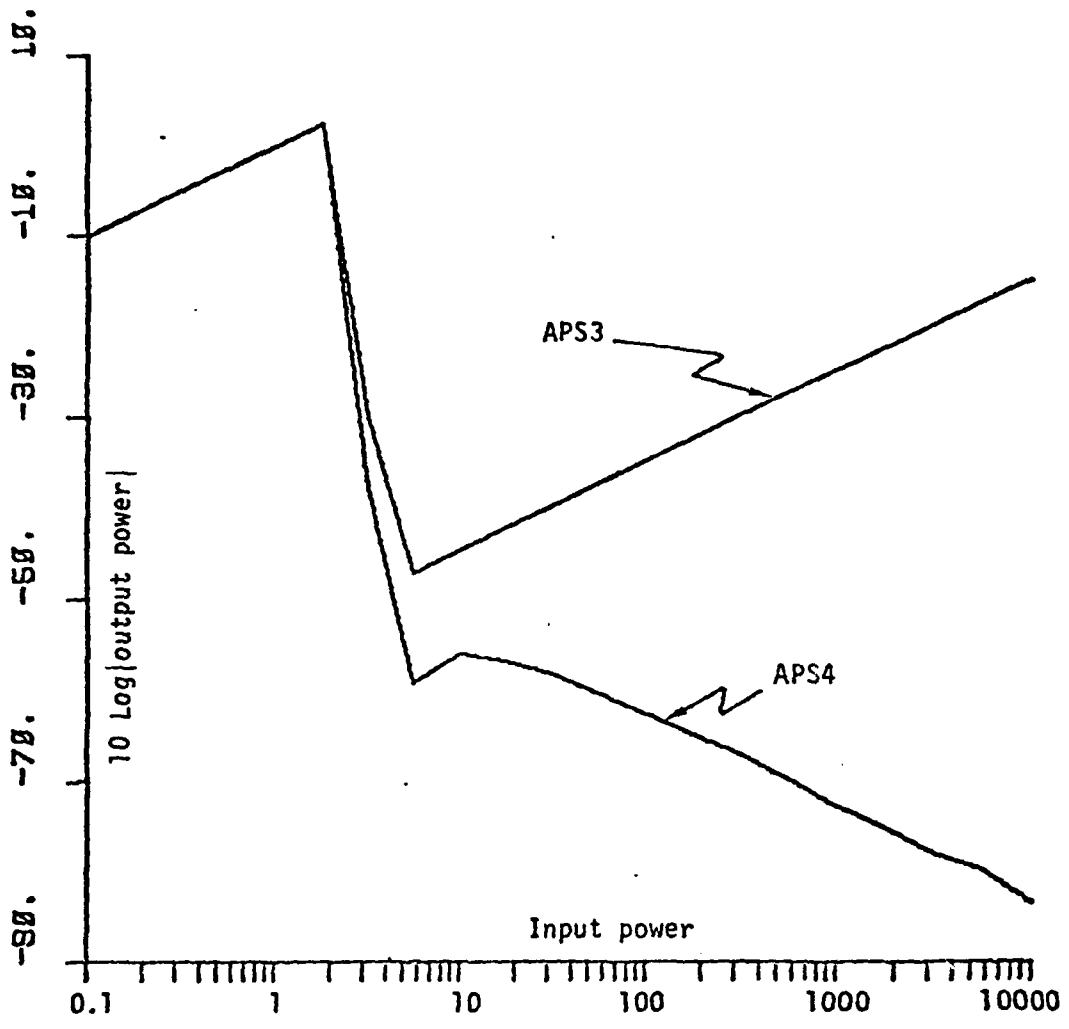

Figure 7-2. Output-power vs. Input-power curves for the APS3 and APS4.

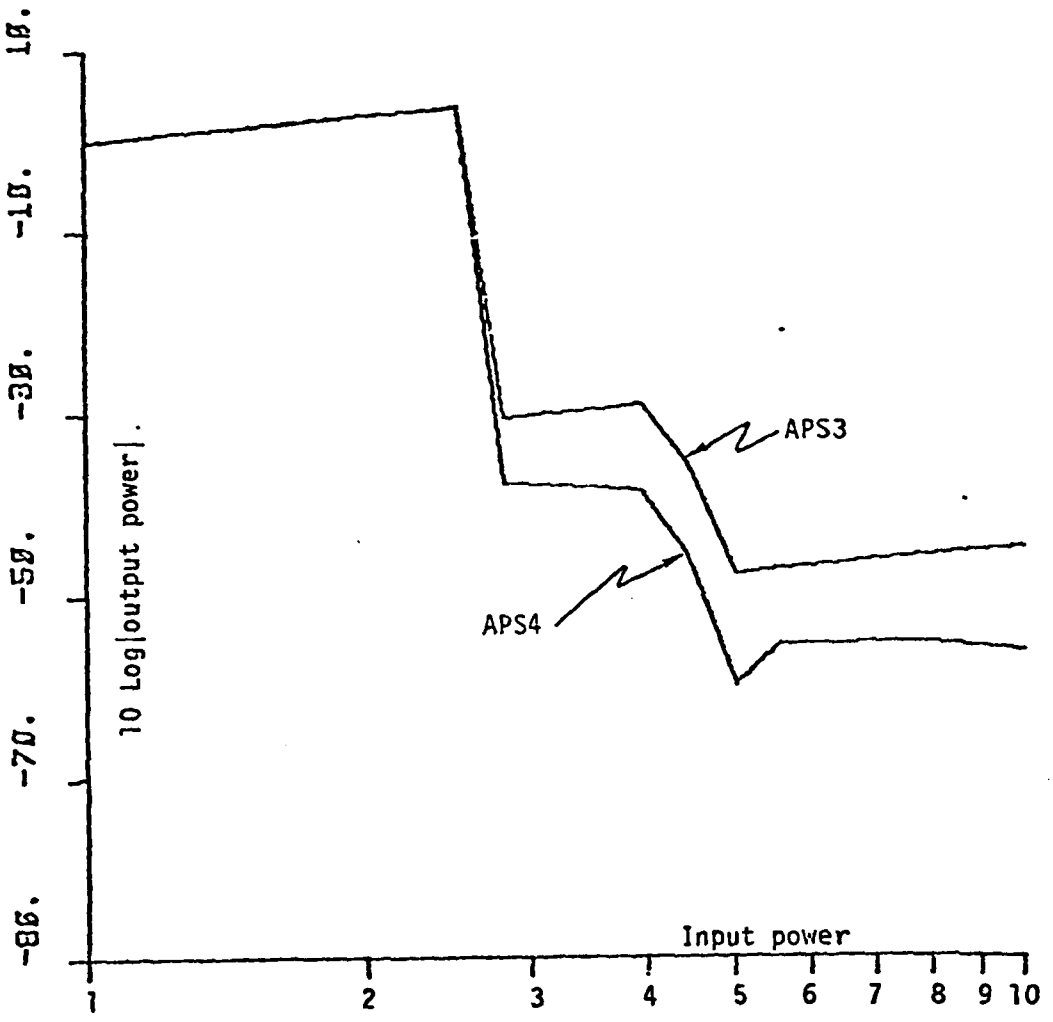

Figure 7-3. Expanded output vs. input power curves for APS3 and APS4.

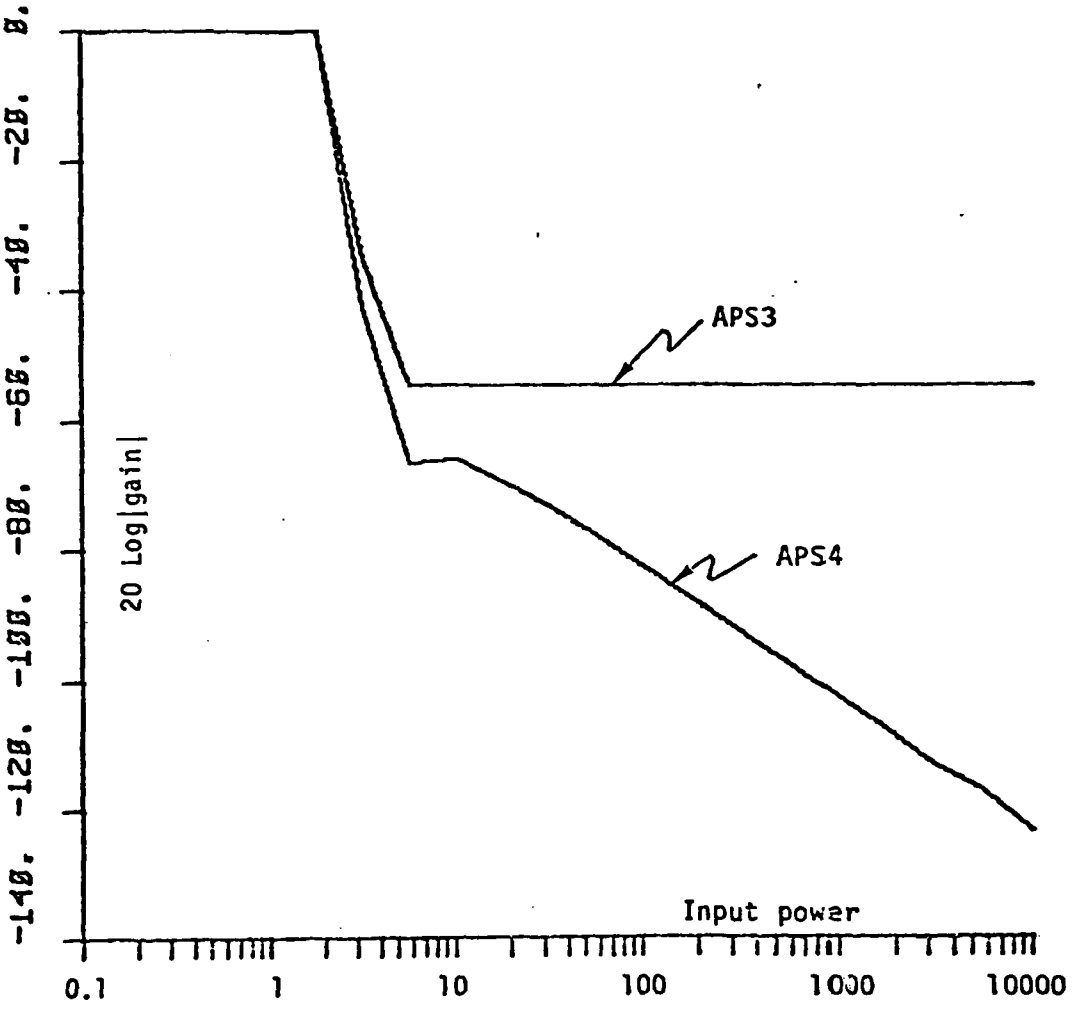

Figure 7-4. Gain vs. input-power curve for APS3 and APS4.

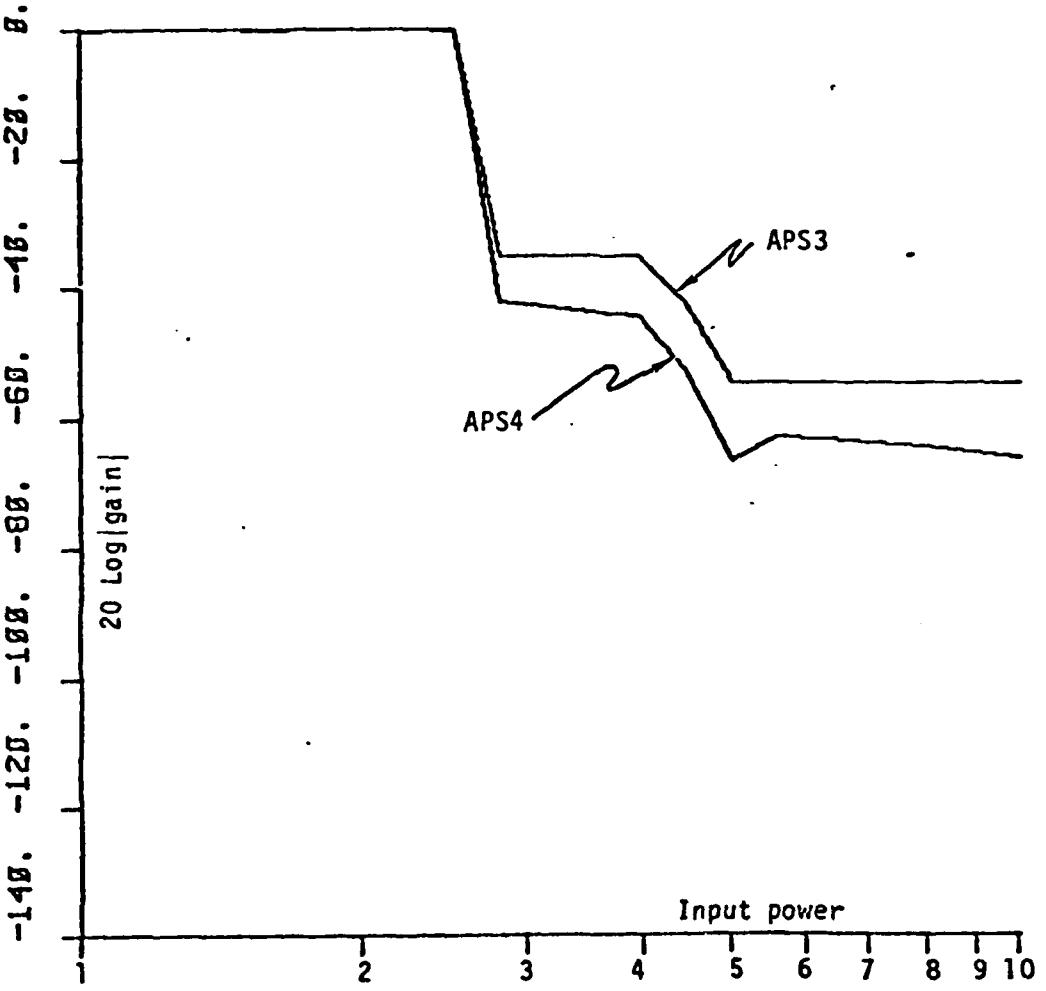

Figure 7-5. Expanded gain vs. input-power curve for APS3 and APS4.

Figures 7-2 and 7-3 show how well the APS4 controls the output power. Also, the sharp threshold is evident, as well as the fact that the APS4 easily meets the design goals. From Fig. 7-3 it is possible to determine that the APS3 meets the design goals over the limited power range that was assumed for the design of the APS3. (The frequency of the sinusoid used to test the power separators was chosen to give the poorest possible results; at other frequencies the output power and filter gain would have been lower for powerful signals.)

For comparison, Fig. 7-6 shows a gain versus input-power curve for a LALE power separator (APS1). The LALE was designed to have a threshold power of 2.5 which gives the best possible signal to jammer enhancement. This figure shows the very slow transition from high gain to low gain that is characteristic of the LALE.

Figures 7-7A and 7-7B show the results of simulating the APS3 with many input sinusoids. In this example there are 10 input sinusoids. Table 7-3 lists the power and frequency of these sinusoids. Figure 7-7A shows a theoretical power spectrum of the input signal and Fig. 7-7B shows a theoretical power spectrum of the output signal. These power spectra are computed from the power of the true input noise, the power of the sinusoids and the gain of the APS3. Figure 7-7B shows that the APS3 has deleted the signals with power 3 or more, and has left unaffected the signals with power 2 or less. Table 7-3 also lists the output powers at the signal frequencies to show the exact effects of the APS3.

Simulations have also been used to determine the frequency resolution of the APS3. It has been determined that a jammer that is

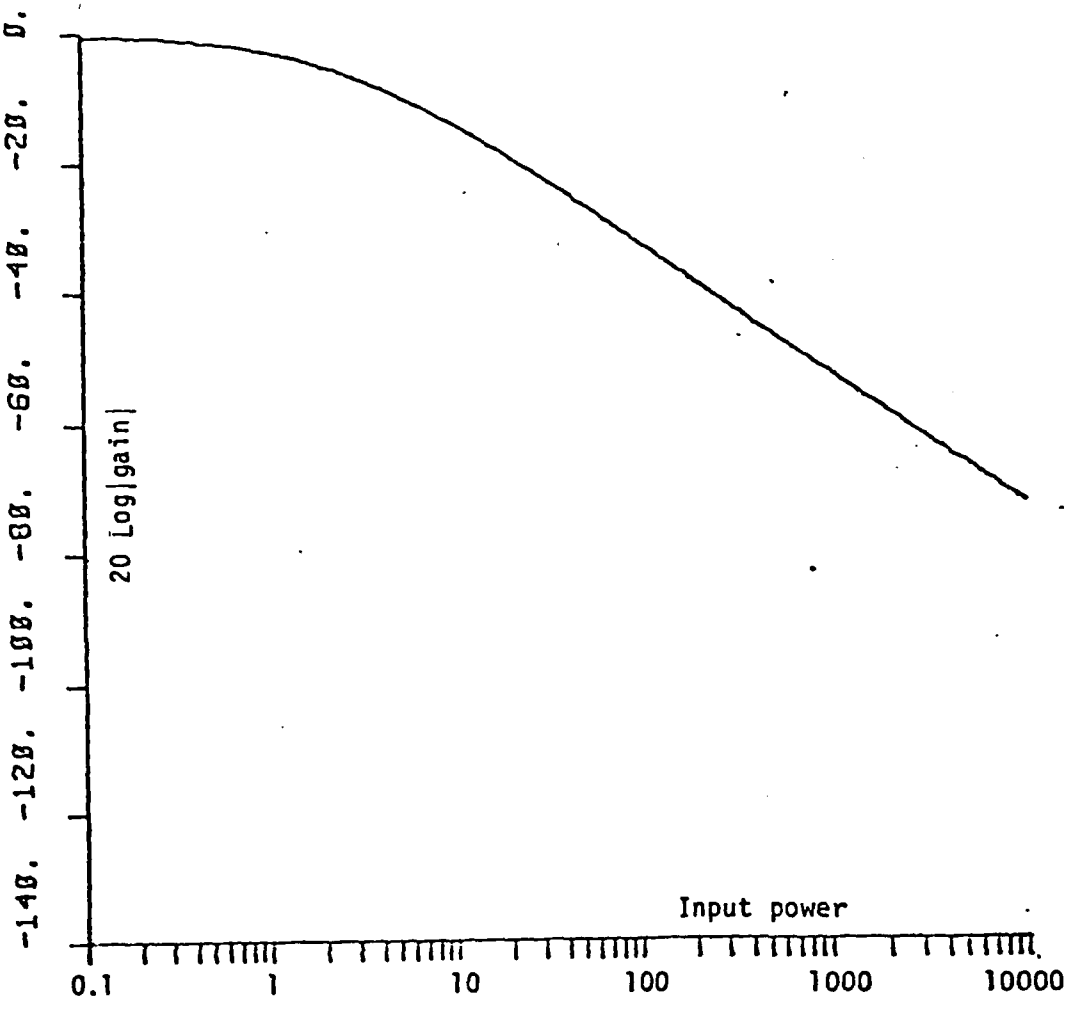

Figure 7-6. Gain vs. Input-power for LALE.

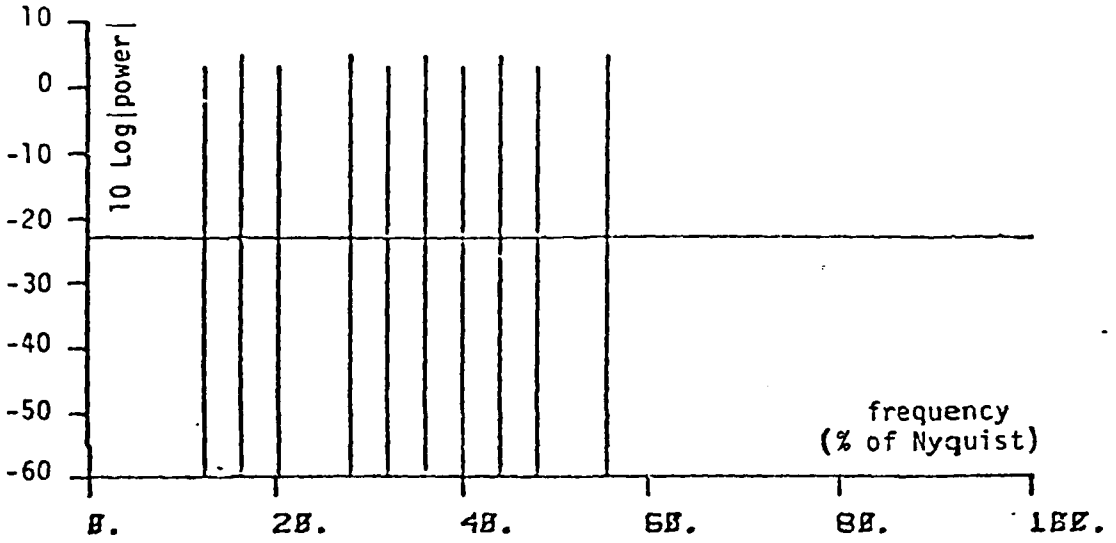

Figure 7-7A. Input power spectrum.

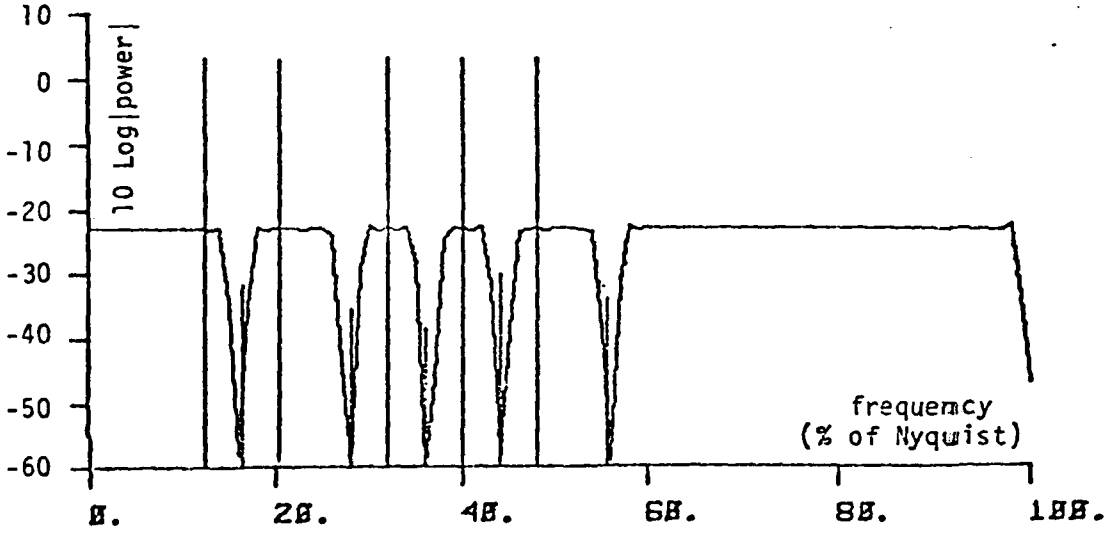

Figure 7-7B. Output power spectrum.

Frequency (% of Nyquist)	Input power	Output power
12.5	2.0	2.00
16.5	3.0	0.00065
20.5	2.0	1.98
28.0	3.0	0.00029
32.0	2.0	2.00
36.0	3.0	0.00014
40.0	2.0	2.06
44.0	3.0	0.00098
48.0	2.0	2.04
55.6	3.0	0.00038

Table 7-3

within one "bin width" (i.e. a frequency of $\frac{1}{nT}$) of a signal can cause the APS3 to erroneously delete the signal. This is caused by a side-lobe of the power spectral estimate of the jammer adding to the spectral estimate of the weak signal and causing the total estimate to exceed the threshold value. Thus for good performance of the APS3, the signals should be separated by at least 1.5 bin widths (4.9% of the Nyquist frequency for a 64 weight APS).

8 -- SUMMARY AND CONCLUSIONS

This thesis has developed the concept of an adaptive power separator and analyzed three implementations of a generic power separator structure. A good example of an APS is the APS3. The APS3 uses a LALE to analyze the input signal, and a DFT of the LALE's weight vector to produce a power spectral estimate. The outputs of the DFT will be large at the frequencies where the input signals are strong, and small elsewhere. The DFT outputs are passed through threshold devices that have zero output whenever their input exceeds a predetermined threshold and unit output otherwise. The outputs of the threshold devices form a desired, or ideal, frequency response. A filter with this frequency response would pass weak signals with unit gain and reject strong signals with zero gain. This ideal frequency response is converted into a weight vector for a finite impulse response filter by a design technique called frequency sampling. The frequency characteristics of the resulting filter can be made as nearly ideal as required by appropriately selecting the length of the filter.

Since the LALE-DFT combination gives good spectral estimates, and since the finite impulse response filter can be made nearly ideal, the APS3 can be designed to have nearly ideal input-to-output characteristics. However, there are other important measures of APS performance such as response time or frequency resolution. Also, the analysis assumed that the input to the APS consisted of a sum of narrowband signals in white noise. This may accurately model many situations,

such as rejection of CW jammers or interference from rotating machinery, but simulations show that the APS3 and APS4 fail to function when the input consists of a wideband signal in white noise. Thus the APS3 and APS4 would provide no protection against wideband jammers.

A possible topic for future work would be the design of an APS that could reject wideband signals as well as narrowband signals. Such an APS might use one of the modern spectral estimation schemes, such as maximum likelihood or maximum entropy, instead of the LALE-DFT combination that is used in the APS3 and APS4.

REFERENCES

[Ber] G. D. Bergland, "A Guided Tour of the Fast Fourier Transform," IEEE Spectrum, Vol. 6, pp. 41-52, July 1969.

[Car] M. S. Carslaw, An Introduction to the Theory of Fourier's Series and Integrals, Dover publications Inc., New York, 1950.

[Che] R. A. Chestek, The Addition of Soft Constraints to the LMS Algorithm, Ph.D. Dissertation, Stanford University, 1979.

[Cin] E. Cinlar, Introduction to Stochastic Processes, Prentice-Hall, Inc., New Jersey, 1975.

[Dan] T. P. Daniell, "Adaptive Estimation with Mutually Correlated Training Sequences," IEEE Trans. on Systems Science and Cybernetics, Vol. SSC-6, No. 1, pp. 12-19, January 1970.

[Der] P. M. Derusso et al., State Variables for Engineers, J. Wiley & Sons, New York, 1965.

[Glo] J. Glover, "Adaptive Noise Cancelling of Sinusoidal Interferences," Ph.D. Dissertation, Stanford University, 1975.

[Gri] L. J. Griffiths, Signal Extraction Using Real-Time Adaption of a Linear Multichannel Filter, Ph.D. Dissertation, Stanford University, 1968.

[Oga] K. Ogata, Modern Control Engineering, Prentice-Hall, Inc., New Jersey, 1970.

[Opp] A. V. Oppenheim and R. W. Schafer, Digital Signal Processing, Prentice-Hall, Inc., New Jersey, 1975.

[Pap] A. Papoulis, Signal Analysis, McGraw-Hill Book Co., New York, 1977.

[Rab] L. R. Rabiner, "Techniques for Designing Finite-Duration Impulse-Response Digital Filters," IEEE Trans. on Communication Technology, Vol. COM-19, pp. 188-195, April 1971.

[Rab2] L. R. Rabiner et al., "An Approach to the Approximation Problem for Nonrecursive Digital Filters," IEEE Transactions on Audio and Electroacoustics, Vol. AU-18, pp. 83-106, June 1970.

[Ros] M. Rosenlicht, Introduction to Analysis, Scott, Foresman and Co., Glenview, IL, 1968.

[Sen] K. D. Senne, Adaptive Linear Discrete-Time Estimation, Ph.D. Dissertation, Stanford University, 1968.

[Tre] J. R. Treichler, The Spectral Line Enhancer -- The Concept, an Implementation and an Application, Ph.D. Dissertation, Stanford University, 1977.

[Trt] S. A. Tretter, Introduction to Discrete-Time Signal Processing, John Wiley & Sons, New York, 1976.

[Wid] B. Widrow and M. Hoff, Jr., "Adaptive Switching Circuits," in IRE WESCON Conv. Rec., Pt. 4, pp. 96-104, 1960.

[Wid2] B. Widrow et al., "Adaptive Noise Cancelling: Principles and Applications," Proc. IEEE, Vol. 63, No. 12, pp. 1692-1716, December 1976.

[Wid3] B. Widrow et al., "Research on Adaptive Antenna Techniques: Final Report," Stanford University, Stanford, March 1977, Naval Air Systems Command Contract N00019-76-C-0250.

[Wid4] B. Widrow et al., "Research on Adaptive Antenna Techniques II: Final Report," Stanford University, Stanford, March 1978, Naval Air Systems Command Contract N00019-77-C-0194.

[Zah] C. L. Zahm, "Application of Adaptive Arrays to Suppress Strong Jammers in the Presence of Weak Signals," IEEE Trans. on Aerospace and Electronic Systems, Vol. AES-9, No. 2, pp. 260-271, March 1973.